

**UNCLASSIFIED**

**419083**

**AD**

---

**DEFENSE DOCUMENTATION CENTER**

**FOR**

**SCIENTIFIC AND TECHNICAL INFORMATION**

**CAMERON STATION, ALEXANDRIA, VIRGINIA**



**UNCLASSIFIED**

**NOTICE:** When government or other drawings, specifications or other data are used for any purpose other than in connection with a definitely related government procurement operation, the U. S. Government thereby incurs no responsibility, nor any obligation whatsoever; and the fact that the Government may have formulated, furnished, or in any way supplied the said drawings, specifications, or other data is not to be regarded by implication or otherwise as in any manner licensing the holder or any other person or corporation, or conveying any rights or permission to manufacture, use or sell any patented invention that may in any way be related thereto.

64-5

CATALOGED BY CLC 419083

AS AD NO. \_\_\_\_\_

419083

THE DYNAMICS OF GYROSCOPE DAMPING FOR  
GEOCENTRIC ATTITUDE CONTROL

by

Martin Messinger and Howard E. Parker

Research Report PIBMRI-1147-63

for

The Air Force Office of Scientific Research

The Army Research Office

The Office of Naval Research

Grant No. AF-AFOSR-62-295

May 1963

MRI

POLYTECHNIC INSTITUTE OF BROOKLYN  
MICROWAVE RESEARCH INSTITUTE  
ELECTRICAL ENGINEERING DEPARTMENT

THE DYNAMICS OF GYROSCOPE DAMPING FOR  
GEOCENTRIC ATTITUDE CONTROL

by  
Martin Messinger  
and  
Howard E. Parker

Polytechnic Institute of Brooklyn  
Microwave Research Institute  
55 Johnson Street  
Brooklyn 1, New York

Research Report No. PIBMRI-1147-63


Grant No. AFOSR-62-295

May 1963

Title Page  
Acknowledgement  
Abstract  
Table of Contents  
Table of Figures  
118 Pages of Text  
References  
Distribution List

  
Martin Messinger

  
Howard E. Parker

  
Mischa Schwartz  
Head, Electrical Engineering Department

Prepared for

The Air Force Office of Scientific Research  
The Army Research Office  
The Office of Naval Research

### ACKNOWLEDGEMENT

The Authors wish to thank their Thesis Advisor Dr. Martin L. Shooman for his expert guidance and friendly advice extended during the development of the project.

The work reported herein was sponsored by the Air Force Office of Scientific Research of the Office of Aerospace Research; the Department of the Army, Army Research Office, and the Department of the Navy, Office of Naval Research under Grant No. AF-AFOSR-62-295,

## ABSTRACT

This study is concerned with the geocentric attitude stabilization of an earth satellite. The system considered in this report utilizes differential gravity to control the vehicle's orientation and gyroscopes to provide vehicle damping. Several different gyroscope configurations that provide indirect gyroscope damping about all three of the vehicle axes are presented. For each of these configurations, the equations governing the dynamics of the system are systematically developed in terms of the attitude deviation angles and the parameters of the orbit. The expressions for the steady state deviation angles and the torque which must be supplied by gyroscope torquers are also obtained.

The analytical procedure utilized, considers the satellite vehicle to be composed of a rigid body to which is affixed internal gyroscopes. The dynamics of an orbiting rigid body are first obtained with the inclusion of the differential gravity torque. This is followed by a development of the equations of dynamics of a gyroscope constrained in an arbitrary position within an orbiting body. The equations obtained for the gyroscope and the rigid body are completely general in that they are valid for an elliptical orbit. The resulting equations of a gyroscope and a rigid body are combined to obtain both the statics and dynamics of an orbiting vehicle containing internally mounted gyroscopes. This analysis is restricted to a circular orbit. To obtain a better understanding of the mechanism of gyroscope damping, an analysis of a simple configuration employing a gyroscope for damping purposes is also included.

## TABLE OF CONTENTS

		Page
Abstract		
Chapter I	- Introduction	1
Chapter II	- Satellite Attitude Dynamics	4
	A - Reference Coordinate System	4
	B - Body Coordinate System	4
	C - The Eulerian Angles and Transformation Matrix	6
	D - Development of Equations of Motion of the Body	8
	E - Inclusion of the Gravity Gradient Torque	14
	F - Solutions of the Equations of Motion for a Circular Orbit	22
Chapter III	- A Simple Analysis of Gyroscope Damping	30
	A - The Mechanism of Gyroscope Damping	30
	B - Analysis of a Simple Configuration Employing Indirect Gyroscope Damping	30
	C - Analysis of a Simple Configuration Employing Direct Gyroscope Damping	56
Chapter IV	- Gyroscope Dynamics	67
	A - The Gyroscope Equations for Symmetrical Design	67
	B - The Transformation Matrix Relating Body and Gyroscope Coordinates	68
	C - The General Gyroscope Equations	70
	D - The Gyroscope Equations for Particular Configurations	75
Chapter V	- Steady State Requirements for an Orbiting Vehicle	8
	A - The General Steady State Torque Equations	84
	B - Specialization for Several Restrictive Cases	85
	C - Choice of a Gyroscope Configuration	88
Chapter VI	- The Dynamics of an Orbiting Vehicle with Internally Mounted Gyroscopes for a Circular Orbit	91
	A - Analysis of a Configuration Employing Gyroscopes with Precession Axes along $X_b$ and $Z_b$	91
	B - Analysis of a "V" Configuration in the $X_b Y_b$ Plane	97
	C - A Configuration Employing a Single Gyroscope to Provide Three Axis Vehicle Damping	100
Chapter VII	- Conclusion	104

TABLE OF FIGURES

	Page
<b>Chapter II</b>	
Fig. 2-1 Satellite Reference Coordinate System	5
Fig. 2-2 Eulerian Angles	7
Fig. 2-3 Drum Shaped Satellite	12
Fig. 2-4 Mechanism of Differential Gravity Torque	14
Fig. 2-5 Signal Flow Graph for the $X_b$ and $Z_b$ axes of the Body in an Elliptical Orbit	19
Fig. 2-6 Signal Flow Graph for the $Y_b$ Axis of the Body in an Elliptical Orbit	20
Fig. 2-7 Response to an Impulsive Torque of Strength $\delta$ Applied About the $X_b$ Axis	25
Fig. 2-8 Response to an Impulsive Torque of Strength $\delta$ Applied About the $Y_b$ Axis	25
Fig. 2-9 Response to an Impulsive Torque of Strength $\delta$ Applied About the $Z_b$ Axis	28
<b>Chapter III</b>	
Fig. 3-1 Configuration to Illustrate Indirect Gyroscope Damping	31
Fig. 3-2 Third Order Pole on the Real Axis	34
Fig. 3-3 Real Pole and a Pair of Complex Poles	34
Fig. 3-4 Variation of $\sigma$ , $H_r$ and $K$ with the Damping Coefficient for Optimization with a Third Order Pole on the Real Axis	36
Fig. 3-5 Settling Time as a Function of the Damping Coefficient for Optimization with a Third Order Pole on the Real Axis	38
Fig. 3-6 Root Locus as a Function of the Damping Coefficient for Optimization with a Third Order Pole on the Real Axis	40
Fig. 3-7 Root Locus as a Function of the Angular Momentum of the Rotor for Optimization with a Third Order Pole on Real Axis	42
Fig. 3-8 Root Locus as a Function of the Spring Constant for Optimization with a Third Order Pole on the Real Axis	44
Fig. 3-9 Root Locus as a Function of the Moment of Inertia of the Gyroscope for Optimization with a Third Order Pole on the Real Axis	46
Fig. 3-10 Variation of $\sigma$ , $H_r$ and $\omega_d$ with the Damping Coefficient for Optimization with a Real Pole and a Pair of Complex Poles	48
Fig. 3-11 Settling Time as a Function of the Damping Coefficient for Optimization with a Real Pole and a Pair of Complex Poles	50
Fig. 3-12 Root Locus as a Function of the Damping Coefficient for Optimization with a Real Pole and a Pair of Complex Poles	51



	<b>Page</b>
Fig. 3-13 Root Locus as a Function of the Angular Momentum of the Rotor for Optimization with a Real Pole and a Pair of Complex Poles	53
Fig. 3-14 Root Locus as a Function of the Spring Constant for Optimization with a Real Pole and a Pair of Complex Poles	55
Fig. 3-15 Root Locus as a Function of the Moment of Inertia of the Gyroscope for Optimization with a Real Pole and a Pair of Complex Poles	57
Fig. 3-16 Configuration to Illustrate Direct Gyroscope Damping	59
Fig. 3-17 Root Locus as a Function of the Damping Coefficient for Direct Damping	62
Fig. 3-18 Root Locus as a Function of the Spring Constant for Direct Damping	64
Fig. 3-19 Root Locus as a Function of the Moment of Inertia of the Gyroscope for Direct Damping	66
<b>Chapter IV</b>	
Fig. 4-1 Transformation Matrix Relating Gyroscope and Body Axes	69
Fig. 4-2 Gyroscope Precession Axis in the $X_b Y_b$ Plane	77
Fig. 4-3 Gyroscope Precession Axis in the $X_b Z_b$ Plane	77
Fig. 4-4 Gyroscope Precession Axis in the $Y_b Z_b$ Plane	79
Fig. 4-5 Gyroscope Precession Axis Along the $X_b$ Axis	79
Fig. 4-6 Gyroscope Precession Axis Along the $Y_b$ Axis	81
Fig. 4-7 Gyroscope Precession Axis Along the $Z_b$ Axis	81
<b>Chapter VI</b>	
Fig. 6-1 Configuration Employing Gyroscopes with Precession Axes Along $X_b$ and $Z_b$	92
Fig. 6-2 "V" Configuration in the $X_b Y_b$ Plane	96
Fig. 6-3 Configuration Employing a Single Gyroscope	101
<b>Appendix A</b>	
Fig. A-1 System of Particles	106
<b>Appendix B</b>	
Fig. B-1 Single Degree of Freedom Gyroscope	111
<b>Appendix C</b>	
Fig. C-1 An Arbitrary Shaped Orbiting Vehicle	115

### Nomenclature

$X, Y, Z$	geocentric reference coordinate system.
$i, j, k$	unit vectors along the $X, Y, Z$ reference coordinate axes.
$\left[ \begin{matrix} \phantom{x} \\ \phantom{y} \\ \phantom{z} \end{matrix} \right]_x, \left[ \begin{matrix} \phantom{x} \\ \phantom{y} \\ \phantom{z} \end{matrix} \right]_y, \left[ \begin{matrix} \phantom{x} \\ \phantom{y} \\ \phantom{z} \end{matrix} \right]_z$	components along the $X, Y, Z$ reference coordinate axes.
$X_b, Y_b, Z_b$	body fixed coordinate system along the body principal axes.
$i_b, j_b, k_b$	unit vectors along the $X_b, Y_b, Z_b$ body axes.
$\left[ \begin{matrix} \phantom{x} \\ \phantom{y} \\ \phantom{z} \end{matrix} \right]_{i_b}, \left[ \begin{matrix} \phantom{x} \\ \phantom{y} \\ \phantom{z} \end{matrix} \right]_{j_b}, \left[ \begin{matrix} \phantom{x} \\ \phantom{y} \\ \phantom{z} \end{matrix} \right]_{k_b}$	components along the $X_b, Y_b, Z_b$ body axes.
$X_g, Y_g, Z_g$	gyroscope fixed coordinate system along the gyroscope principal axes.
$i_g, j_g, k_g$	unit vectors along the $X_g, Y_g, Z_g$ gyroscope axes.
$\left[ \begin{matrix} \phantom{x} \\ \phantom{y} \\ \phantom{z} \end{matrix} \right]_{i_g}, \left[ \begin{matrix} \phantom{x} \\ \phantom{y} \\ \phantom{z} \end{matrix} \right]_{j_g}, \left[ \begin{matrix} \phantom{x} \\ \phantom{y} \\ \phantom{z} \end{matrix} \right]_{k_g}$	components along the $X_g, Y_g, Z_g$ gyroscope axes.
$T$	total torque on the body.
$T_d$	total torque on the body less the differential gravity torque.
$T_{dg}$	differential gravity torque on the body.
$T_e$	external torque applied to the body less the differential gravity torque.
$T_g$	torque on the gyroscope
$I_{x_b}, I_{y_b}, I_{z_b}$	polar moments of inertia of the body about the $X_b, Y_b, Z_b$ axes of the body.
$I_g$	polar moment of inertia of a symmetrical gyroscope.
$H_r$	angular momentum of the gyroscope rotor.
$\Omega$	angular velocity of the reference coordinate system with respect to inertial space.
$\omega_b$	angular velocity of the body with respect to inertial space.
$\omega_g$	angular velocity of the gyroscope with respect to inertial space.
$\theta_x, \theta_y, \theta_z$	set of Eulerian angles relating the reference coordinate system to the body coordinate system.
$\phi_x, \phi_y, \phi_z$	set of Eulerian angles relating the body coordinate system to the gyroscope coordinate system.
$\left[ \begin{matrix} \phantom{x} \\ \phantom{y} \\ \phantom{z} \end{matrix} \right]', \left[ \begin{matrix} \phantom{x} \\ \phantom{y} \\ \phantom{z} \end{matrix} \right]''$	first and second derivatives with respect to time.

Appendix A	-	Derivation of Euler's Equations	Page 106
Appendix B	-	Derivation of Gyroscope Equations	110
Appendix C	-	Derivation of Gravity Gradient Torque	114
Reference			

## Chapter I - INTRODUCTION

There are numerous applications which require a particular axis of a satellite vehicle to be oriented in some specific direction. The need for space vehicle attitude control and stabilization can only be appreciated when consideration is given to the mission that the vehicle is to perform. For example, conversion of solar energy to electrical energy will require solar energy gathering devices which must, by necessity, be oriented toward the sun. Midcourse maneuvers requiring the firing of rocket engines would also require vehicle attitude control to give the proper direction to the thrust. As the satellite moves in orbit around the earth, it might be desired to obtain weather information or obtain surveillance information over enemy territory. The latter applications require a camera to be so oriented that its axis is aligned with the geocentric vertical of the earth.

The various sources of attitude disturbance torques for a vehicle orbiting the earth are worthy of consideration. A brief discussion of disturbance torques is given below:

### a) Aerodynamic Torque

At an altitude of about 500 miles a very sparse atmosphere exists. Nevertheless, the torque produced by aerodynamic drag can be significant. This would be particularly true if the space vehicle was to employ large solar energy collecting panels where the location of the center of aerodynamic pressure might not coincide with the center of mass of the vehicle. The torque produced is a function of the angle of attack of the vehicle and for a constant angle of attack and a circular orbit, the torque produced will be constant.

At an altitude of about 500 miles, the dynamic pressure is approximately  $6 \times 10^{-5}$  dyne/cm<sup>2</sup>. For a space vehicle employing flat solar energy collecting panels, 100 feet<sup>2</sup> in area, with a 2.5 inch offset of the center of aerodynamic pressure from the mass center of the vehicle, a disturbance torque of approximately 56 dyne-cm. will result for the worst angle of attack.<sup>1</sup>

### b) Solar Radiation Pressure

Solar radiation pressure is caused by the impact of photons with the surface of the vehicle. As in the case of aerodynamic drag, torques produced can be significant if large solar energy collecting panels are utilized and if the center of solar radiation pressure does not coincide with the mass center of the vehicle. The torque produced would be periodic; the period being the time of one orbital revolution.

For a satellite employing flat solar energy collecting panels, 100 feet<sup>2</sup> in area, with a 2.5 inch offset from the mass center, a torque of approximately 60 dyne-cm can be produced.<sup>1</sup>

**(c) Earth's Magnetic Field**

There are two primary sources of torque resulting from the interaction with the earth's magnetic field. The first is produced by interaction with the current loops and ferromagnetic material in the vehicle and the second is produced by eddy currents set up by motion of electrically conducting parts of the vehicle relative to the magnetic field. The latter becomes more prevalent as the angular velocity of the vehicle increases. The torque produced depends heavily on the design, altitude and latitude of the vehicle. If large current loops are avoided and nonmagnetic materials are used whenever possible, the torque can be kept to the order of 10 dyne-cm. As in the previous case, the torque produced is periodic.<sup>1</sup>

**(d) Internal Moving Parts**

There is an angular momentum associated with every moving part in the vehicle. The variation of angular velocity of tape recorder reels or any rotating machinery causes a change of angular momentum with respect to inertial space. This in turn produces a reaction torque which is exerted on the vehicle.

**(e) Meteorite Impacts**

Meteorite impacts will produce a torque on the vehicle. The magnitude of this torque will vary in accordance with the kinetic energy of the meteorites and the location of impact. The time average of the resultant torque is of statistical nature.

**(f) Gravity Gradient (Differential Gravity)**

A portion of the vehicle a small distance nearer the earth than another part will experience a slightly larger gravitational force. Depending on the vehicle attitude and geometry, a resultant torque might be produced. The magnitude of this torque will decrease as the altitude of the satellite is increased.

There are a number of basic methods which can be utilized to obtain attitude control. These include:

**(i) Mass Expulsion**

This method utilizes familiar rocket principles for the generation of attitude control torques. Reaction jets are provided and a propellant is stored within the vehicle. This type of system is good for intermittent large angle corrections. Applications of this system are limited since the propellant is exhaustable.

**(ii) Momentum Exchange Within the Vehicle**

This method utilizes the motion of internal parts to provide torques. Externally applied torques can be countered by changing the angular momentum of internally mounted gyroscopes or inertia wheels.

(iii) Interaction with the Environment

This method utilizes prevailing environmental conditions to provide torques. A classic example is the stabilization of aircraft using atmospheric drag. Satellites operating above an altitude of a few hundred miles do not experience enough atmospheric drag to be utilized effectively as a means of stabilization. However, since gravity gradient torques tend to align the axis of least inertia along the geocentric vertical, it can effectively be utilized in controlling the orientation of the vehicle.

The system with which this report is concerned, utilizes gravity gradient torques to control the vehicle's orientation and gyroscopes to provide vehicle damping. Several different gyroscope configurations, utilizing single degree of freedom gyroscopes are considered, and for these configurations the equations governing the statics and dynamics of the system are systematically developed.

This report is subdivided in the following manner: In Chapter II the dynamics of a rigid body orbiting the earth are developed in terms of the attitude deviation angles and the parameters of the orbit. Chapter III presents a simplified analysis of gyroscope damping. In Chapter IV, the dynamics of a gyroscope constrained within a satellite are developed; the equations are obtained in terms of satellite attitude deviation angles, orbit parameters, and the gyroscope precession angle. The equation of constraint, relating the gyroscope precession angle to the satellite deviation angles is also developed. In Chapter V, steady state requirements for an orbiting vehicle with internally mounted gyroscopes are considered. The equations obtained in Chapters II, IV and V are combined in Chapter VI to obtain the dynamics of an orbiting vehicle for various gyroscope configurations.

1

See reference 14 .

## Chapter II - SATELLITE ATTITUDE DYNAMICS

### A) Reference Coordinate System

In order to develop a set of equations suitable for the dynamic analysis of a given system, it is necessary to introduce a coordinate reference for that system. For the problem of attitude control, it is necessary to define a coordinate reference system from which attitude deviations can be measured. For geocentric attitude control it is desirable for the reference coordinate system to be chosen coincident with the desired orientation of the satellite. The desired orientation of the vehicle is determined by the instantaneous geocentric vertical, therefore the reference coordinate system is not fixed and will in general be a variable angular velocity system. With this choice of reference coordinate system, it will be possible to linearize the resulting equations for small angular deviations. ( $\cos \theta = 1$ ,  $\sin \theta = \theta$ ). Indeed, for large angular deviations these approximations cannot be made and the resulting equations of motion will contain nonlinear trigonometric terms.

The reference coordinate system used (which will be denoted by  $X, Y, Z$ ) is shown for an arbitrary position in the orbit. (See Figure 2-1.) The  $Z$  axis is taken along the instantaneous geocentric vertical positive outward. The  $X$  axis is chosen tangential to the orbit and in the general direction of the orbital velocity of the vehicle. The  $Y$  axis is chosen perpendicular to the plane of the orbit, in the direction of the orbital momentum, such that a right-handed system is formed. This system is both translating and rotating with respect to inertial space. It should be noted that the  $X$  axis does not coincide with the direction of the velocity vector of the vehicle for an elliptical orbit.

### B) Body Coordinate System

It is also necessary to define a coordinate system which is fixed with respect to the satellite and which is to be controlled to coincide with the reference coordinate system. It is advantageous to choose the body fixed coordinate system to coincide with the principal axes of the vehicle. This eliminates all product of inertia terms and hence simplifies the differential equations of motion. (The inertia tensor is then diagonal; see Appendix A). This choice of body fixed axes reduces the generality of the results, since it now requires that the control axes be principal axes of the body. Since most satellite vehicles have some sort of symmetry, this reduction in generality is not serious. It is further assumed that the satellite is a rigid body. This is not strictly true due to motion of its internal components (such as tape recorders and gyroscopes). If the mass of such internal components is small in comparison with the overall vehicle mass, then these effects can be neglected.

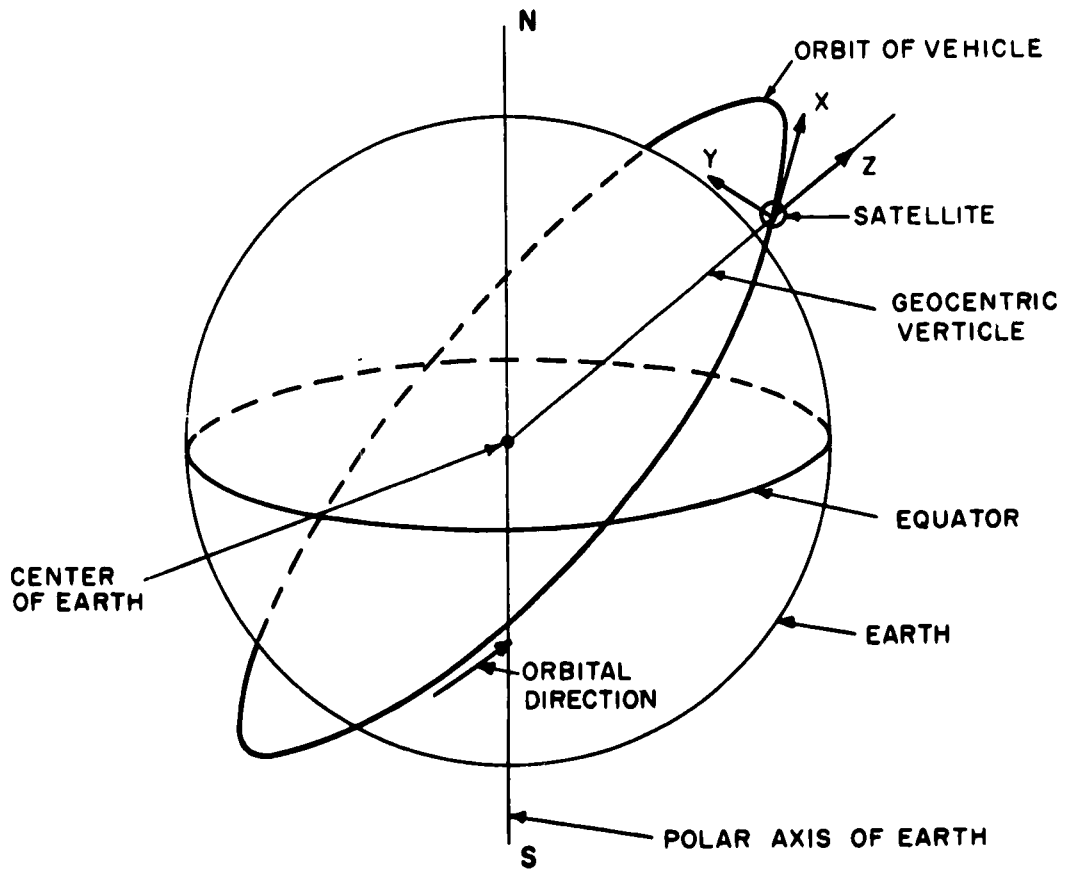


Fig. 2-1 Satellite Reference Coordinate System



It can therefore be assumed that the principal axes are fixed in the satellite. The coordinate system formed by the body principal axes is denoted by  $X_b$ ,  $Y_b$ , and  $Z_b$ .

### C) The Eulerian Angles and Transformation Matrix

The body principal axes can be related to the reference coordinate system by an array of Eulerian angles;  $\theta_x$ ,  $\theta_y$ ,  $\theta_z$ . These angles are defined by successive rotations of the body axes through the angles  $\theta_x$ ,  $\theta_y$  and  $\theta_z$  about the  $X_b$ ,  $Y_b$ ,  $Z_b$  body axes respectively which rotate the vehicle from its reference system into its present position. (see Fig. 2-2). These angles will be taken as positive when the sense of the rotation is equivalent to that of a right-handed screw advancing in the direction of the axis of rotation. Figure 2-2 shows the three successive rotations and their corresponding transformation matrices. Viewing the position vectors as column matrices, the transformation matrix gives the new coordinate system as the product of the transformation matrix and the old coordinate system.

$$\begin{pmatrix} X_b \\ Y_b \\ Z_b \end{pmatrix} = \begin{pmatrix} & & \\ & A & \\ & & \end{pmatrix} \begin{pmatrix} X \\ Y \\ Z \end{pmatrix} \quad (2.1)$$

The overall transformation matrix relating the components of a vector in the X Y Z system to the components of the same vector in the  $X_b$   $Y_b$   $Z_b$  system is given by

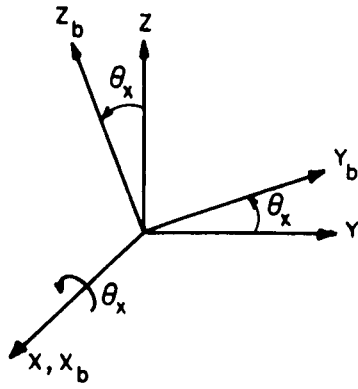
$$A = (A_z) (A_y) (A_x) \quad (2.2)$$

$$A = \begin{pmatrix} \cos \theta_y \cos \theta_z & \begin{bmatrix} \sin \theta_y \sin \theta_x \cos \theta_z \\ + \cos \theta_x \sin \theta_z \end{bmatrix} & \begin{bmatrix} -\cos \theta_x \sin \theta_y \cos \theta_z \\ + \sin \theta_x \sin \theta_z \end{bmatrix} \\ -\cos \theta_y \sin \theta_z & \begin{bmatrix} -\sin \theta_x \sin \theta_y \sin \theta_z \\ + \cos \theta_x \cos \theta_z \end{bmatrix} & \begin{bmatrix} \cos \theta_x \sin \theta_y \sin \theta_z \\ + \sin \theta_x \cos \theta_z \end{bmatrix} \\ \sin \theta_y & -\sin \theta_x \cos \theta_y & \cos \theta_x \cos \theta_y \end{pmatrix} \quad (2.3)$$

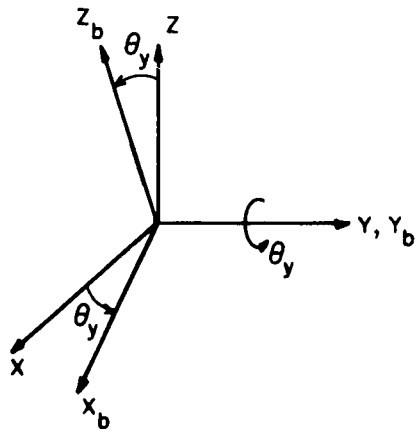
The matrix multiplications are not commutative and therefore must be performed in the order indicated. The physical significance of the non-commutability of the matrix product, is that the order of the rotations cannot be interchanged and must be performed as indicated.

If the deviation angles are small ( $\sin \theta = \theta$ ,  $\cos \theta = 1$ ) the transformation matrix (2.3) becomes

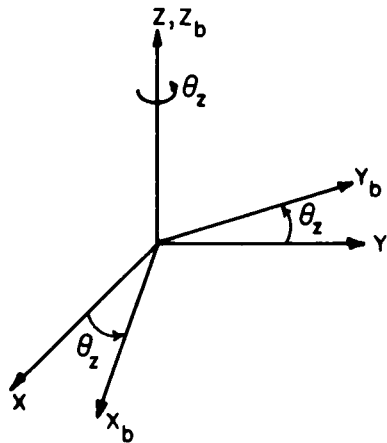
$$A = \begin{pmatrix} 1 & \theta_x \theta_y + \theta_z & -\theta_y + \theta_x \theta_z \\ -\theta_z & -\theta_x \theta_y \theta_z + 1 & \theta_y \theta_z + \theta_x \\ \theta_y & -\theta_x & 1 \end{pmatrix} \quad (2.4)$$



$$\begin{pmatrix} i_b \\ j_b \\ k_b \end{pmatrix} = \underbrace{\begin{pmatrix} 1 & 0 & 0 \\ 0 & \cos \theta_x & \sin \theta_x \\ 0 & -\sin \theta_x & \cos \theta_x \end{pmatrix}}_{A_x} \begin{pmatrix} i \\ j \\ k \end{pmatrix}$$



$$\begin{pmatrix} i_b \\ j_b \\ k_b \end{pmatrix} = \underbrace{\begin{pmatrix} \cos \theta_y & 0 & -\sin \theta_y \\ 0 & 1 & 0 \\ \sin \theta_y & 0 & \cos \theta_y \end{pmatrix}}_{A_y} \begin{pmatrix} i \\ j \\ k \end{pmatrix}$$



$$\begin{pmatrix} i_b \\ j_b \\ k_b \end{pmatrix} = \underbrace{\begin{pmatrix} \cos \theta_z & \sin \theta_z & 0 \\ -\sin \theta_z & \cos \theta_z & 0 \\ 0 & 0 & 1 \end{pmatrix}}_{A_z} \begin{pmatrix} i \\ j \\ k \end{pmatrix}$$

Fig. 2-2 Eulerian Angles

Upon further assuming that the product of two small angles can be neglected compared to a single angle, one obtains

$$A = \begin{pmatrix} 1 & \theta_z & -\theta_y \\ -\theta_z & 1 & \theta_x \\ \theta_y & -\theta_x & 1 \end{pmatrix} \quad (2.5)$$

#### D) Development of Equations of Motion of the Body

The equations of motion of a rigid body in three dimensional space is given by Euler's equations. (A24, A25, A26). A derivation of these equations is given in appendix A .

$$T_{i_b} = I_{x_b} \dot{\omega}_{b_{i_b}} + (I_{z_b} - I_{y_b}) \omega_{b_{j_b}} \omega_{b_{k_b}} \quad (2.6)$$

$$T_{j_b} = I_{y_b} \dot{\omega}_{b_{j_b}} + (I_{x_b} - I_{z_b}) \omega_{b_{i_b}} \omega_{b_{k_b}} \quad (2.7)$$

$$T_{k_b} = I_{z_b} \dot{\omega}_{b_{k_b}} + (I_{y_b} - I_{x_b}) \omega_{b_{j_b}} \omega_{b_{i_b}} \quad (2.8)$$

where  $I_{x_b}, I_{y_b}, I_{z_b}$  are the moments of inertia about the  $X_b, Y_b, Z_b$  principal axes of the body.

$\omega_{b_{i_b}}, \omega_{b_{j_b}}, \omega_{b_{k_b}}$  are the  $X_b, Y_b, Z_b$  components of the angular velocity of the body relative to inertial space.

$T_{i_b}, T_{j_b}, T_{k_b}$  are the  $X_b, Y_b, Z_b$  components of the torque taken about the mass center of the body.

In order to adapt Euler's equations to the problem of attitude control, it is necessary to express the angular velocities ( $\omega_{b_{i_b}}, \omega_{b_{j_b}}, \omega_{b_{k_b}}$ ) and their derivatives ( $\dot{\omega}_{b_{i_b}}, \dot{\omega}_{b_{j_b}}, \dot{\omega}_{b_{k_b}}$ ) in terms of the deviation angles ( $\theta_x, \theta_y, \theta_z$ ) and the angular velocity of the reference system. The angular velocity of the body with respect to inertial space is given as the vector sum of the angular velocity of the vehicle with respect to the reference frame and the angular velocity of the reference frame relative to inertial space.

$$\omega_{b / \text{inertial space}} = \omega_{b / \text{reference frame}} + \omega_{\text{reference frame} / \text{inertial space}} \quad (2.9)$$

The angular velocity of the body relative to the reference frame, is given by

$$\omega_{b / \text{reference frame}} = \dot{\theta}_x i_b + \dot{\theta}_y j_b + \dot{\theta}_z k_b \quad (2.10)$$

The angular velocity of the reference frame with respect to inertial space is given by

$$\omega_{\text{ref/inertial space}} = \Omega_x i + \Omega_y j + \Omega_z k \quad (2.11)$$

where  $\Omega_x, \Omega_y, \Omega_z$  are the components of the angular velocity of the reference frame with respect to inertial space along the X, Y, Z axes of the reference system respectively,

Using the transformation matrix (2.5), the angular velocity of the reference system can be expressed in terms of the body coordinates.

$$\begin{pmatrix} \Omega_{i_b} \\ \Omega_{j_b} \\ \Omega_{k_b} \end{pmatrix} = \begin{pmatrix} 1 & \theta_z & -\theta_y \\ -\theta_z & 1 & \theta_x \\ \theta_y & -\theta_x & 1 \end{pmatrix} \begin{pmatrix} \Omega_x \\ \Omega_y \\ \Omega_z \end{pmatrix} \quad (2.12)$$

$$\begin{aligned} \omega_{\text{ref}} = & [\Omega_x + \theta_z \Omega_y - \theta_y \Omega_z] i_b + [-\theta_z \Omega_x + \Omega_y + \theta_x \Omega_z] j_b \\ & + [\theta_y \Omega_x - \theta_x \Omega_y + \Omega_z] k_b \end{aligned} \quad (2.13)$$

Addition of Equations (2.10) and (2.13), and separation into components yields the following equations for the components of the angular velocities and their derivatives along the body axes.

$$\omega_{b_{i_b}} = \dot{\theta}_x + \Omega_x + \theta_z \dot{\Omega}_y - \theta_y \dot{\Omega}_z \quad (2.14)$$

$$\omega_{b_{j_b}} = \dot{\theta}_y + \Omega_y + \theta_x \dot{\Omega}_z - \theta_z \dot{\Omega}_x \quad (2.15)$$

$$\omega_{b_{k_b}} = \dot{\theta}_z + \Omega_z + \theta_y \dot{\Omega}_x - \theta_x \dot{\Omega}_y \quad (2.16)$$

$$\dot{\omega}_{b_{i_b}} = \ddot{\theta}_x + \dot{\Omega}_x + \theta_z \ddot{\Omega}_y + \dot{\theta}_z \dot{\Omega}_y - \theta_y \ddot{\Omega}_z - \dot{\theta}_y \dot{\Omega}_z \quad (2.17)$$

$$\dot{\omega}_{b_{j_b}} = \ddot{\theta}_y + \dot{\Omega}_y + \theta_x \ddot{\Omega}_z + \dot{\theta}_x \dot{\Omega}_z - \theta_z \ddot{\Omega}_x - \dot{\theta}_z \dot{\Omega}_x \quad (2.18)$$

$$\dot{\omega}_{b_{k_b}} = \ddot{\theta}_z + \dot{\Omega}_z + \theta_y \ddot{\Omega}_x + \dot{\theta}_y \dot{\Omega}_x - \theta_x \ddot{\Omega}_y - \dot{\theta}_x \dot{\Omega}_y \quad (2.19)$$

Substituting these results into Euler's equations (2.6, 2.7, 2.8) yields:

$$\begin{aligned}
 T_{i_b} = I_{x_b} & \left[ \ddot{\theta}_x + \dot{\Omega}_x + \theta_z \ddot{\Omega}_y + \dot{\theta}_z \dot{\Omega}_y - \theta_y \dot{\Omega}_z - \dot{\theta}_y \dot{\Omega}_z \right] \\
 & + (I_{z_b} - I_{y_b}) \left[ \dot{\theta}_y \dot{\theta}_z + \dot{\theta}_y \dot{\Omega}_z + \theta_x \dot{\theta}_y \dot{\Omega}_y + \theta_y \dot{\theta}_y \dot{\Omega}_x + \dot{\theta}_z \dot{\Omega}_y \right. \\
 & + \dot{\Omega}_y \dot{\Omega}_z - \theta_x \dot{\Omega}_y^2 + \theta_y \dot{\Omega}_x \dot{\Omega}_y - \theta_z \dot{\theta}_z \dot{\Omega}_x - \theta_z \dot{\Omega}_x \dot{\Omega}_z \\
 & + \theta_x \theta_z \dot{\Omega}_x \dot{\Omega}_y - \theta_y \theta_z \dot{\Omega}_x^2 + \theta_x \dot{\theta}_z \dot{\Omega}_z + \theta_x \dot{\Omega}_z^2 - \theta_x^2 \dot{\Omega}_y \dot{\Omega}_z \\
 & \left. + \theta_x \theta_y \dot{\Omega}_x \dot{\Omega}_z \right] \quad (2.20)
 \end{aligned}$$

$$\begin{aligned}
 T_{j_b} = I_{y_b} & \left[ \ddot{\theta}_y + \dot{\Omega}_y - \theta_z \dot{\Omega}_x - \dot{\theta}_z \dot{\Omega}_x + \theta_x \dot{\Omega}_z + \dot{\theta}_x \dot{\Omega}_z \right] \\
 & + (I_{x_b} - I_{z_b}) \left[ \dot{\theta}_x \dot{\theta}_z + \dot{\theta}_x \dot{\Omega}_z - \theta_x \dot{\theta}_x \dot{\Omega}_y + \theta_y \dot{\theta}_x \dot{\Omega}_x + \dot{\theta}_z \dot{\Omega}_x \right. \\
 & + \dot{\Omega}_x \dot{\Omega}_z - \theta_x \dot{\Omega}_x \dot{\Omega}_y + \theta_y \dot{\Omega}_x^2 + \theta_z \dot{\theta}_z \dot{\Omega}_y + \theta_z \dot{\Omega}_y \dot{\Omega}_z \\
 & - \theta_x \theta_z \dot{\Omega}_y^2 + \theta_y \theta_z \dot{\Omega}_x \dot{\Omega}_y - \theta_y \dot{\theta}_z \dot{\Omega}_z - \theta_y \dot{\Omega}_z^2 - \theta_y^2 \dot{\Omega}_x \dot{\Omega}_z \\
 & \left. + \theta_x \theta_y \dot{\Omega}_y \dot{\Omega}_z \right] \quad (2.21)
 \end{aligned}$$

$$\begin{aligned}
 T_{k_b} = I_{z_b} & \left[ \ddot{\theta}_z - \dot{\Omega}_z - \theta_x \dot{\Omega}_y - \dot{\theta}_x \dot{\Omega}_y + \theta_y \dot{\Omega}_x + \dot{\theta}_y \dot{\Omega}_x \right] \\
 & + (I_{y_b} - I_{x_b}) \left[ \dot{\theta}_x \dot{\theta}_y + \dot{\theta}_x \dot{\Omega}_y - \dot{\theta}_x \theta_z \dot{\Omega}_x + \theta_x \dot{\theta}_x \dot{\Omega}_z + \dot{\theta}_y \dot{\Omega}_x \right. \\
 & + \dot{\Omega}_x \dot{\Omega}_y - \theta_z \dot{\Omega}_x^2 + \theta_x \dot{\Omega}_x \dot{\Omega}_z + \theta_z \dot{\theta}_z \dot{\Omega}_y + \theta_z \dot{\Omega}_y^2 \\
 & - \theta_z^2 \dot{\Omega}_x \dot{\Omega}_y + \theta_x \theta_z \dot{\Omega}_y \dot{\Omega}_z - \theta_y \dot{\theta}_y \dot{\Omega}_z - \theta_y \dot{\Omega}_y \dot{\Omega}_z \\
 & \left. + \theta_y \theta_z \dot{\Omega}_y \dot{\Omega}_z - \theta_x \theta_y \dot{\Omega}_z^2 \right] \quad (2.22)
 \end{aligned}$$

where  $T_{i_b}$ ,  $T_{j_b}$ ,  $T_{k_b}$  are the components of torque about the center of gravity of the vehicle along  $X_b$ ,  $Y_b$  and  $Z_b$  respectively.

The above equations are valid under the following assumptions:

a) Inertia of internal moving parts of the body are negligible. -  
This assumption is necessary to allow the system to be treated as a rigid body.

b) The fixed body axes coincide with the principal axes. -  
This assumption made the inertia tensor diagonal (see eq. A.21).

c) Small angular deviations. -  
This assumption is utilized in the derivation of the transformation matrix (2.5).

In order to specialize these equations for the problem of attitude control, it is necessary to obtain an expression for the components of the reference system angular

velocity ( $\Omega_x, \Omega_y, \Omega_z$ ). If the earth were a perfect homogeneous sphere, and if the only force acting on the satellite was the earth's gravity, the satellite orbit would be an ellipse whose spatial plane and major axis would be fixed in inertial space. Under these conditions,  $\Omega_x$  and  $\Omega_z$  would be zero and  $\Omega_y$  would be equal to the orbital angular velocity (sometimes referred to as the pitch over rate) predicted by Kepler's laws of planetary motion. There are several perturbations which act on the orbit and change  $\Omega_x, \Omega_y$  and  $\Omega_z$  from these idealized values. They are listed below:

- a) The earth is not a perfect sphere but is closer to an oblate spheroid.
- b) The earth is not homogeneous.
- c) Atmospheric drag.
- d) Gravitational attraction of the moon, sun and other planets.
- e) Electromagnetic forces caused by the satellite's motion through the earth's magnetic field.
- f) Collision with meteorites and other particles.

The changes in angular velocity produced by the perturbations discussed above are several orders of magnitude less than the orbital angular velocity which is in the order of  $10^{-3}$  rad/sec. These perturbations therefore have a negligible effect in the equations of motion when compared to terms containing  $\Omega_y$ . As a result,  $\Omega_x$  and  $\Omega_z$  are considered to be zero in the equations of motion. It is further assumed that there is no time average force acting on the vehicle, since such a force would cause the plane of the orbit to become time varying.

Setting  $\dot{\Omega}_x = \dot{\Omega}_z = \dot{\Omega}_y = 0$  in the torque equations (2.20, 2.21, 2.22) yield:

$$T_{i_b} = I_{x_b} \left[ \ddot{\theta}_x + \theta_z \dot{\Omega}_y + \dot{\theta}_z \Omega_y \right] + (I_{z_b} - I_{y_b}) \left[ \dot{\theta}_y \dot{\theta}_z + \theta_x \dot{\theta}_y \Omega_y + \dot{\theta}_z \Omega_y - \theta_x \Omega_y^2 \right] \quad (2.23)$$

$$T_{j_b} = I_{y_b} \left[ \ddot{\theta}_y + \dot{\Omega}_y \right] + (I_{x_b} - I_{z_b}) \left[ \dot{\theta}_x \dot{\theta}_z - \theta_x \dot{\theta}_x \Omega_y + \theta_z \dot{\theta}_z \Omega_y - \theta_x \theta_z \Omega_y^2 \right] \quad (2.24)$$

$$T_{k_b} = I_{z_b} \left[ \ddot{\theta}_z - \theta_x \dot{\Omega}_y - \dot{\theta}_x \Omega_y \right] + (I_{y_b} - I_{x_b}) \left[ \dot{\theta}_x \dot{\theta}_y + \dot{\theta}_x \Omega_y + \theta_z \dot{\theta}_y \Omega_y + \theta_z \Omega_y^2 \right] \quad (2.25)$$

Further simplification of Eqs. (2.23), (2.24), (2.25) can be obtained if the order of magnitude of the various terms is estimated.

- 1)  $\Omega_y$  is taken to be  $10^{-3}$  rad/sec. This corresponds roughly to a ninety minute, 400 mile high circular orbit.
- 2) An estimate of the angular acceleration can be obtained from a simple example. Consider a 1000 pound drum shaped satellite (see Fig. 2-3) which is 4 feet in length and 4 feet in diameter

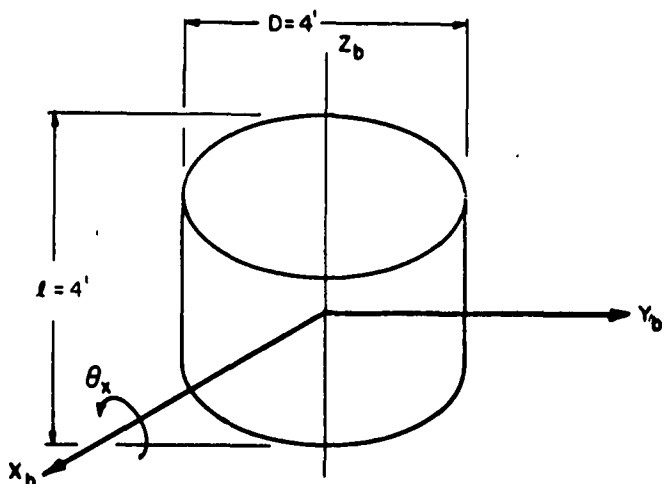


Fig. 2-3 Drum Shaped Satellite

For a cylindrical satellite

$$I_{x_b} = I_{y_b} = \frac{m}{12} (l^2 + 3R^2) \quad (2.26)$$

$$I_{z_b} = \frac{1}{2} mR^2 \quad (2.27)$$

Where  $I_{x_b}$ ,  $I_{y_b}$  and  $I_{z_b}$  are the polar moments of inertia about the  $X_b$ ,  $Y_b$  and  $Z_b$  axes of the body.

$m$  is the mass of the satellite in slugs.

$l$  is the length of the satellite in feet.

$R$  is the radius of the satellite in feet.

Calculation of the moments of inertia yields:

$$I_{x_b} = I_{y_b} = 72.5 \text{ slug} \cdot \text{ft.}^2 \quad (2.28)$$

$$I_{z_b} = 62.2 \text{ slug} \cdot \text{ft.}^2 \quad (2.29)$$

It will be assumed that a sinusoidal disturbance torque of amplitude 80 dyne - cm is applied to the vehicle with a radian frequency of  $\Omega_y$  ( $10^{-3}$  rad/sec) about its  $Z_b$  axis.

$$T_{d_{k_b}} = 80 \sin 10^{-3} t \text{ dyne-cm} \quad (2.30)$$

Converting to ft. - lbs. yields:

$$T_{d_{k_b}} = 5.9 \times 10^{-6} \sin 10^{-3} t \text{ ft} \cdot \text{lbs.} \quad (2.31)$$

Assume for the purpose of estimation that the elementary equation

$$T_{d_{k_b}} = I_{z_b} \ddot{\theta}_z \quad (2.32)$$

applies.

Therefore the angular acceleration is given by

$$\ddot{\theta}_z = \frac{T_{d_{k_b}}}{I_{z_b}} = 0.94 \times 10^{-7} \sin 10^{-3} t \frac{\text{rad}}{\text{sec}^2} \quad (2.33)$$

The maximum value of the angular acceleration about all the axes is seen to be about  $10^{-7}$  rad/sec<sup>2</sup>

$$\ddot{\theta}_x = \ddot{\theta}_y = \ddot{\theta}_z = 10^{-7} \frac{\text{rad}}{\text{sec}^2} \quad (2.34)$$

3) An estimate of the angular velocities and angular deviations can be obtained by integration. Integrating to obtain the angular velocity and deviation, one obtains

$$\dot{\theta} = -10^{-4} \cos 10^{-3} t \quad (2.35)$$

$$\theta = -10^{-1} \sin 10^{-3} t \quad (2.36)$$

Therefore the estimate for the maximum value of the angular velocity will be  $10^{-4}$  rad/sec.

$$\dot{\theta}_x = \dot{\theta}_y = \dot{\theta}_z = 10^{-4} \text{ rad/sec} \quad (2.37)$$

and the estimate for the maximum value of the angular deviation will be 0.1 rad

$$\theta_x = \theta_y = \theta_z = 0.1 \text{ rad} \quad (2.38)$$



The effect of damping on the vehicle will cause these values to be smaller than those used for the estimations.

Substituting the estimated values into equations (2.23), (2.24) and (2.25) and deleting the negligible terms, (a term will be considered negligible if it is at least one order of magnitude smaller than the other terms), yields the final set of equations of motion for a body in a general elliptical and planar orbit.

$$T_{i_b} = I_{x_b} [\ddot{\theta}_x + \theta_z \dot{\Omega}_y + \dot{\theta}_y \Omega_y] + (I_{z_b} - I_{y_b}) [\dot{\theta}_z \Omega_y - \theta_x \Omega_y^2] \quad (2.39)$$

$$T_{j_b} = I_{y_b} [\ddot{\theta}_y + \dot{\Omega}_y] + (I_{x_b} - I_{z_b}) [\dot{\theta}_x \dot{\theta}_z - \theta_x \dot{\theta}_x \Omega_y + \theta_z \dot{\theta}_z \Omega_y - \theta_x \theta_z \Omega_y^2] \quad (2.40)$$

$$T_{k_b} = I_{z_b} [\ddot{\theta}_z - \theta_x \dot{\Omega}_y - \dot{\theta}_x \Omega_y] + (I_{y_b} - I_{x_b}) [\dot{\theta}_x \Omega_y + \theta_z \Omega_y^2] \quad (2.41)$$

E) Inclusion of the Gravity Gradient Torque

It is essential to understand that the left side of equations (2.39), (2.40) and (2.41) represent the components of the total external torques applied to the body.

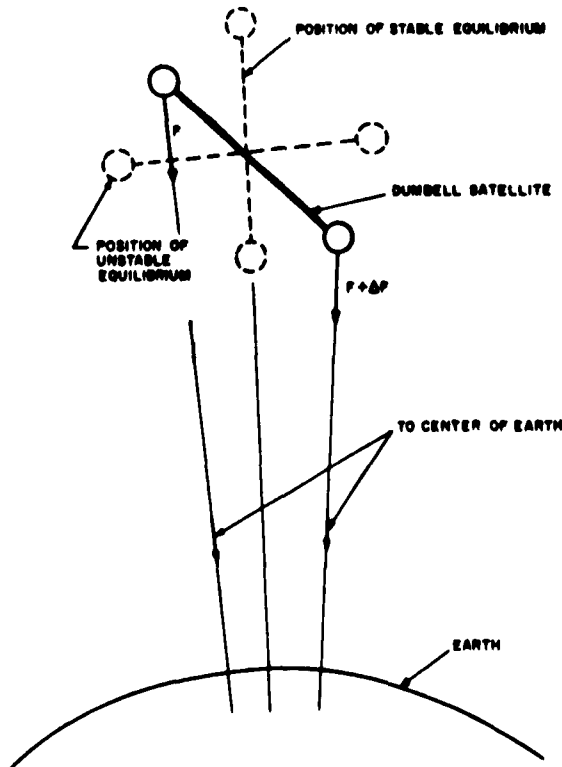


Fig. 2-4 Mechanism of Differential Gravity Torque

In general, the total external torque applied to the vehicle is composed of disturbance torques and control torques. It is advantageous to explicitly include the expressions for the control torques so that the only torque appearing on the left side of the equations are the true disturbance torques.

Differential gravity is a possible source of a control torque. The mechanism, by which differential gravity can be utilized to provide a control torque, can be qualitatively demonstrated with the aid of the following simple example:

Consider the dumbbell shaped vehicle as shown in Fig. 2-4. The difference in force acting at its ends will cause a small torque tending to align the longitudinal axis of the vehicle along the geocentric vertical. As the satellite orbits the earth a torque is thereby produced tending to keep the satellite so aligned. The positions of stable and un-stable equilibrium are also shown in Fig. 2-4. It is of cardinal importance to realize that differential gravity alone can be used as a mechanism for keeping an axis of the satellite aligned in the general direction of the earth. Without damping however, the poles of the system will lie on the imaginary axis and therefore a disturbance torque will cause the vehicle to oscillate.

A derivation for the differential gravity torque, for a sufficiently general body, is given in Appendix C. The results of the derivation are repeated here for convenience. For an elliptical orbit

$$T_{dg} = \frac{3 g_s R_c^2}{\rho_o^3} \left[ i_b \theta_x (I_{z_b} - I_{y_b}) + j_b \theta_y (I_{z_b} - I_{x_b}) \right] \quad (C22)$$

and for a circular orbit

$$T_{dg} = 3\Omega_y^2 \left[ i_b \theta_x (I_{z_b} - I_{y_b}) + j_b \theta_y (I_{z_b} - I_{x_b}) \right] \quad (C23)$$

It is immediately seen from these equations that the component of the gravity gradient torque about the  $Z_b$  axis of the body is zero. Therefore, differential gravity cannot be used to prevent drift about the  $Z_b$  body axis. It is seen from either equation (C22) or (C23) that differential gravity introduces a component of torque on both the  $X_b$  and  $Y_b$  axes of the body that is proportional to the displacement angle about that axis. Since the behavior of the differential gravity torque on both the  $X_b$  and  $Y_b$  axes are similar, only the component along the  $Y_b$  axis will be considered.

Two situations are of interest:

$$1) I_{x_b} < I_{z_b} \quad (2.42)$$

$$2) I_{z_b} < I_{x_b} \quad (2.43)$$

Consider case (1)

$$T_{dg_{j_b}} = + 3 \Omega_y^2 \theta_x |I_{z_b} - I_{x_b}| \quad (2.44)$$

It is seen from equation (2.44) that the differential gravity torque is in the same direction as the angular displacement. This clearly represents an unstable configuration since once a disturbance torque produces a small angular displacement, differential gravity will cause this angle to increase.

Now consider case (2)

$$T_{dg_{j_b}} = - 3 \Omega_y^2 \theta_x |I_{z_b} - I_{x_b}| \quad (2.45)$$

In this case differential gravity is in the opposite direction of the angular displacement. Hence if a disturbance torque produces an angular displacement, differential gravity will tend to restore the vehicle to its unperturbed position. For this configuration, differential gravity introduces position feedback much in the same manner as a body coupled to a spring. Therefore, it is of utmost importance that the moment of inertia about the  $Z_b$  axis of the body be less than the moments of inertia about both the  $X_b$  and  $Y_b$  axes of the body.

From equation (C 22) it is seen that the total external torque on the body is given by

$$T_{i_b} = T_{d_{i_b}} + \frac{3 g_s R_e^2}{\rho_o^3} \theta_x (I_{z_b} - I_{y_b}) \quad (2.46)$$

$$T_{j_b} = T_{d_{j_b}} + \frac{3 g_s R_e^2}{\rho_o^3} \theta_y (I_{z_b} - I_{x_b}) \quad (2.47)$$

$$T_{k_b} = T_{d_{k_b}} \quad (2.48)$$

where  $T_d$  is the total torque on the body less the differential gravity torque.

Substituting equations (2.46), (2.47) and (2.48) into equations (2.39), (2.40) and (2.41), and bringing the differential gravity terms over to the right side of the equations yields:

$$T_{d_{i_b}} = I_{x_b} \left[ \ddot{\theta}_x + \theta_z \dot{\Omega}_y + \dot{\theta}_z \Omega_y \right] + (I_{z_b} - I_{y_b}) \left[ \dot{\theta}_z \Omega_y - \theta_x (\Omega_y^2 + \frac{3g_s R_e^2}{\rho_o^3}) \right] \quad (2.49)$$

$$T_{d_{j_b}} = I_{y_b} \left[ \ddot{\theta}_y + \dot{\Omega}_y \right] + (I_{x_b} - I_{z_b}) \left[ \dot{\theta}_x \dot{\theta}_z - \theta_x \dot{\theta}_x \Omega_y + \theta_z \dot{\theta}_z \Omega_y - \theta_x \theta_z \Omega_y^2 + \frac{3g_s R_e^2}{\rho_o^3} \theta_y \right] \quad (2.50)$$

$$T_{d_{k_b}} = I_{z_b} \left[ \ddot{\theta}_z - \theta_x \dot{\Omega}_y - \dot{\theta}_x \Omega_y \right] + (I_{y_b} - I_{x_b}) \left[ \dot{\theta}_x \Omega_y + \theta_z \Omega_y^2 \right] \quad (2.51)$$

The corresponding equations of motion for a circular orbit can be obtained by setting  $\dot{\Omega}_y = 0$  and

$$\frac{3g_s R_e^2}{\rho_o^3} = 3 \Omega_y^2 \quad (C.16)$$

$$T_{d_{i_b}} = I_{x_b} \left[ \ddot{\theta}_x + \dot{\theta}_z \Omega_y \right] + (I_{z_b} - I_{y_b}) \left[ \dot{\theta}_z \Omega_y - 4 \theta_x \Omega_y^2 \right] \quad (2.52)$$

$$T_{d_{j_b}} = I_{y_b} \ddot{\theta}_y + (I_{x_b} - I_{z_b}) \left[ \dot{\theta}_x \dot{\theta}_z - \theta_x \dot{\theta}_x \Omega_y + \theta_z \dot{\theta}_z \Omega_y - \theta_x \theta_z \Omega_y^2 + 3 \theta_y \Omega_y^2 \right] \quad (2.53)$$

$$T_{d_{k_b}} = I_{z_b} \left[ \ddot{\theta}_z - \dot{\theta}_x \Omega_y \right] + (I_{y_b} - I_{x_b}) \left[ \dot{\theta}_x \Omega_y + \theta_z \Omega_y^2 \right] \quad (2.54)$$

Equations (2.50) and (2.53) can again be simplified if order of magnitude approximations are considered. Using the estimated values given in equations (2.37) and (2.38) it is seen that equation (2.50) simplifies to

$$T_{d_{j_b}} = I_{y_b} \left[ \ddot{\theta}_y + \dot{\Omega}_y \right] + 3(I_{x_b} - I_{z_b}) \frac{\theta_y g_s R_e^2}{\rho_o^3} \quad (2.55)$$

and equation (2.53) simplifies to

$$T_{d_{j_b}} = I_{y_b} \ddot{\theta}_y + 3(I_{x_b} - I_{z_b}) \theta_y \Omega_y^2 \quad (2.56)$$

It should be noted from equations (2.49), (2.51) and (2.55) that the expressions for  $T_{d_{i_b}}$  and  $T_{d_{k_b}}$  are linear, cross coupled, time varying differential equations that depend on  $\theta_x$  and  $\theta_z$  and their derivatives but not on  $\theta_y$  and its derivatives. Therefore,  $\theta_x$  and  $\theta_z$  can be determined from the disturbance torques about the  $X_b$  and  $Z_b$  axis without involving the disturbance torque about the  $Y_b$  axis. Equation (2.55) is a linear, time varying differential equation that only involves  $\theta_y$  and its derivatives and does not depend upon the angular deviations about the other two axes.

As an aid to obtaining an insight into equations (2.49), (2.51) and (2.55), they are put into the following form, and from this form, a signal flow graph can be easily constructed. (see Fig. 2-5 and Fig. 2-6)

$$\ddot{\theta}_x = \frac{T_{d_{i_b}}}{I_{x_b}} - \theta_z \dot{\Omega}_y - \dot{\theta}_z \Omega_y - \frac{(I_{z_b} - I_{y_b})}{I_{x_b}} \left[ \dot{\theta}_z \Omega_y - \theta_x \left( \Omega_y^2 + \frac{3g_s Re^2}{\rho_o^3} \right) \right] \quad (2.57)$$

$$-\ddot{\theta}_y = \frac{T_{d_{j_b}}}{I_{y_b}} - \dot{\Omega}_y - 3 \frac{(I_{x_b} - I_{z_b})}{I_{y_b}} \frac{\theta_y g_s Re^2}{\rho_o^3} \quad (2.58)$$

$$\ddot{\theta}_z = \frac{T_{d_{k_b}}}{I_{z_b}} + \theta_x \dot{\Omega}_y + \dot{\theta}_x \Omega_y - \frac{(I_{y_b} - I_{x_b})}{I_{z_b}} \left[ \dot{\theta}_x \Omega_y + \theta_z \Omega_y^2 \right] \quad (2.59)$$

Figure 2-5 relates the output angles  $\theta_x$  and  $\theta_z$  to the torques about the  $X_b$  and  $Z_b$  axes, and Fig. 2-6 relates  $\theta_y$  to the torque about the  $Y_b$  axis.

With reference to Fig. 2-5, paths  $P_1$  and  $P_2$  represent position feedback terms due to the orbital angular velocity of the vehicle. If  $I_{y_b} > I_{x_b}$  and  $I_{y_b} > I_{z_b}$ , the feedback produced by these paths will be such as to oppose a displacement produced by a disturbance torque. Paths  $P_3$  and  $P_4$  are also due to the orbital angular velocity of the satellite about the earth. These paths introduce feedback depending on the error rates ( $\dot{\theta}_x$  and  $\dot{\theta}_z$ ). Unfortunately these terms do not introduce damping because they appear in the wrong equations. For an elliptical orbit, the angular momentum of the vehicle becomes time varying. The derivative of the orbital rate ( $\dot{\Omega}_y$ ) gives rise to cross coupling between the  $X_b$  and  $Z_b$  axes as shown by paths  $P_5$  and  $P_6$ . With reference to both Figs. 2-5 and 2-6, paths  $P_7$  and  $P_8$  are seen to introduce position feedback on the  $X_b$  and  $Y_b$  axes. These are

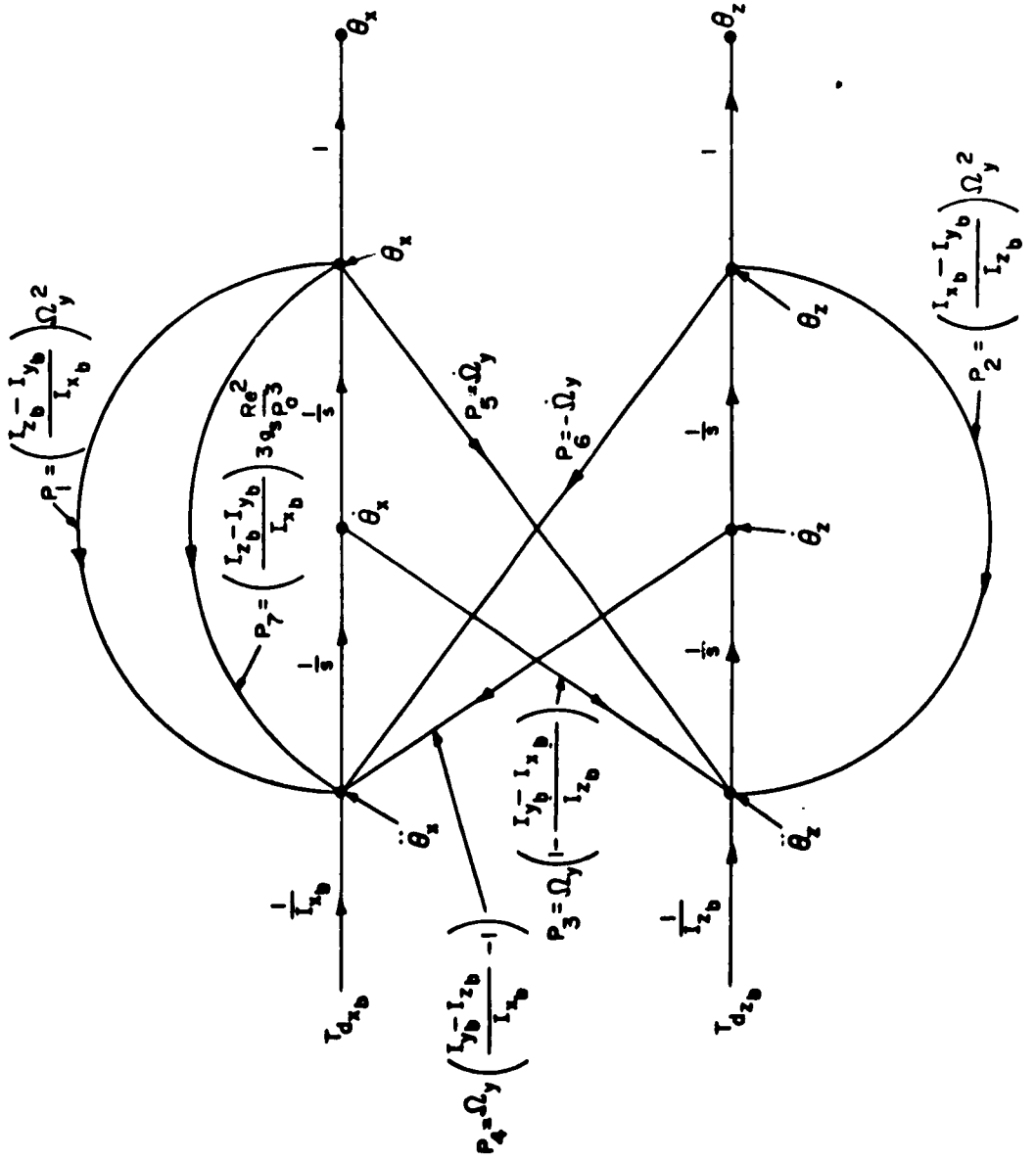


Fig. 2-5 Signal Flow Graph for the  $X_b$  and  $Z_b$  Axes of the Body in an Elliptical Orbit

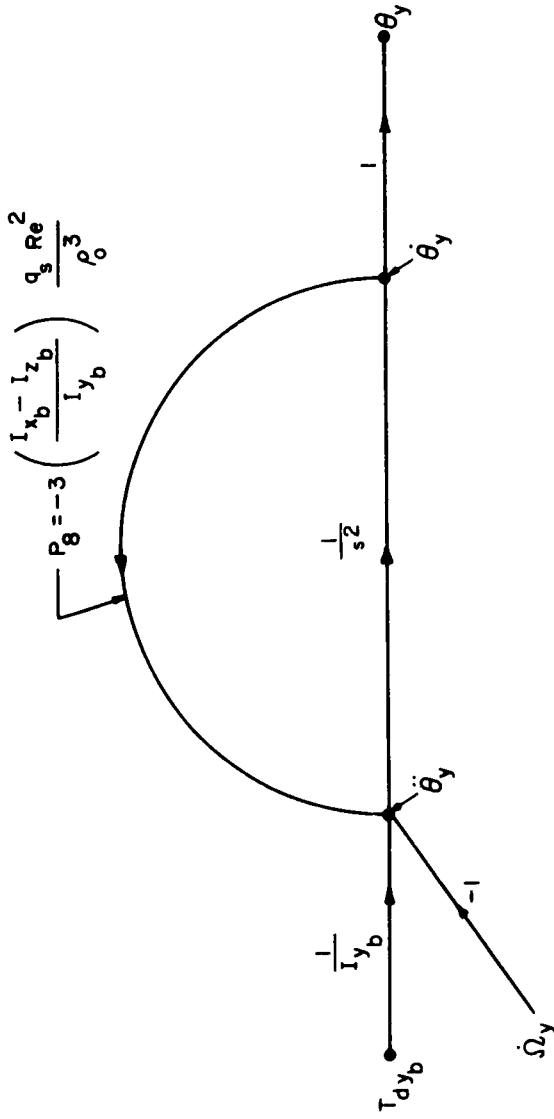


Fig. 2-6 Signal Flow Graph for the  $Y_b$  Axis of the Body in an Elliptical Orbit

the result of differential gravity and, as was previously shown, the feedback will be negative about both axes if the moment of inertia of the body about its  $Z_b$  axis is smaller than the moments of inertia about the other two axes. The corresponding flow graphs for a circular orbit can be obtained from Figs. 2-5 and 2-6 by setting  $\dot{\Omega}_y$  equal to zero and

$$\frac{g_s R_e^2}{\rho_o^3} = \Omega_y^2. \quad (C.16)$$

It is seen from the flow graphs that position feedback terms, for a suitable choice of the moments of inertia, ( $I_{y_b} > I_{x_b} > I_{z_b}$ ) can act as spring type restoring torques about each of the axes of the body. The effective spring constant, defined as the ratio of restoring torque to angular displacement, is given below for each of the axes.

$$K_x = (I_{y_b} - I_{z_b}) \left[ \Omega_y^2 + \frac{3g_s R_e^2}{\rho_o^3} \right] \quad (2.60)$$

$$K_y = 3(I_{x_b} - I_{z_b}) \frac{g_s R_e^2}{\rho_o^3} \quad (2.61)$$

$$K_z = (I_{y_b} - I_{x_b}) \Omega_y^2 \quad (2.62)$$

It is of interest to obtain some appreciation, as to the order of magnitude of these terms. Consider again the drum satellite of Fig. 2-3. Assuming a circular orbit and using the moments of inertia calculated for this satellite, yields:

$$K_x = 4.11 \times 10^{-5} \frac{\text{ft.} \cdot \text{lbs.}}{\text{rad}} \quad (2.63)$$

$$K_y = \frac{3}{4} K_x = 3.11 \times 10^{-5} \frac{\text{ft.} \cdot \text{lbs.}}{\text{rad}} \quad (2.64)$$

$$K_z = 0$$



F) Solution of the Equations of Motion for a Circular Orbit

Introducing Laplace transform notation into equations (2.52), (2.54) and (2.56) yields:

$$T_{d_{i_b}}(s) = I_{x_b} \left[ s^2 \theta_x(s) + s \theta_z(s) \Omega_y \right] + (I_{z_b} - I_{y_b}) \left[ s \theta_z(s) \Omega_y - 4 \theta_x(s) \Omega_y^2 \right] \quad (2.66)$$

$$T_{d_{j_b}}(s) = I_{y_b} s^2 \theta_y(s) + 3(I_{x_b} - I_{z_b}) \theta_y(s) \Omega_y^2 \quad (2.67)$$

$$T_{d_{k_b}}(s) = I_{z_b} \left[ s^2 \theta_z(s) - s \theta_x(s) \Omega_y \right] + (I_{y_b} - I_{x_b}) \left[ s \theta_x(s) \Omega_y + \theta_z(s) \Omega_y^2 \right] \quad (2.68)$$

Solving equations (2.66), (2.67) and (2.68) one obtains:

$$\theta_x(s) = \frac{T_{d_{i_b}}(s) \left[ s^2 I_{z_b} + (I_{y_b} - I_{x_b}) \Omega_y^2 \right] - T_{d_{k_b}}(s) \left[ s \Omega_y (I_{x_b} + I_{z_b} - I_{y_b}) \right]}{s^2 \Omega_y^2 (I_{x_b} + I_{z_b} - I_{y_b})^2 + \left[ s^2 I_{x_b} + 4(I_{y_b} - I_{z_b}) \Omega_y^2 \right] \left[ s^2 I_{z_b} + (I_{y_b} - I_{x_b}) \Omega_y^2 \right]} \quad (2.69)$$

$$\theta_y(s) = \frac{T_{d_{j_b}}(s)}{s^2 I_{y_b} + 3(I_{x_b} - I_{z_b}) \Omega_y^2} \quad (2.70)$$

$$\theta_z(s) = \frac{T_{d_{k_b}}(s) \left[ s^2 I_{x_b} + 4(I_{y_b} - I_{z_b}) \Omega_y^2 \right] + T_{d_{i_b}}(s) \left[ s \Omega_y (I_{x_b} + I_{z_b} - I_{y_b}) \right]}{s^2 \Omega_y^2 (I_{x_b} + I_{z_b} - I_{y_b})^2 + \left[ s^2 I_{x_b} + 4(I_{y_b} - I_{z_b}) \Omega_y^2 \right] \left[ s^2 I_{z_b} + (I_{y_b} - I_{x_b}) \Omega_y^2 \right]} \quad (2.71)$$

In order to better understand the nature of the response of the body to disturbance torques, several examples will be considered.

Example No. 1

The moments of inertia about the  $X_b$  and  $Y_b$  axes are equal and greater than the moment of inertia about the  $Z_b$  axis. An impulsive torque of strength  $\delta$  is applied about the  $X_b$  axis and no torques are applied about the other two axes. Impulsive torques are characteristic of meteorite impacts.

When appropriate substitutions are made in equation (2.69) one obtains for  $\theta_x(s)$

$$\theta_x(s) = \frac{\frac{1}{I_{x_b}} \delta}{s^2 + \Omega_y^2 \frac{(4 I_{x_b} - 3 I_{z_b})}{I_{x_b}}} \quad (2.72)$$

Since  $I_{x_b} > I_{z_b}$  the poles of  $\theta_x(s)$  lie on the imaginary axis and the system will oscillate with a radian frequency of

$$\omega_o = \Omega_y \sqrt{\frac{4 I_{x_b} - 3 I_{z_b}}{I_{x_b}}} \quad (2.73)$$

If  $I_{x_b} < I_{z_b}$  there will be a pole of  $\theta_x(s)$  in the right half plane and the angular deviation will increase with time. For  $I_{x_b} > I_{z_b}$

$$\theta_x(t) = \frac{\delta}{I_{x_b} \omega_o} \sin \omega_o t U(t) \quad (2.74)$$

Clearly from equation (2.70)

$$\theta_y(t) = 0 \quad (2.75)$$

From equation (2.71)

$$\theta_z(s) = \frac{\Omega_y \delta}{s \left[ s^2 I_{x_b} + \Omega_y^2 (4 I_{x_b} - 3 I_{z_b}) \right]} = \frac{\delta}{s \Omega_y (4 I_{x_b} - 3 I_{z_b})} - \frac{s I_x \delta}{\Omega_y (4 I_{x_b} - 3 I_{z_b}) \left[ s^2 I_{x_b} + \Omega_y^2 (4 I_{x_b} - 3 I_{z_b}) \right]} \quad (2.76)$$

Therefore for  $I_{x_b} > I_{z_b}$

$$\theta_z(t) = \frac{\delta}{\Omega_y (4 I_{x_b} - 3 I_{z_b})} [1 - \cos \omega_o t] U(t) \quad (2.77)$$

From equation (2.74) it is seen that the angular deviation about the  $X_b$  axis is oscillatory with zero mean, whereas from equation (2.77) it is seen that the deviation about the  $Z_b$  axis is also oscillatory but with a non-zero mean. The results of this example are summarized in Fig. 2-7.

### Example No. 2

The same satellite configuration as in Example 1 but now the impulsive torque of strength  $\delta$  is applied about the  $Y_b$  axis and no torques are applied about the other two axes.

Substitution into equations (2.69) and (2.71), it is clearly seen that

$$\theta_x(t) = \theta_z(t) = 0 \quad (2.78)$$

Substitution into equation (2.70) yields for  $\theta_y(s)$

$$\theta_y(s) = \frac{\frac{1}{I_{y_b}} \delta}{s^2 + 3 \frac{(I_{x_b} - I_{z_b})}{I_{y_b}} \Omega_y^2} \quad (2.79)$$

Therefore

$$\theta_y(t) = \frac{\delta}{\omega_1 I_{y_b}} \sin \omega_1 t U(t) \quad (2.80)$$

where

$$\omega_1 = \Omega_y \sqrt{\frac{3(I_{x_b} - I_{z_b})}{I_{y_b}}} \quad (2.81)$$

(observe that  $\omega_1 < \omega_o$ ).

It is seen from equation (2.80) that the angular deviation about the  $Y_b$  axis is sinusoidal with zero mean. The result of this example is summarized in Fig. 2-8.

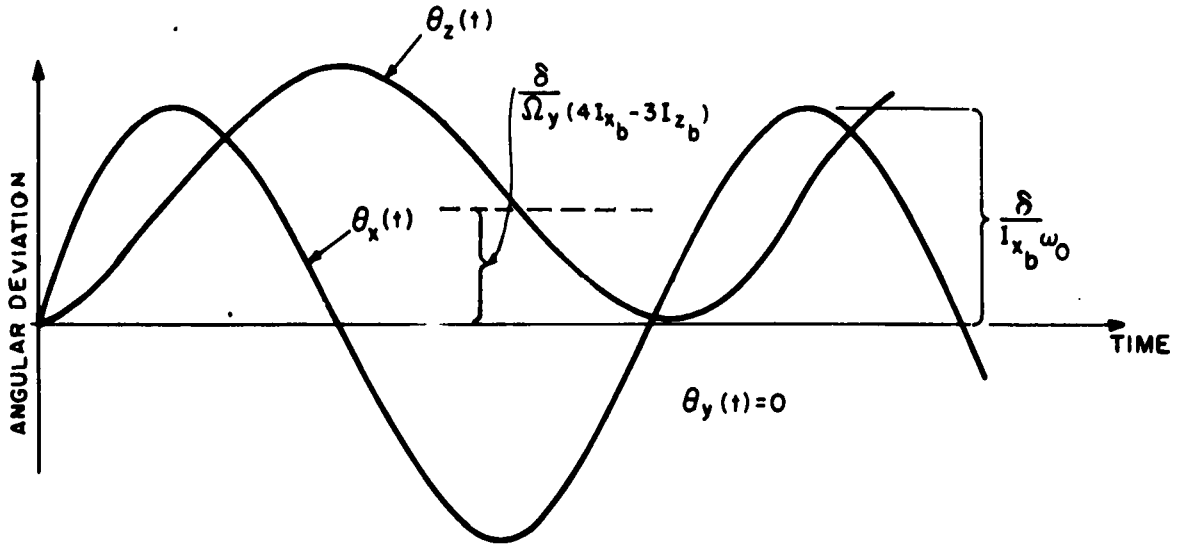


Fig. 2-7 Response to an Impulsive Torque of Strength  $\delta$  Applied about the  $X_b$  Axis

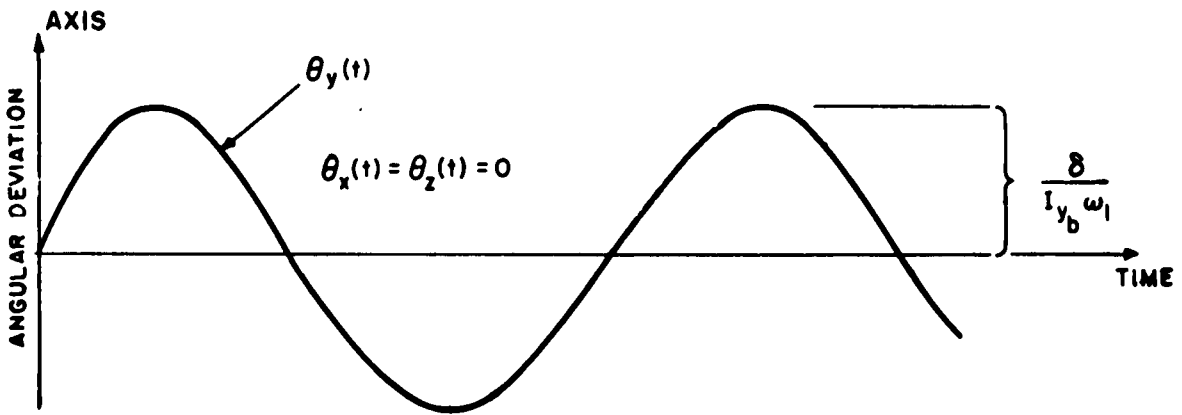


Fig. 2-8 Response to an Impulsive Torque of Strength  $\delta$  Applied About the  $Y_b$  Axis

Example No. 3

The same satellite configuration as in Example 1, but now an impulsive torque of strength  $\delta$  is applied about the  $Z_b$  axis and no torques are applied about the other two axes.

Substitution into equation (2.69) yields for  $\theta_x(s)$

$$\theta_x(s) = \frac{-\Omega_y \delta}{s \left[ s^2 I_{x_b} + \Omega_y^2 (4 I_{x_b} - 3 I_{z_b}) \right]} = \frac{\delta}{s \Omega_y (4 I_{x_b} - 3 I_{z_b})} + \frac{s I_x \delta}{\Omega_y (4 I_{x_b} - 3 I_{z_b}) \left[ s^2 I_{x_b} + \Omega_y^2 (4 I_{x_b} - 3 I_{z_b}) \right]} \quad (2.82)$$

Therefore

$$\theta_x(t) = \frac{\delta}{\Omega_y (4 I_{x_b} - 3 I_{z_b})} [\cos \omega_o t - 1] U(t) \quad (2.83)$$

Clearly from equation (2.70)

$$\theta_y(t) = 0 \quad (2.84)$$

Substitution into equation (2.71) yields for  $\theta_z(s)$

$$\theta_z(s) = \frac{\delta \left[ s^2 I_{x_b} + 4(I_{x_b} - I_{z_b}) \Omega_y^2 \right]}{s^2 I_{z_b} \left[ s^2 I_{x_b} + (4 I_{x_b} - 3 I_{z_b}) \Omega_y^2 \right]} = \frac{\frac{1}{I_{z_b}} \delta}{s^2 + \frac{(4 I_{x_b} - 3 I_{z_b}) \Omega_y^2}{I_{x_b}}} + \frac{4(I_{x_b} - I_{z_b}) \delta}{s^2 I_{z_b} (4 I_{x_b} - 3 I_{z_b})} - \frac{4(I_{x_b} - I_{z_b}) \delta}{I_{z_b} (4 I_{x_b} - 3 I_{z_b}) \left[ s^2 + \frac{(4 I_{x_b} - 3 I_{z_b}) \Omega_y^2}{I_{x_b}} \right]} \quad (2.85)$$

Taking the inverse Laplace transform, one obtains

$$\theta_z(t) = \frac{\delta}{(4 I_{x_b} - 3 I_{z_b}) \omega_o} \left[ \sin \omega_o t + \frac{(4 I_{x_b} - I_{z_b})}{I_{z_b}} t \right] U(t) \quad (2.86)$$

It is seen from equation (2.86) that when an impulsive torque is applied about the  $Z_b$  axis drift occurs. Differential gravity is not available to help stabilize the vehicle about that axis. Furthermore, since it was assumed that  $I_{x_b} = I_{y_b}$ , the gyroscopic

action due to the orbital rate of the vehicle was not able to produce position feedback. (see Fig. 2-5 and equation (2.62)). The results of this example are summarized in Fig. 2-9. If the moments of inertia of the vehicle were chosen such that  $I_{y_b} > I_{x_b} > I_{z_b}$ , drift would not occur about any of the vehicle's axes as a result of an impulsive disturbance. Consider the following example. Choose the moments of inertia of the vehicle such that  $I_{y_b} > I_{x_b} > I_{z_b}$  and

$$I_{x_b} + I_{z_b} = I_{y_b} \quad (2.87)$$

(For example:  $I_x = \frac{2}{3} I_y$ ,  $I_z = \frac{1}{3} I_y$ ). Equations (2.69), (2.70) and (2.71) degenerate to

$$\theta_x(s) = \frac{T_{d_{j_b}}(s) \left[ s^2 I_{z_b} + (I_{y_b} - I_{x_b}) \Omega^2 \right]}{\left[ s^2 I_{x_b} + 4(I_{y_b} - I_{z_b}) \Omega^2 \right] \left[ s^2 I_{z_b} + (I_{y_b} - I_{x_b}) \Omega^2 \right]} \quad (2.88)$$

$$\theta_y(s) = \frac{T_{d_{j_b}}(s)}{s^2 I_{y_b} + 3(I_{x_b} - I_{z_b}) \Omega^2} \quad (2.89)$$

$$\theta_z(s) = \frac{T_{d_{k_b}}(s) \left[ s^2 I_{x_b} + 4(I_{y_b} - I_{z_b}) \Omega^2 \right]}{\left[ s^2 I_{x_b} + 4(I_{y_b} - I_{z_b}) \Omega^2 \right] \left[ s^2 I_{z_b} + (I_{y_b} - I_{x_b}) \Omega^2 \right]} \quad (2.90)$$

It is apparent from these equations, that when the moments of inertia of the body satisfy equation (2.87), the three axes of the body are completely uncoupled. i.e. a disturbance applied about one axis will only produce a displacement about that axis and none about the other axes. Also, it is seen that no drift will occur about any of the axes due to an impulsive disturbance. The free response consists of the sum of two sinusoids of different frequency. This is certainly an improvement over the drum-shaped satellite discussed in Example 1, 2, and 3.

We have seen in this chapter that, with proper vehicle design, the impulsive response of the system consists of only oscillatory terms. Since the system is linear, if an arbitrary torque is applied, the output will consist of terms of the same form as the input plus the terms of the impulsive response. Hence for impulse-like torques,

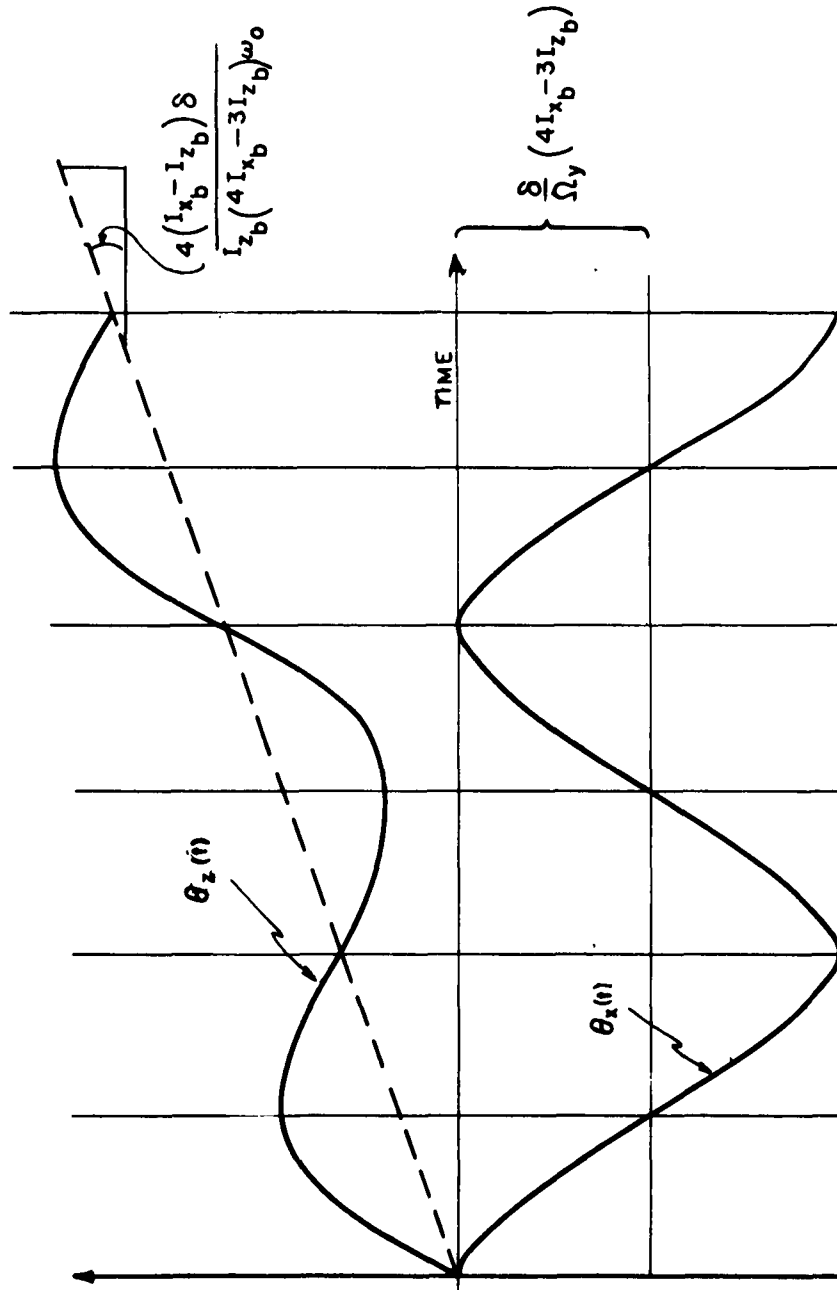


Fig. 2-9 Response to an Impulsive Torque of Strength  $\delta$  Applied About the  $Z_b$  Axis

low level step torques and sinusoidal torques, drift would never occur. If damping devices are incorporated into the system, (this can be done passively) it should be possible to remove the oscillatory components and keep the vehicle reasonably aligned with the geocentric vertical. It is possible to utilize gyroscopes to provide damping. In order to better understand how this can be effected, a simple analysis of gyroscope damping will be presented in Chapter III.



### Chapter III - A SIMPLE ANALYSIS OF GYROSCOPE DAMPING

#### A) The Mechanism of Gyroscope Damping

The mechanism by which gyroscopic action can be utilized to provide vehicle damping can be qualitatively explained as follows. When a disturbance torque is applied to the vehicle, angular motion of the vehicle with respect to inertial space will occur. This motion will cause relative motion between the gimbal of the gyroscope and the body. If viscous damping at the gyroscope gimbal is provided (this can be provided through electrical means) a damping term will couple into the equations of motion of the body.

Vehicle damping can either be of direct or indirect nature. By indirect damping, it is meant that vehicle rotation will produce precession of the gyroscope which causes vehicle damping due to relative motion between the gyroscope and the vehicle. If the vehicle rotation is about the precession axis of the gyroscope, direct damping will occur. In this case the relative motion between the vehicle and the gyroscope gimbal is brought about without the mechanism of gyroscope precession.

#### B) Analysis of a Simple Configuration Employing Indirect Gyroscope Damping

Indirect damping can be demonstrated with the following example. Consider the geometry shown in Figure 3-1. In the geometry pictured, the body is constrained to rotate with respect to inertial space only about its X axis and the gyroscope is constrained to rotate relative to the body about the Z axis of the body. Consider a disturbance torque applied to the body about its X axis. This torque is countered by the inertia torque of the body, the spring torque, and the gyroscopic torque.

$$T_d = I_x \ddot{\theta}_x + K \theta_x - \dot{\theta}_g H_r \cos \theta_g \quad (3.1)$$

Where  $I_x$  is the sum of the moments of inertia of the body and the gyroscope about the X axis.

$K$  is the spring constant

$H_r$  is the angular momentum of the gyroscope rotor.

The torque on the gyroscope about the Z axis is given by:

$$T_{g_z} = -D \dot{\theta}_g \quad (3.2)$$

Where  $D$  is the damping coefficient between the body and the gyroscope gimbal. This torque, (3.2), is countered by the inertia torque of the gyroscope and the gyroscopic torque.

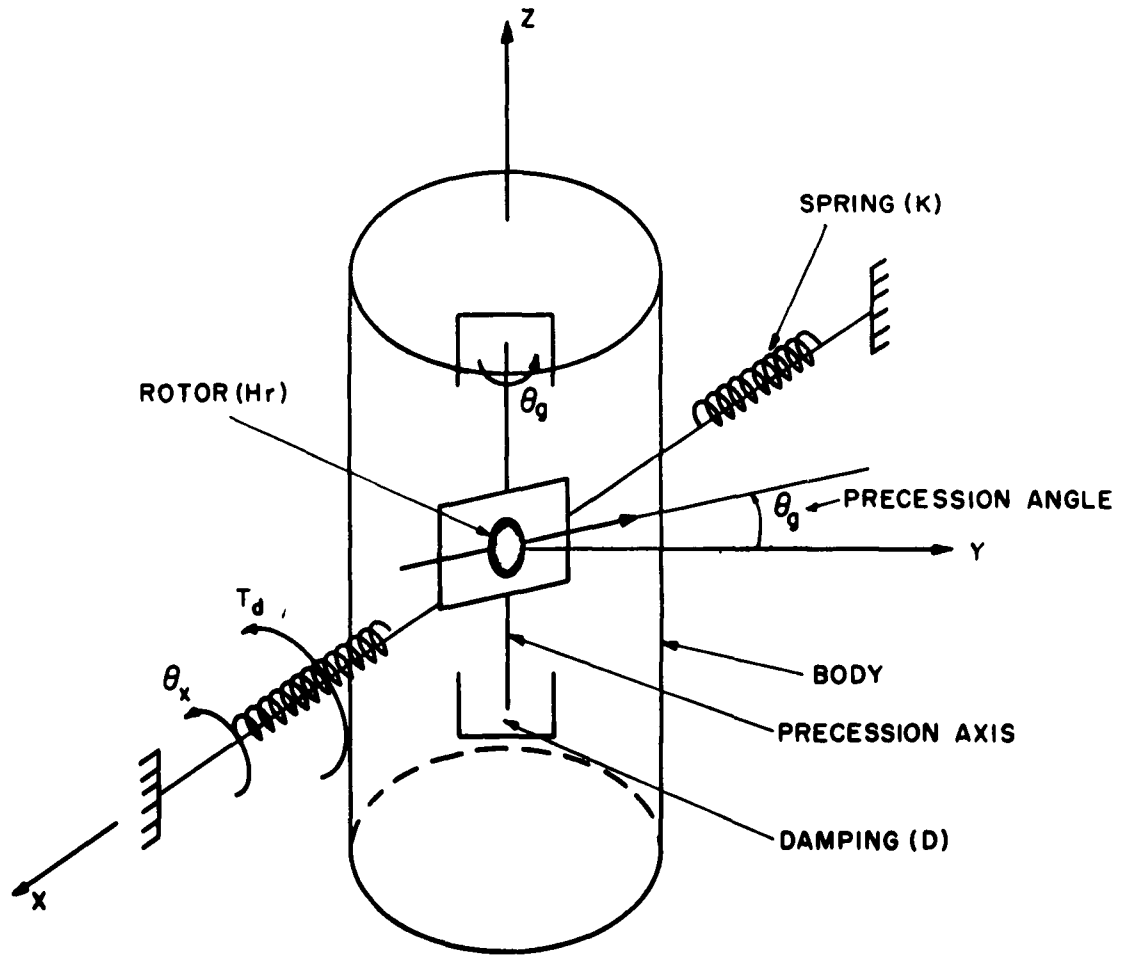


Fig. 3-1 Configuration to Illustrate Indirect Gyroscope Damping

$$T_{g_z} = -D\dot{\theta}_g = I_g \ddot{\theta}_g + \dot{\theta}_x H_r \cos \theta_g \quad (3.3)$$

where  $I_g$  is the moment of inertia of the gyroscope about the Z axis of the body. Equations (3.1) and (3.3) can be linearized for small angular deviations.

$$T_d = I_x \ddot{\theta}_x + K \theta_x - \dot{\theta}_g H_r \quad (3.4)$$

$$-D\dot{\theta}_g = I_g \ddot{\theta}_g + \dot{\theta}_x H_r \quad (3.5)$$

Introducing Laplace transform notation to these linearized equations yields:

$$T_d(s) = I_x s^2 \theta_x(s) + K \theta_x(s) - H_r s \theta_g(s) \quad (3.6)$$

$$-Ds \theta_g(s) = I_g s^2 \theta_g(s) + H_r s \theta_x(s) \quad (3.7)$$

Solving for  $\theta_x(s)$  in equation (3.7) in terms of  $\theta_g(s)$  yields:

$$\theta_x(s) = \frac{-H_r}{D + s I_g} \theta_g(s) \quad (3.8)$$

Substituting into Equation (3.6) yields:

$$T_d(s) [D + s I_g] = \theta_x(s) \left[ s^3 I_x I_g + s^2 D I_x + s(K I_g + H_r^2) + K D \right] \quad (3.9)$$

The characteristic equation of the system is therefore

$$s^3 + \frac{s^2 D}{I_g} + s \frac{(K I_g + H_r^2)}{I_x I_g} + \frac{K D}{I_x I_g} = 0 \quad (3.10)$$

The stability of this system can be demonstrated by applying the Routh stability criterion. Consider the following third order equation.

$$a s^3 + b s^2 + c s + d = 0 \quad (3.11)$$

corresponding to this equation, the Routh array is

$$\begin{array}{cc} a & c \\ b & d \\ \frac{bc-ad}{b} & \\ d & \end{array}$$

If the coefficients (a, b, c, d) of equation (3.11) are positive, a necessary and

sufficient condition for stability is that

$$b c - a d > 0 \quad (3.12)$$

applying this condition to the characteristic equation (3.10) yields:

$$I_x D (K I_g + H_r^2) - I_x I_g K D > 0 \quad (3.13)$$

which simplifies to

$$I_x D H_r^2 > 0 \quad (3.14)$$

which clearly is always satisfied. Hence stability of the system is assured. Intuitively this is to be expected.

Since the characteristic equation (3.10) has only real coefficients, the set of roots can only be of two types, i. e.

- 1) three real roots
- 2) one real root and a pair of complex conjugate roots.

It is seen from the characteristic equation (3.10) that the sum of the roots is given by:

$$r_1 + r_2 + r_3 = - \frac{D}{I_g} \quad (3.15)$$

where  $D$  is the damping coefficient

$I_g$  is the moment of inertia of the gyroscope

$r_1, r_2, r_3$  represent the roots of the equation

Since the imaginary parts of the complex conjugate roots cancel on addition

$$\text{Re}(r_1) + \text{Re}(r_2) + \text{Re}(r_3) = - \frac{D}{I_g} \quad (3.16)$$

where  $\text{Re}(\sigma_i)$  represents the real part of the  $i^{\text{th}}$  root.

For a fixed gyroscope moment of inertia ( $I_g$ ) and for a fixed damping coefficient ( $D$ ), the sum of the real parts of the roots is constant. As  $K$ , the spring constant, and  $H_r$ , the angular momentum of the rotor are varied, the roots of the characteristic equation must migrate such that the sum of their real parts remains constant. As some of the roots migrate toward the left, the others must move toward the imaginary axis. This strongly suggests that optimum damping is attained, i. e. steady state is attained in minimum time, when the real part of all the roots are equal. This condition can occur in two ways.

- i) a third order pole on the real axis (see Fig. 3-2)

ii) a real pole and a pair of complex conjugate poles all with the same real part. (see Fig. 3-3)

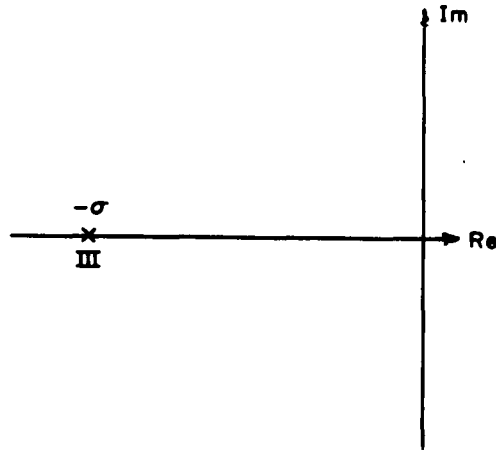


Fig. 3-2 Third Order Pole on the Real Axis

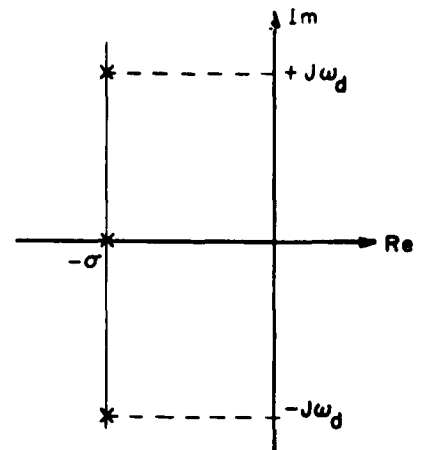


Fig. 3-3 Real Pole and a Pair of Complex Poles

Consider case (i) where a third order pole on the real axis occurs. For this case, the characteristic equation (3.10) must reduce to the form

$$(s + \sigma)^3 = 0 \quad (3.17)$$

Expanding, and equating to the expression for the characteristic equation (3.10), yields:

$$s^3 + 3\sigma s^2 + 3\sigma^2 s + \sigma^3 = s^3 + \frac{D}{I_g} s^2 + \frac{(K I_g + H_r^2)}{I_x I_g} s + \frac{K D}{I_x I_g} \quad (3.18)$$

Equating coefficients of like order terms yields:

$$3\sigma = \frac{D}{I_g} \quad (3.19)$$

$$3\sigma^2 = \frac{K I_g + H_r^2}{I_x I_g} \quad (3.20)$$

$$\sigma^3 = \frac{K D}{I_x I_g} \quad (3.21)$$

Solving for  $\sigma$ ,  $H_r$  and  $K$  yields:

$$\sigma = \frac{D}{3I_g} \quad (3.22)$$

$$H_r = D \sqrt{\frac{8I_x}{27I_g}} \quad (3.23)$$

$$K = \frac{I_x D^2}{27 I_g^2} \quad (3.24)$$

Clearly, for a fixed  $D$  and  $I_x$  these equations are parametric in  $I_g$ . For a specified  $I_x$  and  $I_g$ ,  $\sigma$ ,  $H_r$  and  $K$  can be plotted as a function of  $D$ . In order to obtain an appreciation for the order of magnitude of  $\sigma$ ,  $H_r$  and  $K$ , graphs are drawn as functions of  $D$  for a body whose moment of inertia is  $27.7 \text{ slug-ft.}^2$  (see Fig. 3-4). The moment of inertia of the gyroscope will be taken as one percent of the moment of inertia of the vehicle ( $I_g = 0.3 \text{ slug-ft.}^2$ ). In a satellite vehicle, it is of utmost importance to keep the gyroscope as small as possible so that more data gathering payload can be included. The range of  $D$  chosen is from  $0.5 \times 10^{-3}$  to  $4.0 \times 10^{-3} \text{ ft.-lb./} \frac{\text{rad}}{\text{sec}}$ . These values are typical of the damping attainable in a gyroscope. It is seen from Fig. 3-4 that  $\sigma$  and  $H_r$  are linear functions of  $D$ , whereas  $K$  varies with the square of  $D$ . In order to obtain an estimate of the settling time of the system, it is necessary to look at its free response. The free response of a system, which has a third order pole on the real axis, is of the form

$$\theta(t) = (K_0 + K_1 t + K_2 t^2) e^{-\sigma t} \quad (3.25)$$

It is clear that the term  $K_0 e^{-\sigma t}$  will decay to  $e^{-4}$  or 2% of its maximum value when

$$t = \frac{4}{\sigma} \text{ sec.} \quad (3.26)$$

The term  $K_1 t e^{-\sigma t}$  will decay to  $e^{-4}$  of its maximum value when

$$t e^{-\sigma t} = \frac{e^{-5}}{\sigma} \quad (3.27)$$

The solution of this equation yields:

$$t = \frac{6.9}{\sigma} \text{ sec.} \quad (3.28)$$

The term  $K_2 t^2 e^{-\sigma t}$  will decay to  $e^{-4}$  of its maximum value when

$$t^2 e^{-\sigma t} = \frac{4}{\sigma^2} e^{-6} \quad (3.29)$$

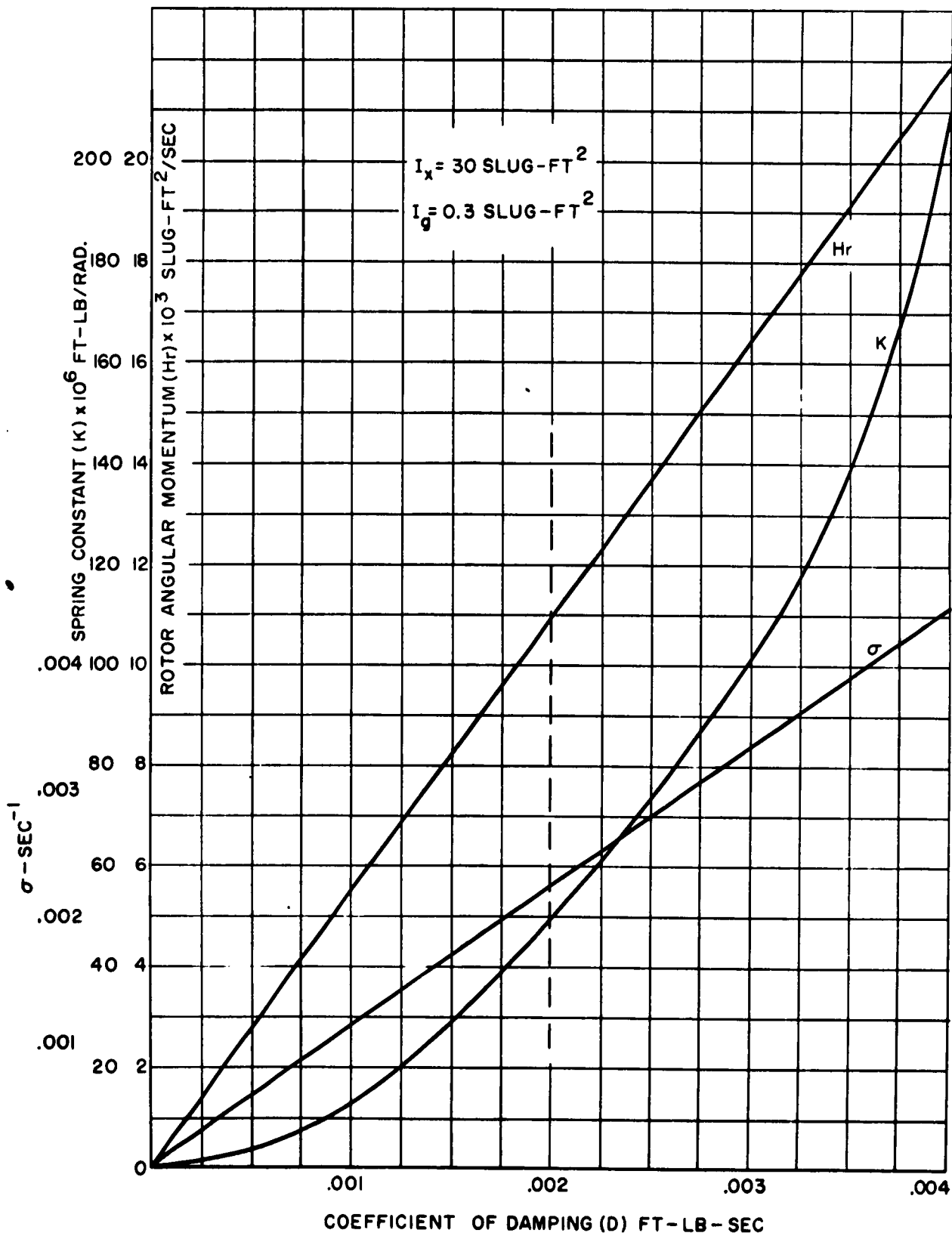


Fig. 3-4 Variation of  $\sigma$ ,  $H_r$  and  $K$  with the Damping Coefficient for Optimization with a Third Order Pole on the Real Axis

The solution of this equation yields:

$$t = \frac{9}{\sigma} \text{ sec.} \quad (3.30)$$

To see which term predominates, it is necessary to consider the transfer function of the system (3.9). Since the system has a third order pole on the real axis, the transfer function becomes

$$\theta_x(s) = \frac{(D + s I_g)}{I_x I_g (s + \sigma)^3} T_d(s) \quad (3.31)$$

The free response of the system is given by its response to an impulse torque ( $T_d(s) = 1$ ). For this torque

$$\theta_x(s) = \frac{D + s I_g}{I_x I_g (s + \sigma)^3} \quad (3.32)$$

Taking the inverse Laplace transform

$$\theta_x(t) = \frac{1}{I_x} t e^{-\sigma t} U(t) + \frac{D}{3 I_x I_g} t^2 e^{-\sigma t} U(t) \quad (3.33)$$

For

$$D = 2 \times 10^{-3} \text{ ft-lbs} / \frac{\text{rad}}{\text{sec}}$$

$$I_g = 0.3 \text{ slug-ft.}^2$$

$$I_x = 30 \text{ slug-ft.}^2$$

$$\theta_x(t) = 33.3 \times 10^{-3} t e^{-2.22 \times 10^{-3} t} U(t) + 74 \times 10^{-6} t^2 e^{-2.22 \times 10^{-3} t} U(t) \quad (3.34)$$

Clearly, the term  $33.3 \times 10^{-3} t e^{-2.22 \times 10^{-3} t} U(t)$  predominates, hence it will be assumed that the system damps in 6.9 time constants. In Fig. 3-5 the settling time is plotted as a function of the damping coefficient. The time is represented as a percentage of a 90 minute orbit.

It will be instructive to sketch the root-loci of the system as a function of the damping coefficient ( $D$ ), the angular momentum of the rotor ( $H_r$ ), the spring constant ( $K$ ), and the moment of inertia of the gyroscope ( $I_g$ ). From Fig. 3-4 it is seen that when  $I_x = 30$ ,  $I_g = 0.3$ , a third order pole occurs on the real axis at  $\sigma = -2.22 \times 10^{-3}$  when  $H_r = 10.9 \times 10^{-3}$ ,  $K = 49.4 \times 10^{-6}$  and  $D = 0.002$ . In sketching



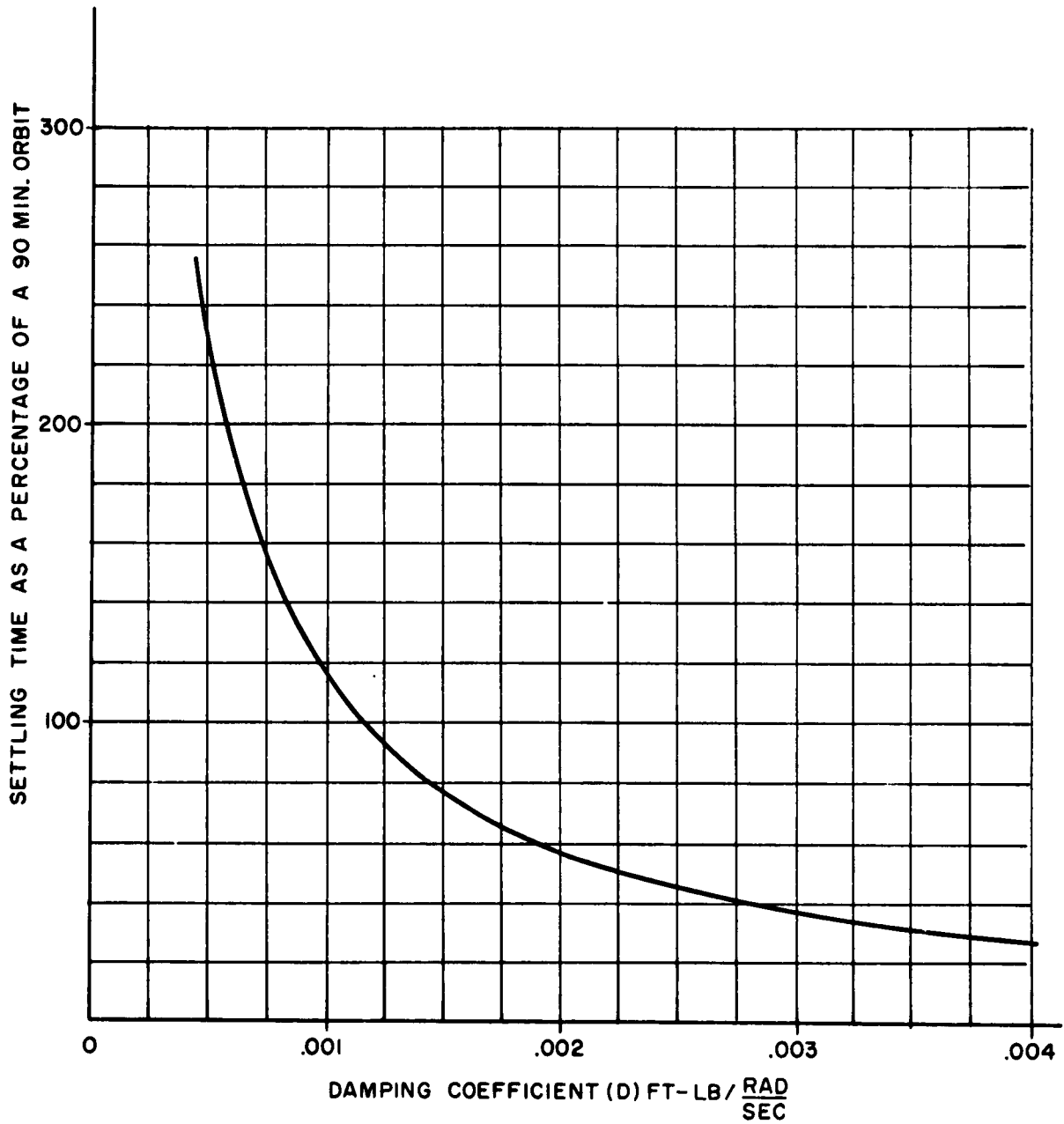


Fig. 3-5 Settling Time as a Function of the Damping Coefficient for Optimization with a Third Order Pole on the Real Axis

the root-loci, each of the parameters will be in-turn varied while the remaining parameters are held fixed at the values given above. Therefore, for each of the root-loci, all the branches will coalesce at  $s = -2.22 \times 10^{-3}$

a) Root-locus as a function of the damping coefficient (D). (See Fig. 3-6) .

The characteristic equation (3.10) can be factored into the form:

$$(s^3 + b s) \left( 1 + \frac{D(a s^2 + c)}{s(s^2 + b)} \right) = 0 \quad (3.35)$$

where

$$a = \frac{1}{I_g} \quad (3.36)$$

$$b = \frac{K I_g + H_r^2}{I_x I_g} \quad (3.37)$$

$$c = \frac{K}{I_x I_g} \quad (3.38)$$

The roots of the characteristic equation (3.10) are therefore seen to satisfy the equation

$$\frac{D(a s^2 + c)}{s(s^2 + b)} = -1 \quad (3.39)$$

The poles and zeros of the expression on the left side of equation (3.39) are given by:

$$p_1 = 0$$

$$p_2, p_3 = \pm j \sqrt{b} = \pm j \sqrt{\frac{K}{I_x} + \frac{H_r^2}{I_x I_g}} \quad (3.40)$$

$$z_1, z_2 = \pm j \sqrt{\frac{c}{a}} = \pm j \sqrt{\frac{K}{I_x}} \quad (3.41)$$

Substituting the chosen values yields:

$$p_1 = 0$$

$$p_2, p_3 = \pm j (3.86 \times 10^{-3}) \quad (3.42)$$

$$z_1, z_2 = \pm j (1.29 \times 10^{-3}) \quad (3.43)$$

The root-locus can now be easily constructed.

At  $D = 0$ , the poles of the system, are as expected, on the imaginary

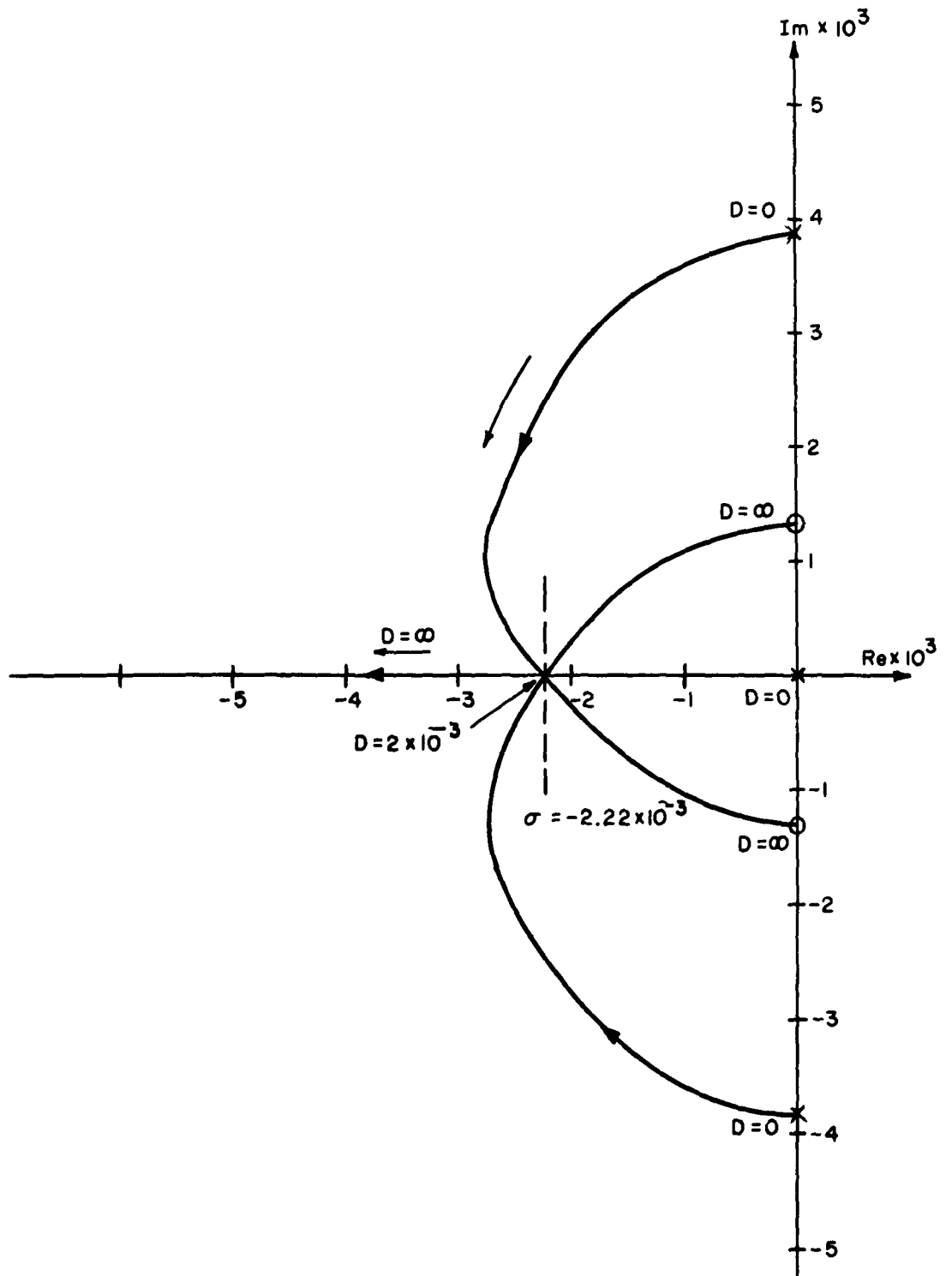


Fig. 3-6 Root Locus as a Function of the Damping Coefficient for Optimization with a Third Order Pole on the Real Axis

axis, and the system is unstable. Maximum stability occurs when

$D = 2.0 \times 10^{-3} \frac{\text{ft. lbs.}}{\text{rad/sec.}}$ . For this value of  $D$ , a third order pole exists on the

real axis; the values of  $H_r$ ,  $K$ , and  $I_g$  were chosen so that this would happen. As  $D$  is increased beyond this value, the free response of the system deteriorates. It should be noted that for very large  $D$ , two of the roots return to the imaginary axis. This occurs because for a very large damping coefficient, relative motion between the gyroscope gimbal and the body cannot occur and thus the system behaves as a rigid body.

b) Root-locus as a function of the angular Momentum of the rotor ( $H_r$ ) (see Fig. 3-7).

For this case the characteristic equation can be factored into the form:

$$(s^3 + a s^2 + b s + d) \left( 1 + \frac{c s H_r^2}{s^3 + a s^2 + b s + d} \right) = 0 \quad (3.44)$$

$$\text{where } a = \frac{D}{I_g} \quad (3.45)$$

$$b = \frac{K}{I_x} \quad (3.46)$$

$$c = \frac{1}{I_x I_g} \quad (3.47)$$

$$d = \frac{K D}{I_x I_g} \quad (3.48)$$

For the chosen values of  $D$ ,  $I_g$ , and  $K$ , the poles and zeros of the expression

$$\frac{c s H_r^2}{s^3 + a s^2 + b s + d} \quad (3.49)$$

become

$$z_1 = 0 \quad (3.50)$$

$$p_1 = -6.7 \times 10^{-3} \quad (3.51)$$

$$p_2, p_3 = \pm j (1.29 \times 10^{-3})$$

It is noted from the root-locus plot (Fig. 3-7) that the damped radian frequency increases as  $H_r$  increases. This is to be expected since as can be seen from the

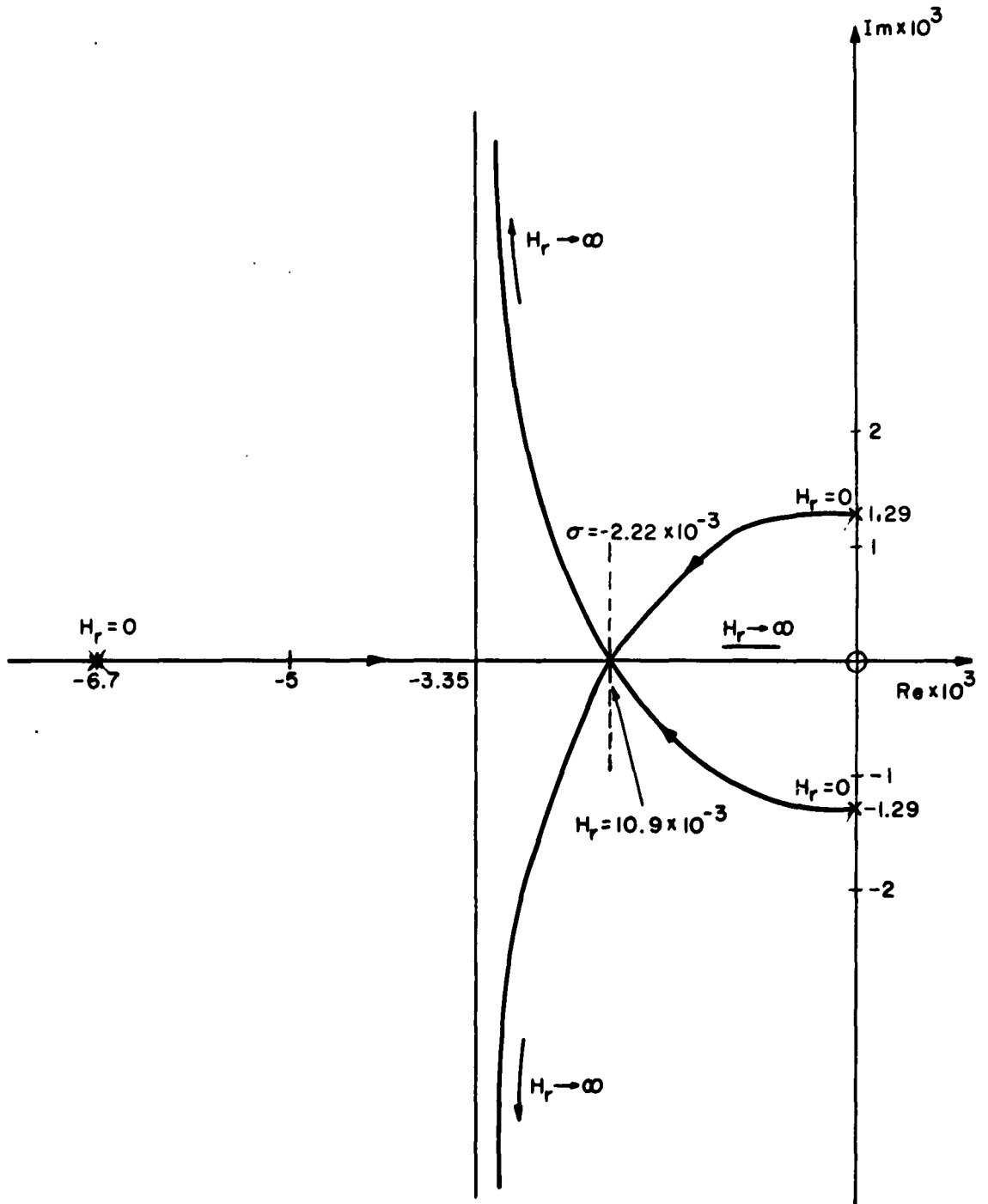


Fig. 3-7 Root Locus as a Function of the Angular Momentum of the Rotor for Optimization with a Third Order Pole on the Real Axis

characteristic equation (3.10), the coefficient of the linear term is given by

$$\frac{K}{I_x} + \frac{H_r^2}{I_x I_g} \quad (3.52)$$

Therefore,  $H_r$  affects the system in the same manner as the spring term. Hence as  $H_r$  increases, the system becomes "stiffer" and therefore the damped radian frequency increases.

c) Root-locus as a function of the spring constant (K) (see Fig. 3-8).

For this case the characteristic equation (3.10) can be factored into the form:

$$(s^3 + a s^2 + b s) \left( 1 + \frac{K(c s + d)}{s^3 + a s^2 + b s} \right) \quad (3.53)$$

where  $a = \frac{D}{I_g}$  (3.54)

$$b = \frac{H_r^2}{I_x I_g} \quad (3.55)$$

$$c = \frac{1}{I_x} \quad (3.56)$$

$$d = \frac{D}{I_x I_g} \quad (3.57)$$

For the chosen values of  $D$ ,  $I_g$  and  $H_r$ , the poles and zeros of the expression

$$\frac{K(c s + d)}{s^3 + a s^2 + b s} \quad (3.58)$$

become

$$z_1 = -6.67 \times 10^{-3} \quad (3.59)$$

$$p_1 = 0 \quad (3.61)$$

$$p_2, p_3 = -3.34 \times 10^{-3} \pm j(1.37 \times 10^{-3})$$

For large values of  $K$ , the characteristic equation (3.10) reduces to

$$s^3 + s^2 \frac{D}{I_g} + s \frac{K}{I_x} + \frac{K D}{I_x I_g} = \left( s + \frac{D}{I_g} \right) \left( s^2 + \frac{K}{I_x} \right) \quad (3.61)$$

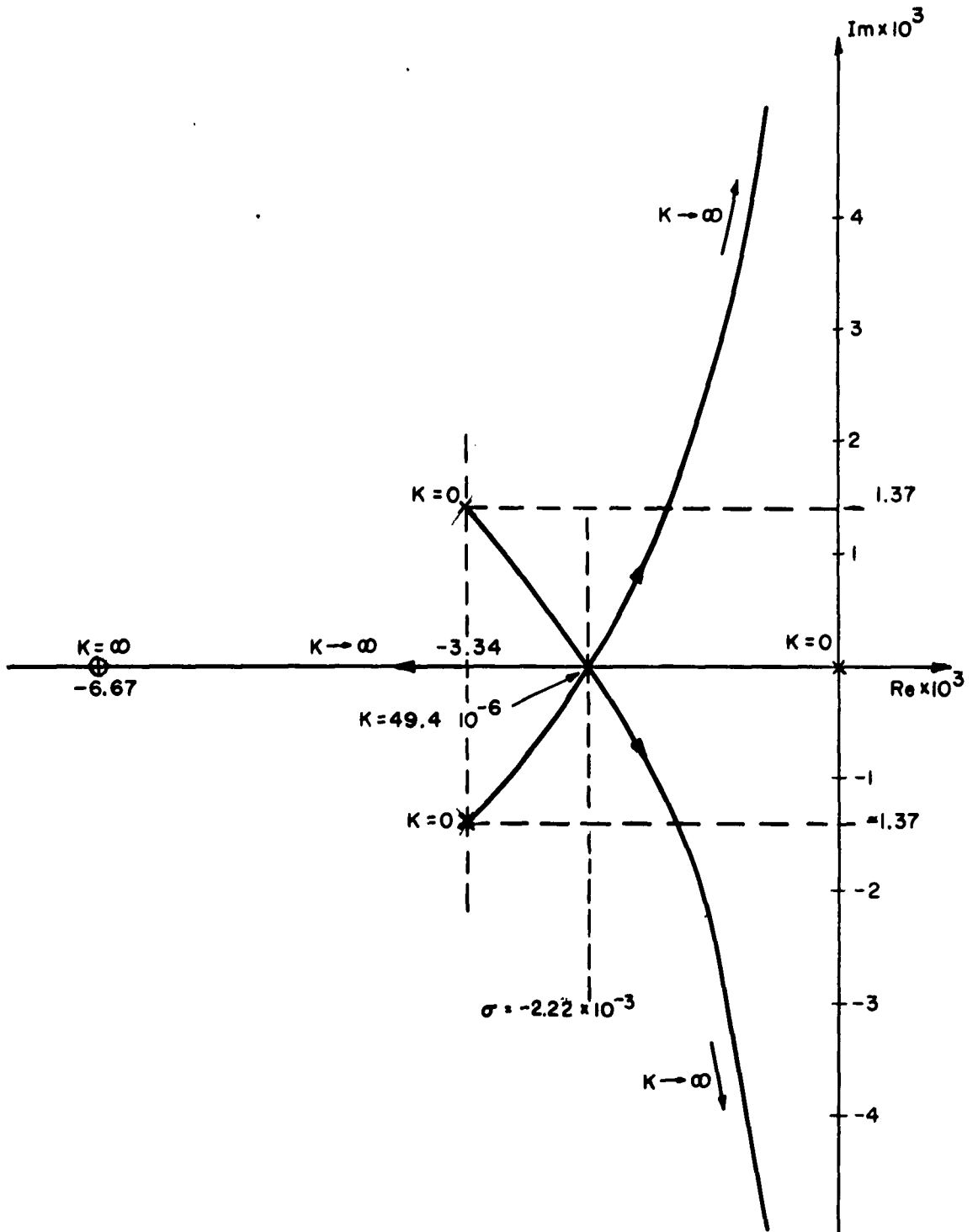


Fig. 3-8 Root Locus as a Function of the Spring Constant for Optimization with a Third Order Pole on the Real Axis

For large  $K$ , the system will have a pole on the real axis at  $s = -\frac{D}{I_g}$  and will oscillate with a radian frequency of  $\omega_n = \sqrt{\frac{K}{I_x}}$ . Hence as  $K$  is increased, the natural radian frequency increases, and an undamped oscillatory mode is approached. This is to be expected since as  $K$  is increased, the system becomes "stiffer" and more energy is stored in the spring which will take longer to dissipate.

d) Root-locus as a function of moment of inertia of the gyroscope ( $I_g$ ) (see Fig. 3-9)

For this case the characteristic equation (3.10) can be factored into the form:

$$(s^3 + b s) \left( 1 + \frac{1}{I_g} \frac{a s^2 + c s + d}{s(s^2 + b)} \right) \quad (3.62)$$

$$\text{where } a = D \quad (3.63)$$

$$b = \frac{K}{I_x} \quad (3.64)$$

$$c = \frac{H_r^2}{I_x} \quad (3.65)$$

$$d = \frac{K D}{I_x} \quad (3.66)$$

For the chosen values of  $D$ ,  $H_r$  and  $K$  the poles and zeros of the expression

$$\frac{1}{I_g} \frac{a s^2 + c s + d}{s(s^2 + b)} \quad (3.67)$$

become

$$p_1 = 0 \quad (3.68)$$

$$p_2, p_3 = \pm j (1.29 \times 10^{-3})$$

$$z_1, z_2 = -0.99 \times 10^{-3} \pm j (0.82 \times 10^{-3}) \quad (3.69)$$

When the moment of inertia of the gyroscope becomes very large, the characteristic equation (3.10) reduces to

$$s(s^2 + \frac{K}{I_x}) = 0 \quad (3.70)$$



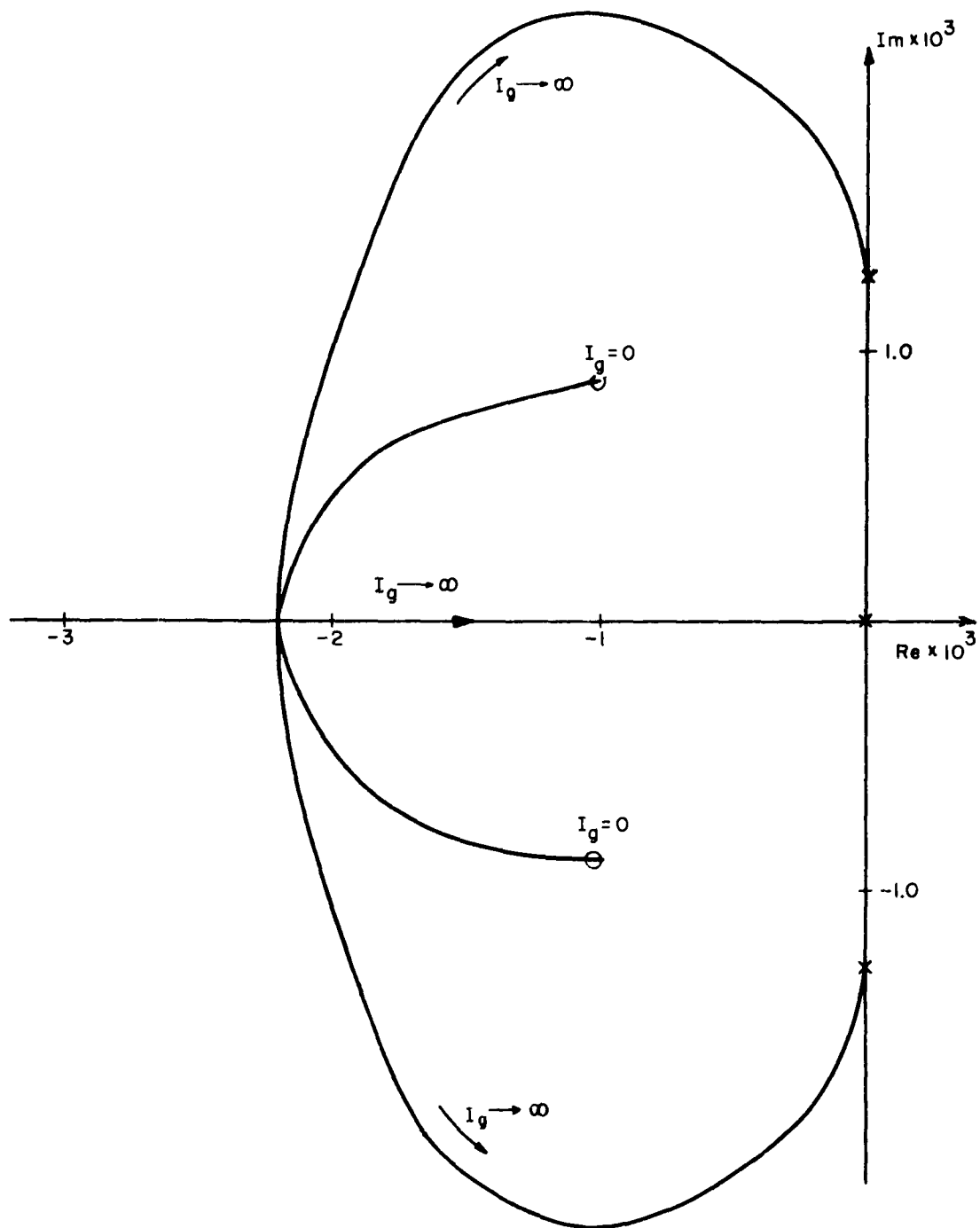


Fig. 3-9 Root Locus as a Function of the Moment of Inertia of the Gyroscope for Optimization with a Third Order Pole on the Real Axis

The roots of this equation are

$$s = 0, s = \pm j \sqrt{\frac{K}{I_x}} \quad (3.71)$$

Therefore, as  $I_g$  increases the damping of the system decreases because the gyroscope precession rate becomes small and relative motion between the gyroscope gimbal and the body is curtailed.

Now consider case (ii) where optimization is obtained with a real pole and a pair of complex conjugate poles all with equal real parts. For this case, the characteristic equation (3.10) must reduce to the form:

$$(s + \sigma)(s + \sigma - j\omega_d)(s + \sigma + j\omega_d) = \quad (3.72)$$

$$s^3 + 3\sigma s^2 + (\omega_n^2 + 2\sigma^2)s + \sigma\omega_n^2 = 0$$

where

$$\omega_n^2 = \omega_d^2 + \sigma^2 \quad (3.73)$$

Clearly  $\sigma^2$  cannot be made larger than  $\omega_n^2$  putting an upper bound on the damping coefficient that can be used in this type of optimization. Equating expression (3.72) to the characteristic equation (3.10) and comparing like order terms yields:

$$\frac{D}{I_g} = 3\sigma \quad (3.74)$$

$$\frac{K I_g + H_r^2}{I_x I_g} = \omega_n^2 + 2\sigma^2 \quad (3.75)$$

$$\sigma \omega_n^2 = \frac{K D}{I_x I_g} \quad (3.76)$$

Solving for  $\omega_n^2$  yields:

$$\omega_n^2 = \frac{3 K}{I_x} \quad (3.77)$$

It is noted from the above equations that three independent quantities must be specified.  $K$  and  $I_g$  will be fixed, and  $H_r$ ,  $\sigma$ , and  $\omega_d$  will be obtained as a function of  $D$ . As in the previous case, the moment of inertia of the body plus gyroscope ( $I_x$ ) will be taken to be 30-slug-ft.<sup>2</sup> and the moment of inertia of the gyroscope will be taken to be 1% of  $I_x$  or 0.3 slug-ft.<sup>2</sup>  $K$  will be chosen for convenience to be  $10^{-5} \frac{\text{ft. lbs.}}{\text{rad}}$ . Corresponding to this value of  $K$ ,  $\omega_n^2 = 10^{-6} \left(\frac{\text{rad}}{\text{sec}}\right)^2$  and the upper bound for  $D$  is

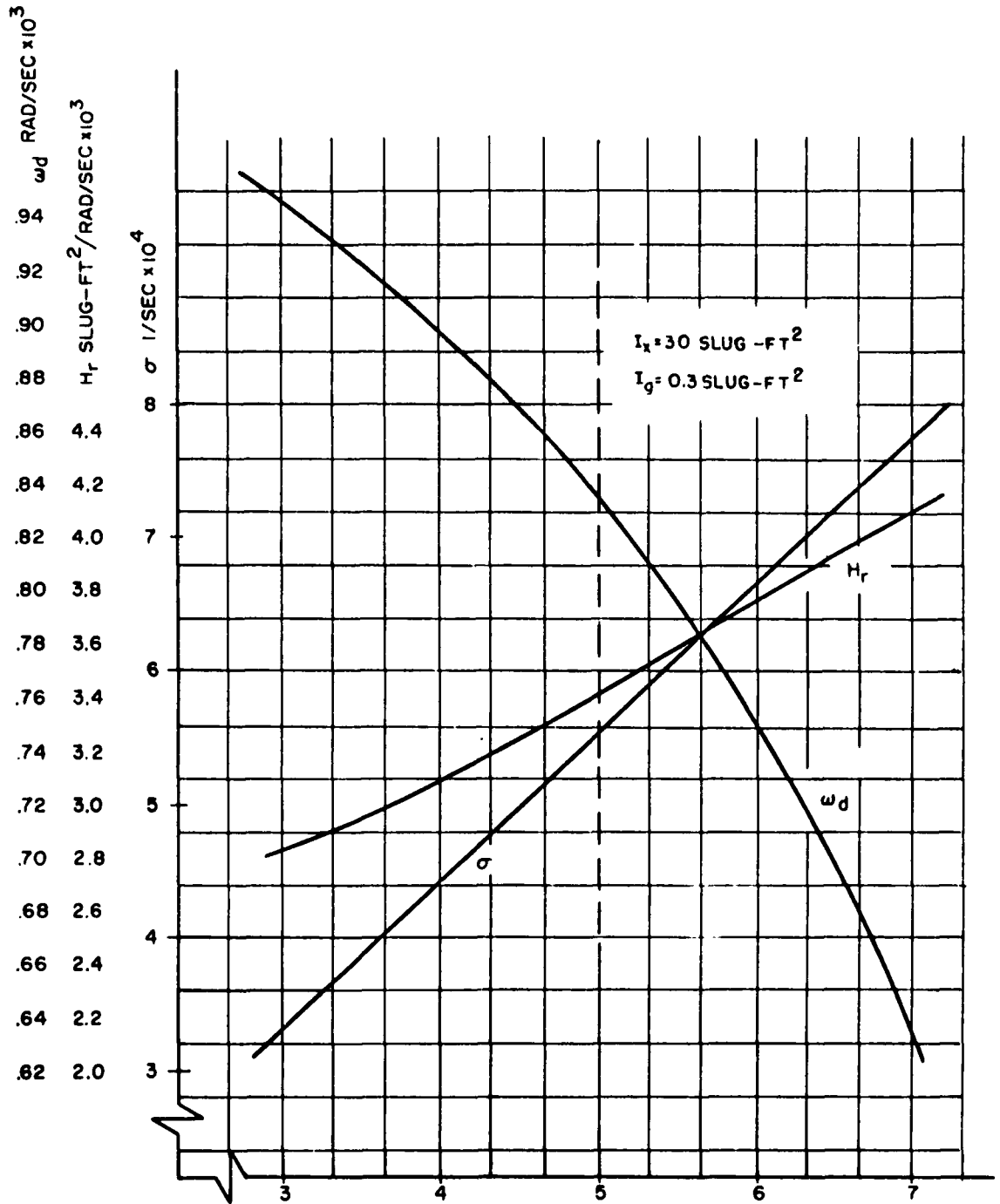


Fig. 3-10 Variation of  $\sigma$ ,  $H_r$  and  $\omega_d$  with the Damping Coefficient for Optimization with a Real Pole and a Pair of Complex Poles

$0.9 \times 10^{-3} \frac{\text{ft. -lbs.}}{\text{rad/sec.}}$ . Using these values,  $H_r$ ,  $\sigma$ , and  $\omega_d$  are plotted as a function of damping. (see Fig. 3-10).

The free response of a system that has a pole on the real axis and a pair of complex conjugate poles, is given by:

$$\theta(t) = K_1 e^{-\sigma t} + K_2 e^{-\sigma t} \cos(\omega_d t + \phi) \quad (3.78)$$

The settling time of this system is clearly

$$t_s = \frac{4}{\sigma} \quad (3.79)$$

In Fig. 3-11, the settling time is plotted as a function of damping coefficient as a percentage of a 90 minute orbit. Comparing Fig. 3-11 with Fig. 3-5 one sees that faster settling times can be obtained for the situation employing a pair of complex poles. This is accomplished at the expense of permitting the system to ring while it settles.

As was done previously, the root-loci of the system will be sketched as a function of the damping coefficient ( $D$ ), the angular momentum of the rotor ( $H_r$ ), the spring constant ( $K$ ) and the moment of inertia of the gyroscope ( $I_g$ ). From Fig. 3-10 it is seen that for  $I_x = 30$ ,  $I_g = 0.3$ ,  $K = 10^{-5}$  the complex poles and the real pole will have equal real parts when  $D = 5 \times 10^{-4}$ ,  $H_r = 3.41 \times 10^{-3}$ . It is also seen from Fig. 3-10 that corresponding to these parameter values,  $\sigma = 5.55 \times 10^{-3}$  and  $\omega_d = 0.835 \times 10^{-3}$ . In sketching the root-loci, each of the parameters will be in-turn varied while the remaining parameters are held fixed at the values given above.

a) Root-locus as a function of damping coefficient ( $D$ ) (See Fig. 3-12).

The characteristic equation (3.10) can be factored into the form of equation (3.35). Substituting the chosen parameters into equations (3.40) and (3.41) yields:

$$p_1 = 0 \quad (3.80)$$

$$p_2, p_3 = \pm j(1.28 \times 10^{-3})$$

$$z_1, z_2 = \pm j(0.57 \times 10^{-3}) \quad (3.81)$$

At  $D = 0$  the poles of the system are on the imaginary axis and the system is unstable. As  $D$  becomes very large, two of the roots return to the imaginary axis causing the free response of the system to deteriorate. As in the case of optimization with a third order pole, the system begins to behave as a rigid body.

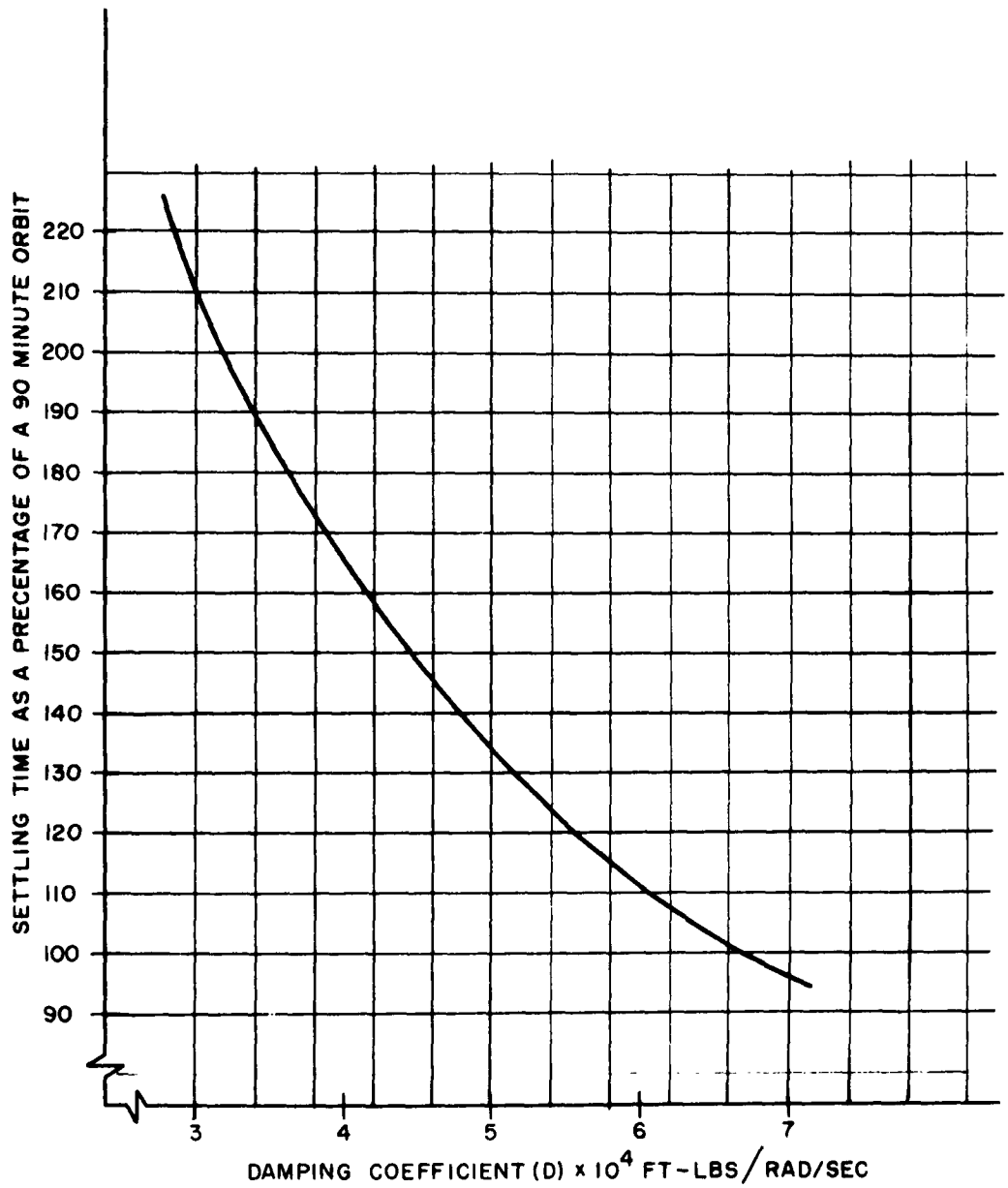


Fig. 3-11 Settling Time as a Function of the Damping Coefficient for Optimization with a Real Pole and a Pair of Complex Poles

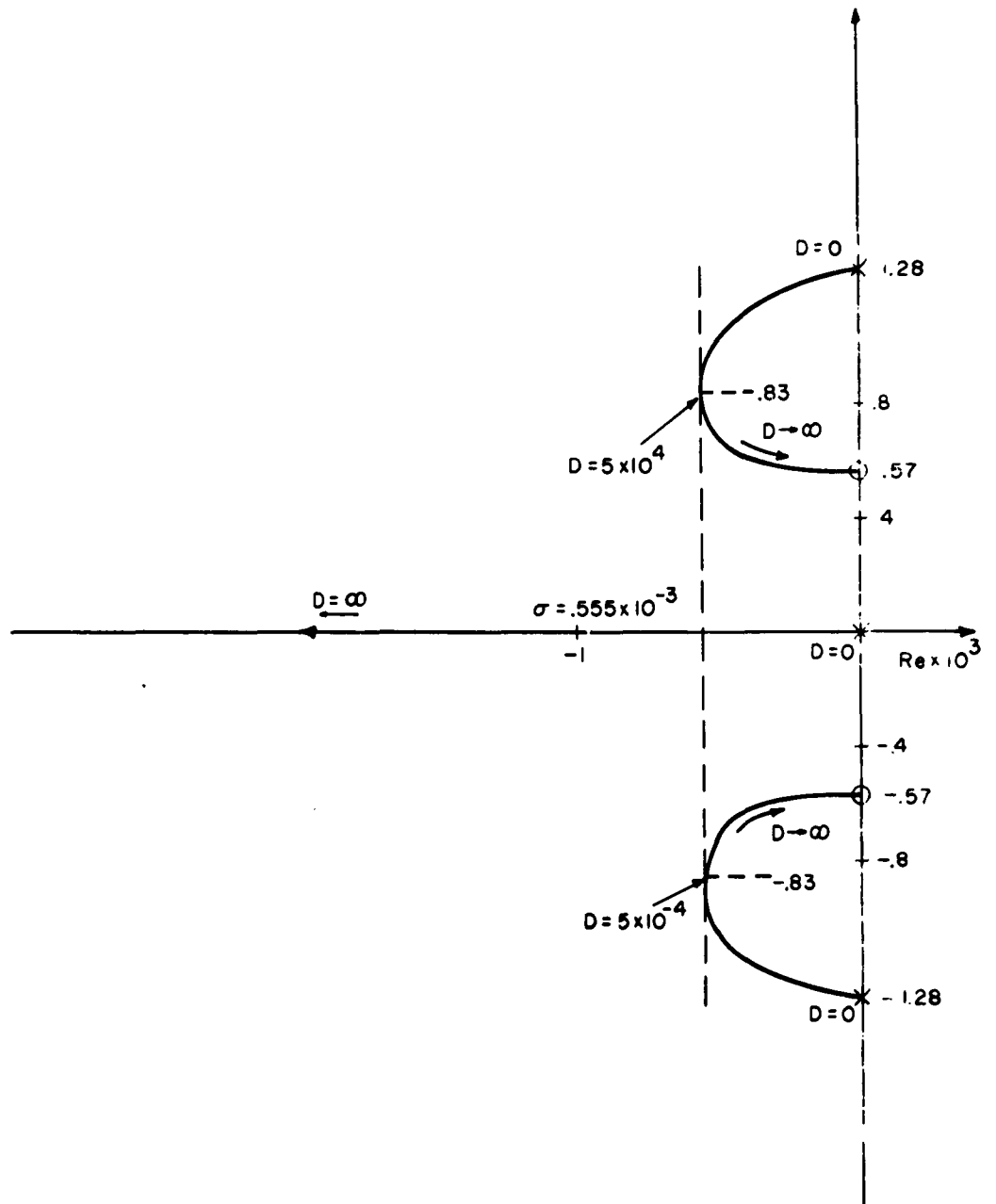


Fig. 3-12 Root Locus as a Function of the Damping Coefficient for Optimization with a Real Pole and a Pair of Complex Poles

When  $D = 5 \times 10^{-4}$  all the roots of the characteristic equation have equal real parts. This is the approximate value of  $D$  where optimum damping occurs. An examination of Fig. 3-10 indicates that the root-locus appears tangent to  $\sigma = -5.55 \times 10^{-3}$ . In actuality however, there is a range for  $D$  where all the roots of the characteristic equation lie to the left of the line  $\sigma = -5.55 \times 10^{-3}$ . This can be shown in the following manner:  $(s + |\sigma|)$  is substituted for  $s$  in equation (3.10) thereby increasing all the roots of the characteristic equation by  $|\sigma|$ . The resulting equation is:

$$s^3 + s^2 \left( -3\sigma + \frac{D}{I_g} \right) + s \left( 5\sigma^2 - \frac{2\sigma D}{I_g} + \omega_n^2 \right) - 3|\sigma|^3 + \frac{D\sigma^2}{I_g} + \frac{D\omega_n^2}{3I_g} - |\sigma|\omega_n^2 = 0 \quad (3.82)$$

If for some range of  $D$  all the roots of this equation lie in the left-half plane, then for that range of  $D$ , all the roots of the characteristic equation (3.10) must lie to the left of the line  $\sigma = -5.55 \times 10^{-3}$ .

Applying the Routh test to equation (3.82), it is seen that the values of  $D$  which place the roots in the left-half plane must satisfy the inequality

$$\frac{2\sigma D^2}{I_g^2} + D \left( -\frac{2\omega_n^2}{3I_g} - \frac{10\sigma^2}{I_g} \right) + 12\sigma^3 + 2\sigma\omega_n^2 > 0 \quad (3.83)$$

If the left side of the above expression is set equal to zero, and the resulting quadratic equation in  $D$  is solved, either

- 1) a pair of complex conjugate roots
- 2) two equal positive real roots
- 3) two distinct positive real roots

is obtained. The first case indicates that all of the roots of the characteristic equation never exist simultaneously on or to the left of the line  $\sigma = -5.55 \times 10^{-3}$ . The second case indicates that for some value of  $D$  the complex pair of roots of the characteristic equation lie on the line  $\sigma = -5.55 \times 10^{-3}$ , and the real root lies either on or to the left of the line. The third case indicates that there is some range of  $D$  where all the roots of the characteristic equation lie to the left of the line  $\sigma = -5.55 \times 10^{-3}$ . For the equation under consideration, the two roots are indeed positive and distinct.

$$D_1 = I_g \left( \frac{\omega_n^2}{3\sigma} + 2\sigma \right) \quad (3.84)$$

$$D_2 = 3\sigma I_g \quad (3.85)$$

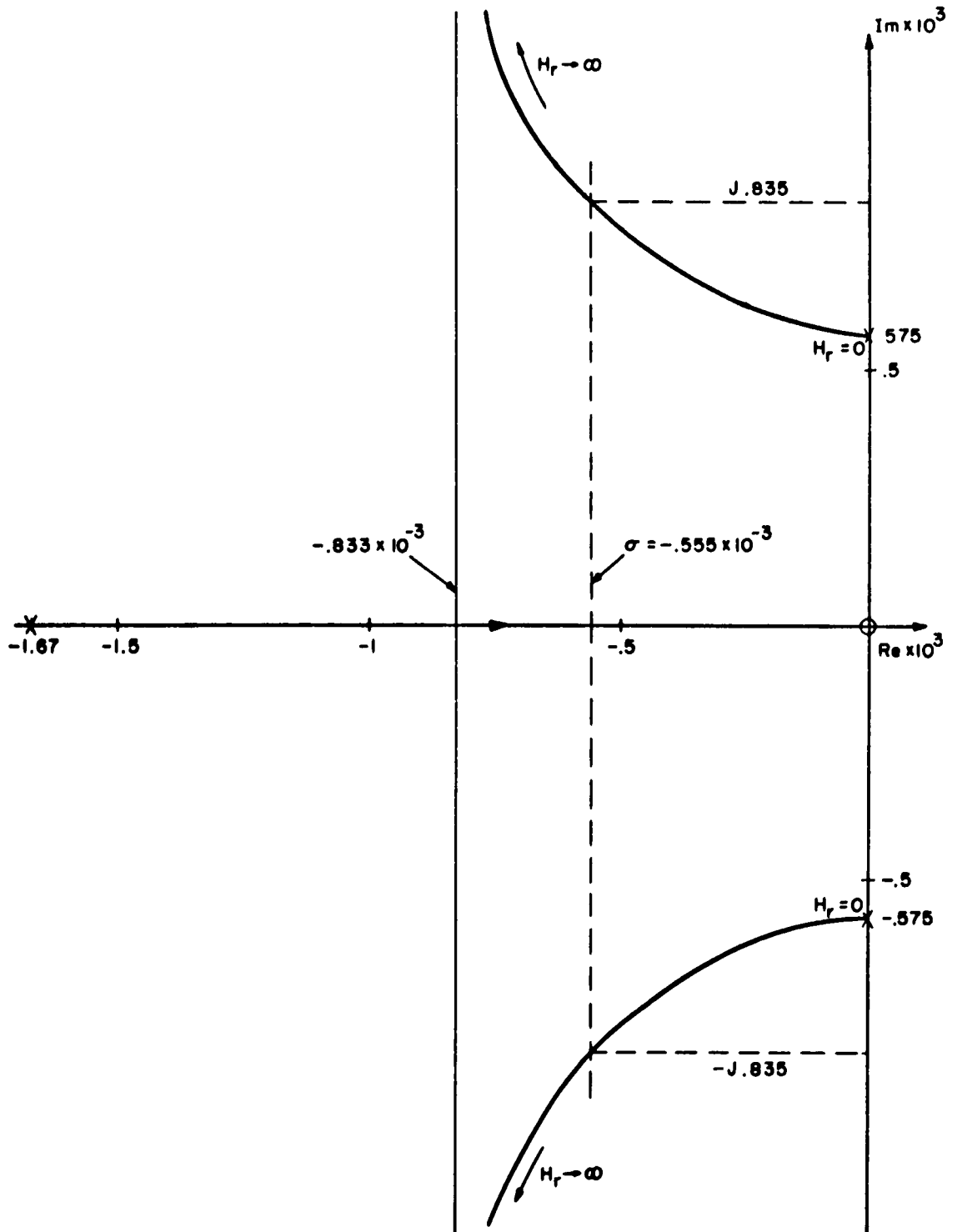


Fig. 3-13 Root Locus as a Function of the Angular Momentum of the Rotor for Optimization with a Real Pole and a Pair of Complex Poles



Hence it is assured that there is a range of  $D$  where a better settling time, than predicted by the optimization procedure, is possible. From Fig. 3-12 it is obvious that the difference is slight and the optimization procedure will give very close to the best possible settling time. The reason for the optimization procedure not yielding the smallest settling time is that the procedure assumed that the sum of the roots remained constant. This is not true since the sum of the roots depends on  $D$ , and  $D$  is varying (see equation 3.16)

b) Root-locus as a function of the angular momentum of the rotor ( $H_r$ ). See Fig. 3-13).

For this case the characteristic equation (3.10) can be factored into the form of equation (3.44). Substituting the chosen parameters, equations (3.50) and (3.51) become

$$z_1 = 0 \quad (3.86)$$

$$p_1 = -1.667 \times 10^{-3} \quad (3.87)$$

$$p_2, p_3 = \pm j (0.575 \times 10^{-3})$$

As  $H_r$  is increased, the damped frequency of oscillation increases. The explanation for this is identical to that given for the case of optimization with a third order pole when the corresponding root locus was discussed.

c) Root-locus as a function of the spring constant ( $K$ ), (see Fig. 3-14).

For this case the characteristic equation (3.10) can be factored into the form of equation (3.53). Substituting the chosen parameters, equations (3.59) and (3.60) becomes

$$z_1 = -1.67 \times 10^{-3} \quad (3.88)$$

$$p_1 = 0 \quad (3.89)$$

$$p_2, p_3 = -0.833 \times 10^{-3} \pm j (0.77 \times 10^{-3})$$

The analysis of the system, for large values of  $K$  is identical to that described for the case of optimization with a third order pole when the corresponding root-locus was discussed.

d) Root-locus as a function of gyroscope moment of inertia ( $I_g$ ). (see Fig. 3-15)

For this case, the characteristic equation (3.10) can be factored into the

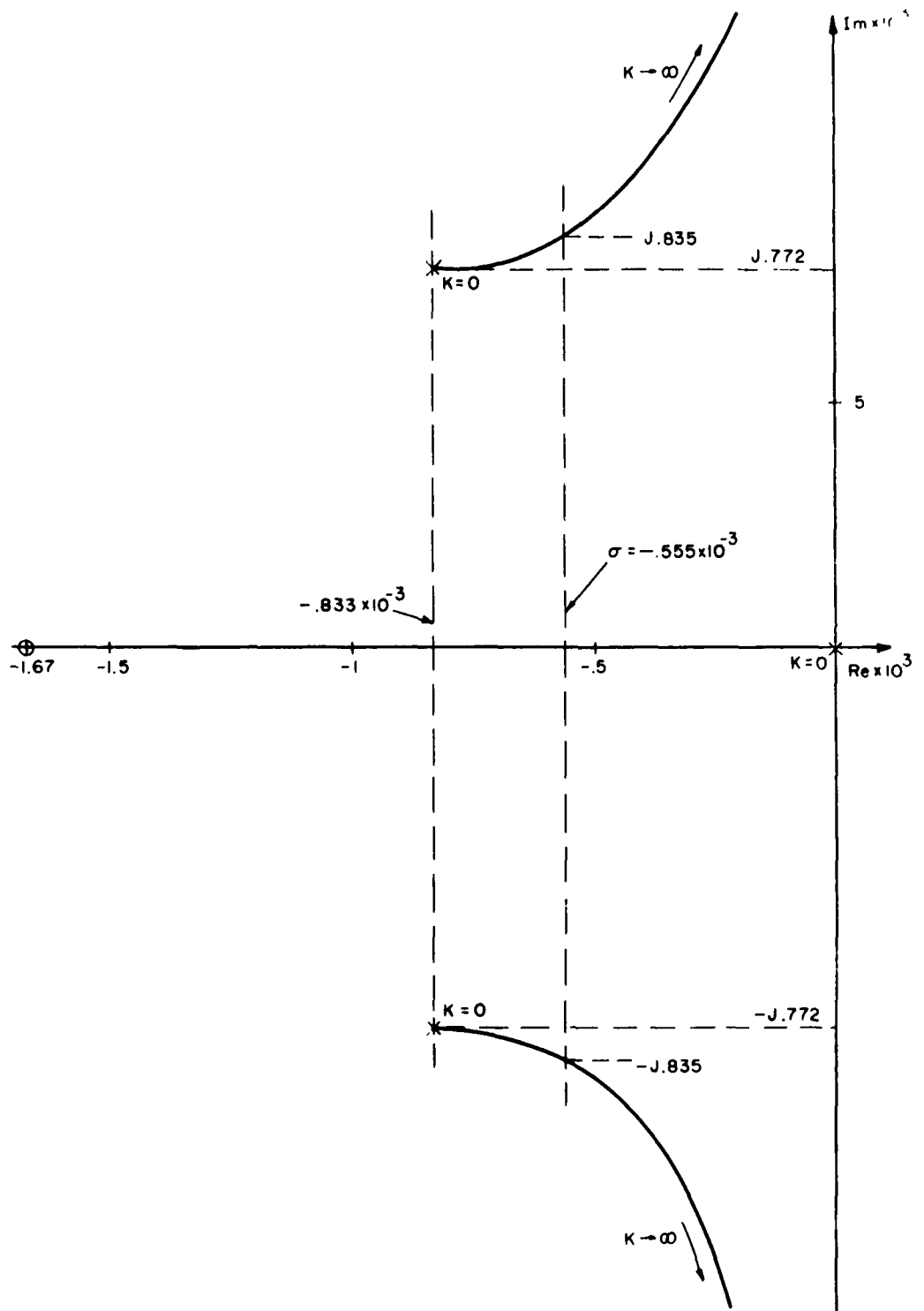


Fig. 3-14 Root Locus as a Function of the Spring Constant for Optimization with a Real Pole and a Pair of Complex Poles

form of equation (3.62). Substituting the chosen parameters, equations (3.68) and (3.69) become

$$p_1 = 0 \quad (3.90)$$

$$p_2, p_3 = \pm j (0.577 \times 10^{-3})$$

$$z_1, z_2 = -0.387 \times 10^{-3} \pm j (0.43 \times 10^{-3}) \quad (3.91)$$

It is seen from Fig. 3-15 that there is a range of  $I_g$  where the response of the system is better than that obtained by the optimization procedure. However, the optimization procedure will yield a value which is reasonably close. The reason for the optimization procedure not yielding the best result is that the sum of the roots depend on  $I_g$  and therefore, for a varying  $I_g$ , is not constant. (See equation (3.16)). The analysis of the system for large values of  $I_g$  is identical to that described for the case of optimization with a third order pole when the corresponding root-locus was discussed.

### C) Analysis of a Simple Configuration Employing Direct Gyroscope Damping

Direct Damping can be demonstrated with the following example. Consider the geometry shown in Fig. 3-16. In the geometry pictured, the body is constrained to rotate, with a spring type restoring torque, about the  $z$  axis of the body. The gyroscope is again constrained to precess relative to the body about the  $z$  axis. Consider a disturbance torque applied to the body about its  $z$  axis. In this case one obtains

$$T_d = I_z \ddot{\theta}_z + K \theta_z + D(\dot{\theta}_z - \dot{\theta}_g) \quad (3.92)$$

where

$I_z$  is the moment of inertia of the body about the  $z$  axis of the body

$K$  is the spring constant

$D$  is the coefficient of damping between the body and the gyroscope gimbal.

The torque applied to the gyroscope is given by

$$D(\dot{\theta}_z - \dot{\theta}_g) = I_g \ddot{\theta}_g \quad (3.93)$$

where

$I_g$  is the moment of inertia of the gyroscope about the  $z$  axis of the body.

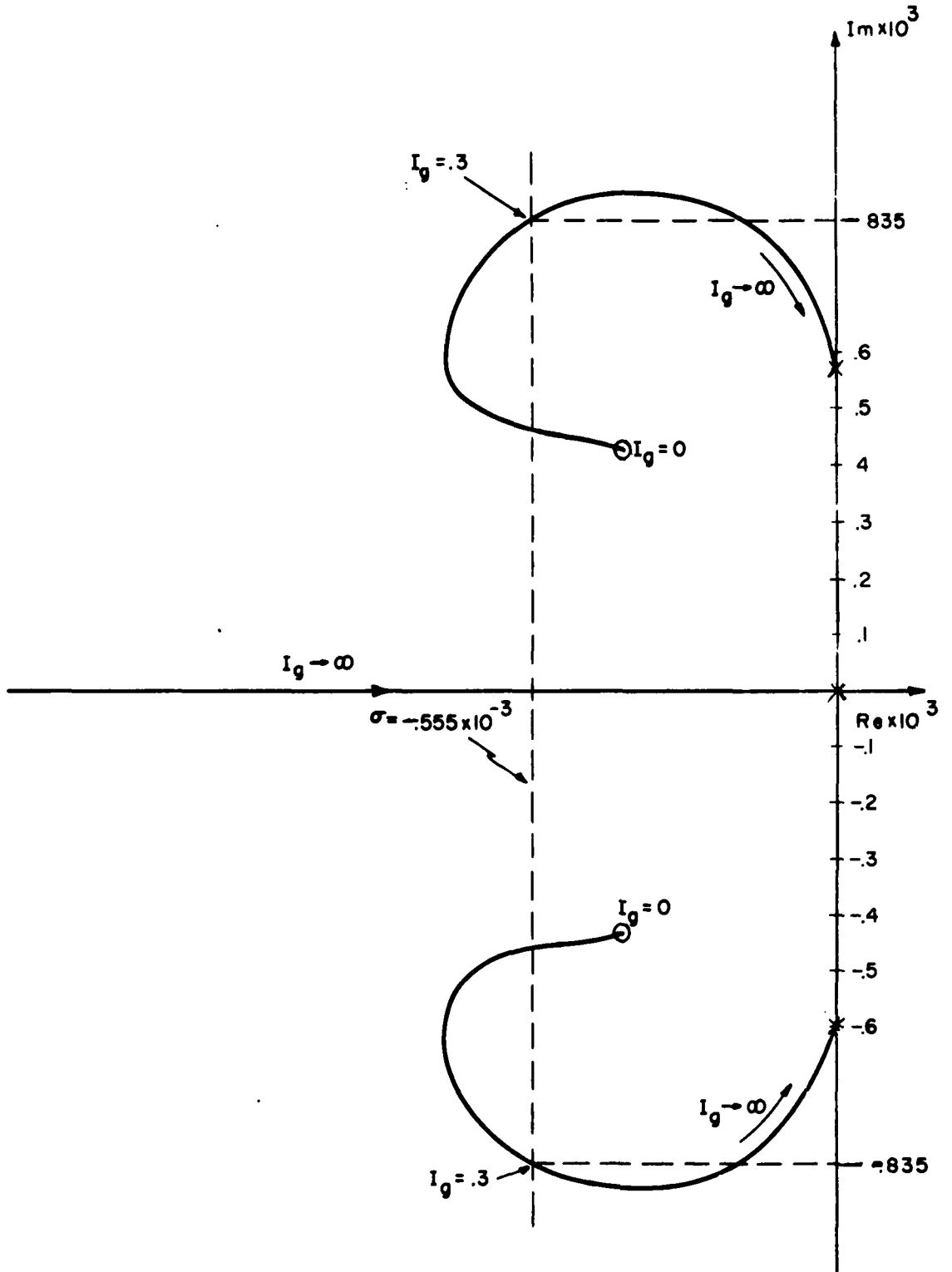


Fig. 3-15 Root Locus as a Function of the Moment of Inertia of the Gyroscope for Optimization with a Real Pole and a Pair of Complex Poles.

Introducing Laplace transform notation, one obtains

$$T_d(s) = I_z s^2 \theta_z(s) + K \theta_z(s) + D s \theta_z(s) - D s \theta_g(s) \quad (3.94)$$

and

$$D s \theta_z(s) - D s \theta_g(s) = I_g s^2 \theta_g(s) \quad (3.95)$$

Solving these equations for  $\theta_z(s)$  yields:

$$T_d(s) [D + s I_g] = \theta_z(s) \left[ s^3 I_z I_g + s^2 D (I_g + I_z) + s I_g K + K D \right] \quad (3.96)$$

Therefore the characteristic equation for a system employing direct damping is:

$$s^3 + s^2 \frac{D(I_z + I_g)}{I_z I_g} + \frac{sK}{I_z} + \frac{KD}{I_z I_g} = 0 \quad (3.97)$$

Applying the Routh stability criterion yields as a necessary and sufficient condition for stability

$$D(I_g + I_z) K I_g - I_z I_g K D > 0 \quad (3.98)$$

which reduces to

$$K D I_g^2 > 0$$

which is clearly always satisfied. Therefore the system is always stable. This was intuitively expected.

As in the case of indirect damping, the characteristic equation (3.97) has only real coefficients. Therefore, the set of roots can only be of two types, i e.

- 1) three real roots
- 2) one real root and a pair of complex conjugate roots.

The sum of the real part of the roots of equation (3.97) is given by:

$$\text{Re}(r_1) + \text{Re}(r_2) + \text{Re}(r_3) = - \frac{D(I_g + I_z)}{I_z I_g} \quad (3.100)$$

For a given body (fixed  $I_z$ ), and for a fixed  $D$  and  $I_g$ , the sum of the real part of the roots is constant. This strongly suggests that optimum damping can be obtained through the same procedures used for indirect damping. It should be noted that the angular momentum of the rotor ( $H_r$ ) does not enter into the characteristic equation (3.97), hence there are less parameters that can be adjusted to meet the required constraints than for the case of indirect damping. It will be shown that neither of the two optimization methods will yield any realizable results.

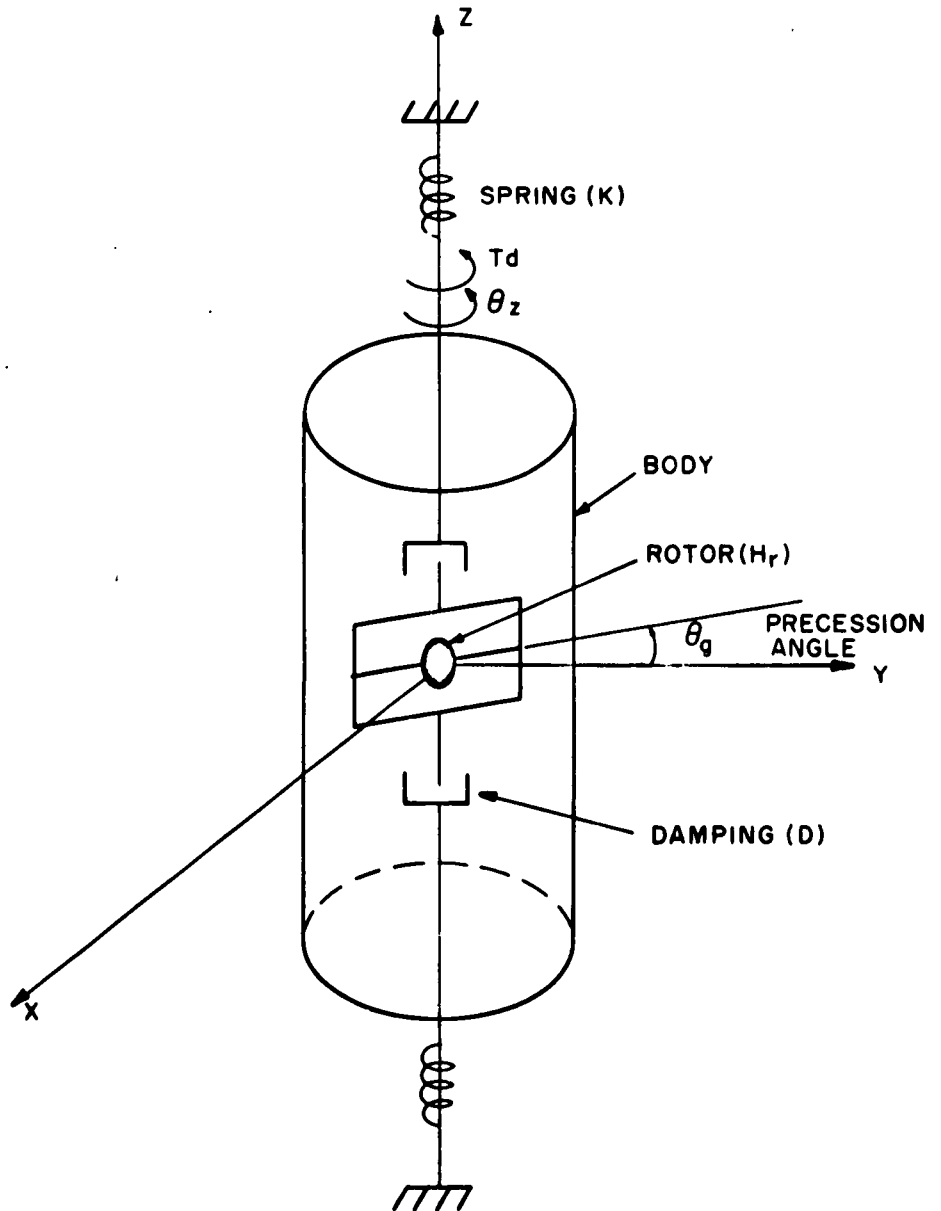


Fig. 3-16 Configuration to Illustrate Direct Gyroscope Damping

Optimization with a third order pole on the real axis will be considered first. The characteristic equation (3.97) must again reduce to the form of equation (3.17). Therefore:

$$s^3 + 3\sigma s^2 + 3\sigma^2 s + \sigma^3 = s^3 + s^2 \frac{D(I_g + I_z)}{I_g I_z} + \frac{sK}{I_z} + \frac{KD}{I_z I_g} \quad (3.101)$$

Equating coefficients yields:

$$3\sigma = \frac{D(I_g + I_z)}{I_g I_z} \quad (3.102)$$

$$3\sigma^2 = \frac{K}{I_z} \quad (3.103)$$

$$\sigma^3 = \frac{KD}{I_z I_g} \quad (3.104)$$

A solution to the above equation is only possible if

$$I_g = 8I_z \quad (3.105)$$

Clearly, this is not a practical situation; optimization of this form is not attainable.

Now consider optimization with one real root and a pair of complex conjugate roots. The characteristic equation (3.97) must reduce to the form of equation (3.72). Therefore:

$$s^3 + 3\sigma s^2 + (\omega_n^2 + 2\sigma^2) s + \sigma \omega_n^2 = s^3 + s^2 \frac{D(I_g + I_z)}{I_z I_g} + \frac{sK}{I_z} + \frac{KD}{I_z I_g} \quad (3.106)$$

Equating like order coefficients yields:

$$3\sigma = \frac{D(I_g + I_z)}{I_g I_z} \quad (3.107)$$

$$\omega_n^2 + 2\sigma^2 = \frac{K}{I_z} \quad (3.108)$$

$$\sigma \omega_n^2 = \frac{KD}{I_z I_g} \quad (3.109)$$

Combining equation (3.107) and (3.109) one obtains

$$\omega_n^2 = \frac{3K}{I_g + I_z} \quad (3.110)$$

Substituting equation (3.110) into equation (3.108) yields:

$$\frac{K}{I_z} - \frac{3K}{I_g + I_z} = 2\sigma^2 \quad (3.111)$$

Since  $\sigma^2$  must be greater than zero,

$$\frac{K}{I_z} > \frac{3K}{I_g + I_z} \quad (3.112)$$

or

$$I_g > 2I_z \quad (3.113)$$

As for the case of optimization with a third order pole on the real axis, optimization with a real pole and a pair of complex conjugate poles requires the moment of inertia of the gyroscope to be larger than the moment of inertia of the vehicle itself. This is, of course, not practical.

In order to obtain some appreciation as to the nature of direct damping, root-loci of the system will be sketched as a function of the damping coefficient (D), the spring constant (K) and the moment of inertia of the gyroscope ( $I_g$ ). The following values will be chosen for the parameters:

$$D = 2 \times 10^{-3} \quad \frac{\text{ft.-lbs.}}{\text{rad/sec.}}$$

$$K = 49.4 \times 10^{-6} \quad \text{ft.-lbs./rad}$$

$$I_z = 30 \quad \text{slug-ft.}^2$$

$$I_g = 0.3 \quad \text{slug-ft.}^2$$

These values correspond to those used for optimization of indirect damping with a third order pole.

a) Root-locus as a function of damping coefficient (D). (See Fig. 3-17).

For this case the characteristic equation (3.97) can be factored into the form:

$$(s^3 + bs) \left( 1 + \frac{D(as^2 + c)}{s(s^2 + b)} \right) = 0 \quad (3.114)$$



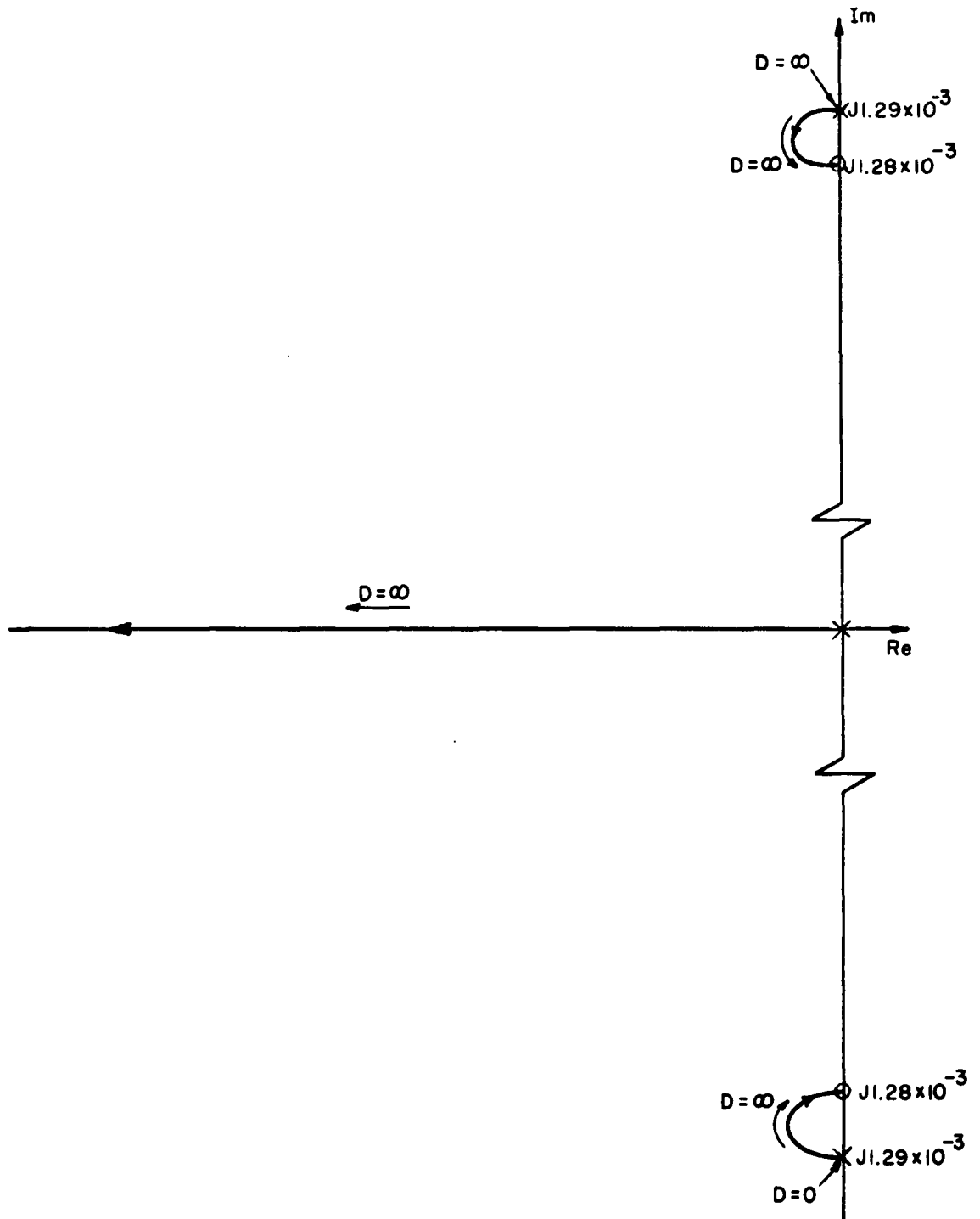


Fig. 3-17 Root Locus as A Function of the Damping Coefficient for Direct Damping

where

$$a = \frac{I_g + I_z}{I_g I_z} \quad (3.115)$$

$$b = \frac{K}{I_z} \quad (3.116)$$

$$c = \frac{K}{I_z I_g} \quad (3.117)$$

Substituting the chosen values, the poles and zeros of the expression

$$\frac{as^2 + c}{s(s^2 + b)} \quad (3.118)$$

become

$$z_1, z_2 = \pm j(1.28 \times 10^{-3}) \quad (3.119)$$

$$p_1 = 0 \quad (3.120)$$

$$p_2, p_3 = \pm j(1.29 \times 10^{-3})$$

It is seen from Fig. 3-17 that very little damping is attainable. When indirect damping was used, it was possible to obtain considerably more damping for the same parameters. The reason for this is that in the indirect case, relative motion between the gyroscope gimbal and the body was produced as a result of gyroscopic precession. The velocity gain of the gyroscope, the ratio of precession velocity to input velocity, is available to give a large relative velocity for a small input velocity. With direct damping however, relative velocity between the gyroscope gimbal and the body is the same as the input velocity, hence no velocity gain is present.

b) Root-locus as a function of the spring constant (K) (See Fig. 3-18)

For this case the characteristic equation (3.97) can be factored into the form:

$$(s^3 + as^2) \left( 1 + \frac{K(bs + c)}{s^2(s + a)} \right) \quad (3.121)$$

where

$$a = \frac{D(I_g + I_z)}{I_g I_z} \quad (3.122)$$

$$b = \frac{1}{I_z} \quad (3.123)$$

$$c = \frac{D}{I_z I_g} \quad (3.124)$$

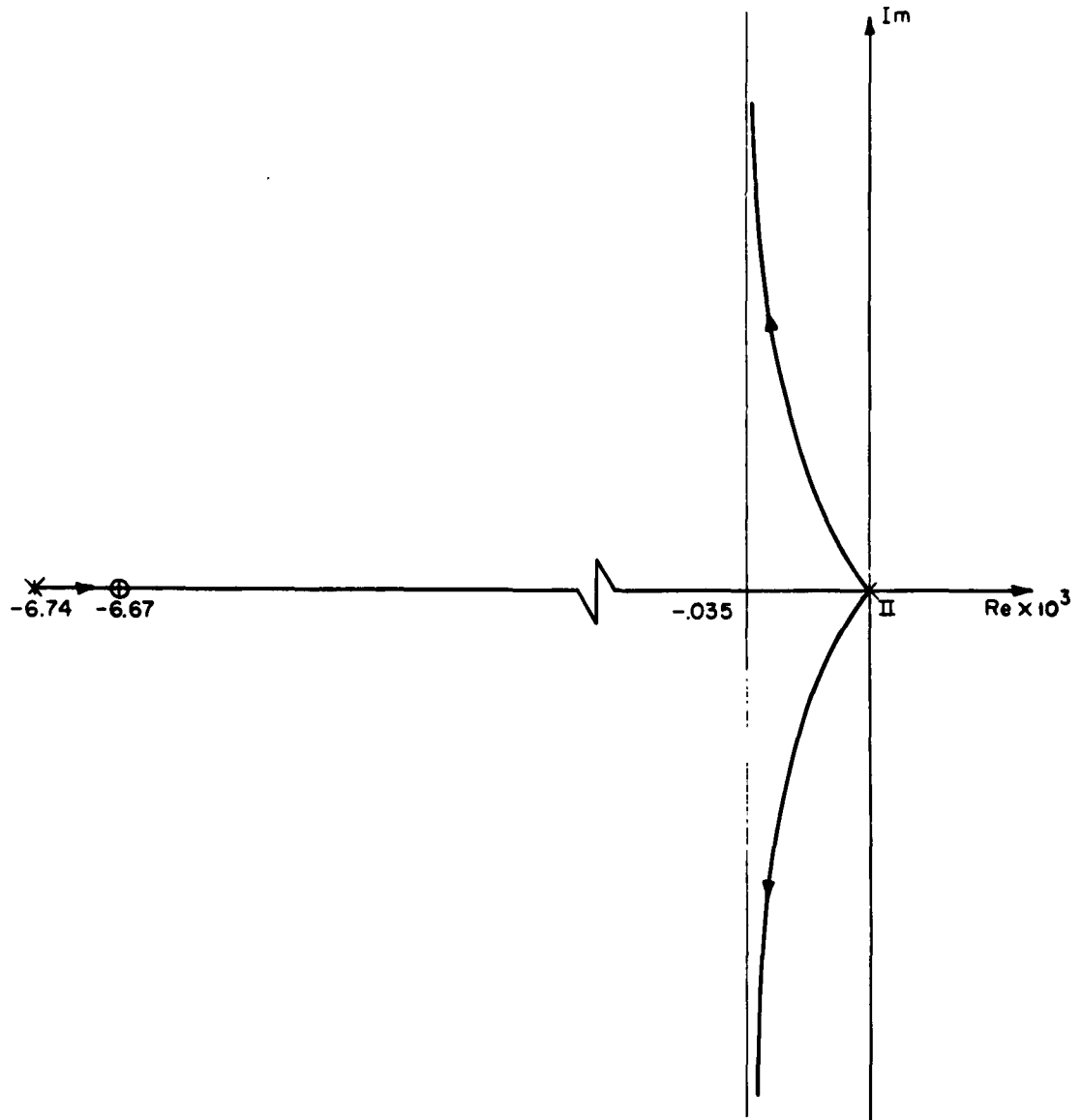


Fig. 3-18 Root Locus as a Function of the Spring Constant for Direct Damping

Substituting the chosen values, the poles and zeros of the expression

$$\frac{(bs + c)}{s^2(s + a)} \quad (3.125)$$

become

$$z_1 = -6.67 \times 10^{-3} \quad (3.126)$$

$$p_1, p_2 = 0 \quad (3.127)$$

$$p_3 = -6.74 \times 10^{-3}$$

c) Root-locus as a function of the moment of inertia of the gyroscope ( $I_g$ )  
(See Fig. 3-19).

For this case the characteristic equation (3.97) can be factored into the form:

$$(s^3 + as^2 + cs) \left( 1 + \frac{\frac{1}{I_g}(bs^2 + d)}{s(bs^2 + as + c)} \right) \quad (3.128)$$

Substituting the chosen values, the poles and zeros of the expression

$$\frac{(bs^2 + d)}{s(s^2 + as + c)} \quad (3.129)$$

become

$$z_1, z_2 = \pm j(1.29 \times 10^{-3}) \quad (3.130)$$

$$p_1 = 0 \quad (3.131)$$

$$p_2, p_3 = \pm j(1.28 \times 10^{-3})$$

Comparing indirect damping with direct damping, it is seen that a much higher damping coefficient is required to obtain a reasonable settling time for the directly damped case. In a satellite vehicle employing a single gyroscope, whose precession axis is along one of the body axes of the satellite, direct damping will occur on one of the axes whereas indirect damping will occur on another. If the damping coefficient is chosen to provide adequate damping for the directly damped axis, the damping on the indirectly damped axis will be well beyond the optimum point, hence poor settling time about that axis will be obtained. This suggests that either the gyroscope precession axis be offset from the body axes or several gyroscopes be employed so that indirect damping can be provided about each of the axes to be controlled.

In order to analyze the dynamics of a satellite containing internally mounted gyroscopes, it will be first necessary to analyze the dynamics of a gyroscope mounted, in an arbitrary position, within an orbiting vehicle. This will be accomplished in Chapter IV.

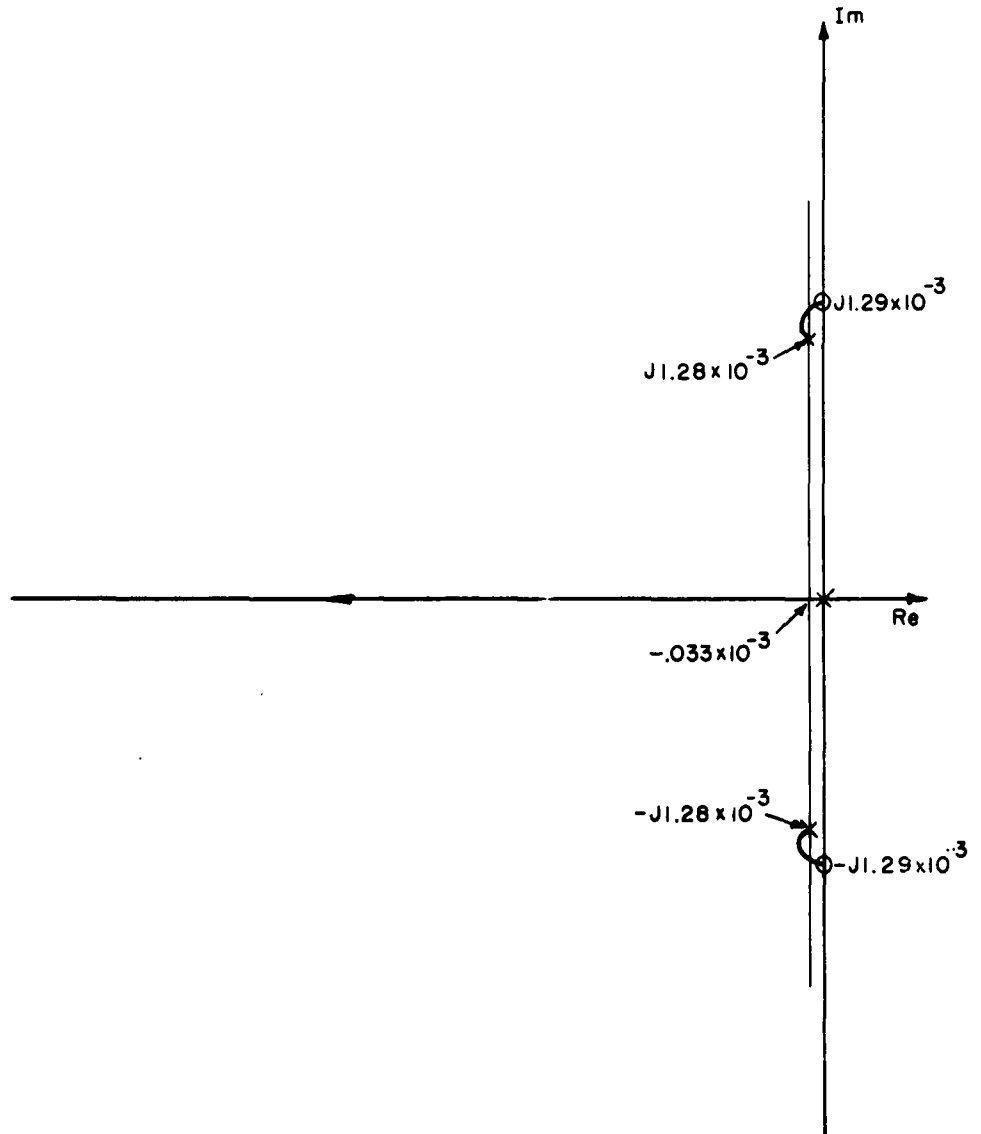


Fig. 3-19 Root Locus as a Function of the Moment of Inertia of the Gyroscope for Direct Damping

## CHAPTER IV - GYROSCOPE DYNAMICS

It was noted in the examples at the end of Chapter II that an orbiting vehicle would, at best, have only an oscillatory free response. Any practical vehicle must, of course, have damping which reduces disturbance oscillations in a reasonable period of time. Since a conventional form of damping, atmospheric drag, present in vehicles which travel in the atmosphere, is not available, some other means of damping must be provided. It was noted in Chapter III that a gyroscope with a damping fluid constraint may be used to provide this damping. In this chapter the equations of motion of a gyroscope mounted within an orbiting vehicle will be developed for an arbitrary orientation of the precession and spin axes relative to the coordinate system of the vehicle. From this general derivation special cases will be cited.

### A) The Gyroscope Equations for Symmetrical Design

The equations of motion of a gyroscope are developed in Appendix B of this report. They are repeated here for convenience.

$$T_{g_i g} = I_{x_g} \dot{\omega}_{g_i g} + (I_{z_g} - I_{y_g}) \omega_{g_j g} \omega_{g_k g} - H_r \omega_{g_k g} \quad (B.9)$$

$$T_{g_j g} = \dot{H}_r + I_{y_g} \dot{\omega}_{g_j g} + (I_{x_g} - I_{z_g}) \omega_{g_i g} \omega_{g_k g} \quad (B.10)$$

$$T_{g_k g} = I_{z_g} \dot{\omega}_{g_k g} + (I_{y_g} - I_{x_g}) \omega_{g_i g} \omega_{g_j g} + H_r \omega_{g_i g} \quad (B.11)$$

where  $X_g, Y_g, Z_g$  are the principal axes of the gyroscope (see Fig. B-1)

$T_{g_i g}, T_{g_j g}, T_{g_k g}$  are the components of torque on the gyroscope along the  $X, Y,$  and  $Z$  axes of the gyroscope respectively

$I_{x_g}, I_{y_g}, I_{z_g}$  are the polar moments of inertia of the gyroscope along the  $X, Y$  and  $Z$  axes of the gyroscope

$\omega_{g_i g}, \omega_{g_j g}, \omega_{g_k g}$  are the components of the angular velocity of the gimbal along the  $X, Y$  and  $Z$  axes of the gyroscope with respect to inertial space

$H_r$  is the angular momentum of the rotor

These equations are similar to Euler's equations of motion except that the angular momentum of the gyroscope rotor introduces some additional terms. The angular momentum of the rotor will normally be held constant through the use of an appropriate speed control system. Therefore  $\dot{H}_r$  can be taken to be zero. The equations reduce to a particularly simple form if symmetrical design of the gyroscope is assumed. ( $I_{x_g} = I_{y_g} = I_{z_g} = I_g$ ). In order to facilitate the analysis, symmetrically

designed gyroscopes will be used throughout this report. It is anticipated that this restriction will not cause a significant loss in generality. Making the appropriate substitutions, equations (B.9), (B.10) and (B.11) become

$$T_{g_i g} = I_g \dot{\omega}_{g_i} - H_r \omega_{g_k g} \quad (4.1)$$

$$T_{g_j g} = I_g \dot{\omega}_{g_j} \quad (4.2)$$

$$T_{g_k g} = I_g \dot{\omega}_{g_k} + H_r \omega_{g_i g} \quad (4.3)$$

It is further assumed that the body, to which the gyroscope is affixed, is reasonably aligned with the reference coordinate system so that the equations developed for small angular deviations in Chapter II can be applied.

#### B) The Transformation Matrix Relating Body and Gyroscope Coordinates

In the derivation to follow in Section C, the gyroscope will be assumed mounted at an arbitrary position within the vehicle. The coordinate system of the gyroscope will be denoted by  $i_g$ ,  $j_g$  and  $k_g$  where  $i_g$  is along the precession axis of the gyroscope,  $j_g$  is along the angular momentum of the rotor and  $k_g$  is chosen to form a right handed coordinate system. (See Fig. B-1). The gyroscope coordinate axes can be related to the body coordinate axes through an appropriate array of Eulerian angles. This procedure is similar to that used in Chapter II, (Section C), where a transformation matrix, relating the body coordinate axes to the reference coordinate axes was obtained. Though the transformation matrix, (2.3) can be applied to the present situation, it will not represent an intelligent choice. It is advantageous to choose the set of Eulerian angles so that the location of the precession axis fixes two of the Eulerian angles, and precession of the gyroscope causes only the third Eulerian angle to vary. Examination of equation (2.3) reveals that if the transformation matrix, developed to relate the body coordinate axes to the reference coordinate axes, is used to relate the gyroscope coordinate axes to the body coordinate axes, precession of the gyroscope will in general cause all three Eulerian angles to change. Precession of the gyroscope represents a rotation about the  $i_g$  axis of the gyroscope; it would therefore be wise to perform this rotation last. The Eulerian angles that will be used will be denoted by  $\phi_y$ ,  $\phi_z$  and  $\phi_x$ . These angles are defined by successive rotations of the gyroscope axes in the order  $\phi_y$ ,  $\phi_z$ ,  $\phi_x$  which rotate the gyroscope axes from coincidence with the body axes into its actual position. (See Fig. 4-1). These angles will be taken as positive when the sense of rotation is equivalent to that of a right handed screw advancing in the direction of the axis of

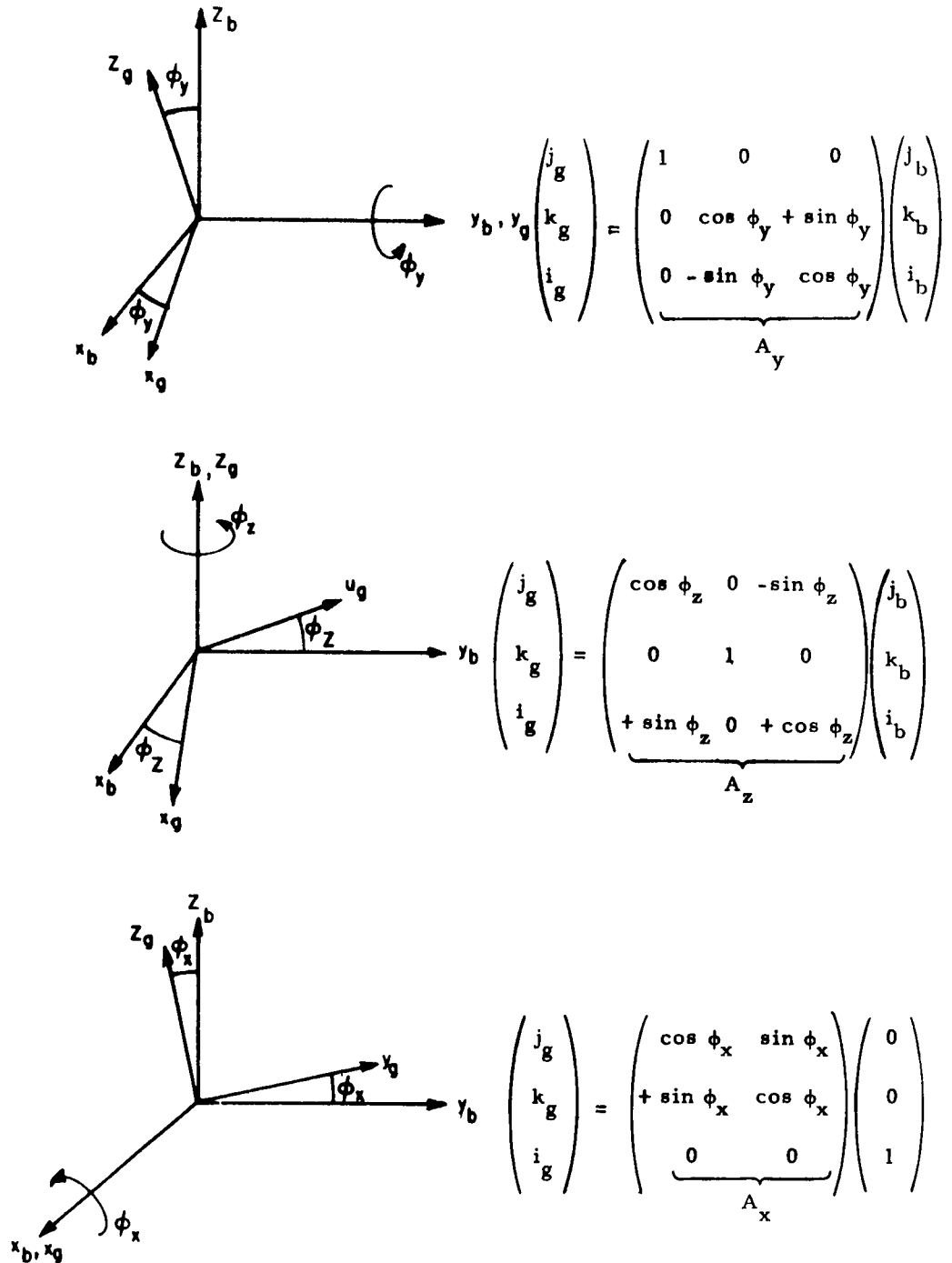


Fig. 4-1 Transformation Matrix Relating Gyroscope and Body Axes



rotation. Fig. 4-1 shows the three successive rotations and their corresponding transformation matrices. The overall transformation matrix relating the components of a vector in body coordinates to the components of the same vector in gyroscope coordinates is given by

$$\begin{pmatrix} j_g \\ k_g \\ i_g \end{pmatrix} = \begin{pmatrix} A \end{pmatrix} \begin{pmatrix} j_b \\ k_b \\ i_b \end{pmatrix} \quad (4.4)$$

where

$$A = (A_x)(A_z)(A_y) \quad (4.5)$$

and

$$A = \begin{pmatrix} \cos \phi_x \cos \phi_z & \cos \phi_x \sin \phi_y \sin \phi_z & -\cos \phi_x \cos \phi_y \sin \phi_z \\ & + \sin \phi_x \cos \phi_y & + \sin \phi_x \sin \phi_y \\ -\sin \phi_x \cos \phi_z & -\sin \phi_x \sin \phi_y \sin \phi_z & \sin \phi_x \cos \phi_y \sin \phi_z \\ & + \cos \phi_x \cos \phi_y & + \cos \phi_x \sin \phi_y \\ \sin \phi_z & -\sin \phi_y \cos \phi_z & \cos \phi_y \cos \phi_z \end{pmatrix} \quad (4.6)$$

As for the transformation matrix relating the body and reference coordinates, matrix multiplication is not commutative and must be performed in the order indicated. This again signifies that the order in which the rotations are performed is of utmost importance. It should be noted that the first two rotations, through the angles  $\phi_y$  and  $\phi_z$ , determine the location of the precession axis of the gyroscope. Precession of the gyroscope, merely changes the remaining Eulerian angle  $\phi_x$ .

### C) The General Gyroscope Equations

The angular velocity of the gyroscope with respect to inertial space is the vector sum of the angular velocity of the gyroscope with respect to the body and the angular velocity of the body with respect to inertial space.

$$\omega_{g/\text{Inertial space}} = \omega_{g/\text{body}} + \omega_{\text{body}/\text{Inertial space}} \quad (4.7)$$

The angular velocity of the body with respect to inertial space, in terms of body coordinates, is given as

$$\omega_{b/I} = \omega_{b,i_b} i_b + \omega_{b,j_b} j_b + \omega_{b,k_b} k_b \quad (4.8)$$

where

$$\omega_{b_i b} = \dot{\theta}_x + \theta_z \Omega_y \quad (4.9)$$

$$\omega_{b_j b} = \dot{\theta}_y + \Omega_y \quad (4.10)$$

$$\omega_{b_k b} = \dot{\theta}_z - \theta_x \Omega_y \quad (4.11)$$

These equations were obtained from equations (2.14), (2.15) and (2.16) by setting  $\Omega_x = \Omega_z = 0$ . Using the vector transformation matrix, derived in the previous section, (equation 4.6), one can express the components of the angular velocity of the body with respect to inertial space in terms of gyroscope coordinates. The resulting equation then becomes

$$\omega_{b/I} = \omega_{b_i g} i_g + \omega_{b_j g} j_g + \omega_{b_k g} k_g \quad (4.12)$$

where

$$\omega_{b_i g} = \sin \phi_x (\dot{\theta}_y + \Omega_y) - \sin \phi_y \cos \phi_z (\dot{\theta}_z - \theta_x \Omega_y) + \cos \phi_y \cos \phi_z (\dot{\theta}_x + \theta_z \Omega_y) \quad (4.13)$$

$$\omega_{b_j g} = \cos \phi_x \cos \phi_z (\dot{\theta}_y + \Omega_y) + (\cos \phi_x \sin \phi_y \sin \phi_z + \sin \phi_x \cos \phi_y) (\dot{\theta}_z - \theta_x \Omega_y) + (-\cos \phi_x \cos \phi_y \sin \phi_z + \sin \phi_x \sin \phi_y) (\dot{\theta}_x + \theta_z \Omega_y) \quad (4.14)$$

$$\omega_{b_k g} = -\sin \phi_x \cos \phi_z (\dot{\theta}_y + \Omega_y) + (\cos \phi_x \cos \phi_y - \sin \phi_x \sin \phi_y \sin \phi_z) (\dot{\theta}_z - \theta_x \Omega_y) + (\cos \phi_x \sin \phi_y + \sin \phi_x \cos \phi_y \sin \phi_z) (\dot{\theta}_x + \theta_z \Omega_y) \quad (4.15)$$

Since the gyroscope is constrained to rotate, relative to the vehicle, about its precession axis ( $i_g$ ), the angular velocity of the gyroscope gimbal with respect to the body can be expressed as

$$\omega_{g/b} = \dot{\phi}_x i_g \quad (4.16)$$

Therefore, from equation (4.7), the angular velocity of the gyroscope gimbal with respect to inertial space is given by

$$\omega_{g/\text{space}} = \omega_{g_i} i_g + \omega_{g_j} j_g + \omega_{g_k} k_g \quad (4.17)$$

where

$$\omega_{g_i} = \omega_{b_i} + \dot{\phi}_x \quad (4.18)$$

$$\omega_{g_j} = \omega_{b_j} \quad (4.19)$$

$$\omega_{g_k} = \omega_{b_k} \quad (4.20)$$

Differentiating the components of equation (4.17) with respect to time, yields the components of the angular acceleration of the gyroscope gimbal with respect to inertial space in terms of gyroscope coordinates. It should be noted that the location of the precession axis is fixed for a given gyroscope orientation, therefore  $\phi_y$  and  $\phi_z$  are fixed constants and the only Eulerian angle that will vary in time is  $\phi_x$  (This angle will vary as the gyroscope precesses).

$$\begin{aligned} \dot{\omega}_{g_i} = & \sin \phi_z (\ddot{\theta}_y + \dot{\Omega}_y) - \sin \phi_y \cos \phi_z (\ddot{\theta}_z - \theta_x \dot{\Omega}_y - \dot{\theta}_x \Omega_y) \\ & + \cos \phi_y \cos \phi_z (\ddot{\theta}_x + \theta_z \dot{\Omega}_y + \dot{\theta}_z \Omega_y) + \ddot{\phi}_x \end{aligned} \quad (4.21)$$

$$\begin{aligned} \dot{\omega}_{g_j} = & -\dot{\phi}_x \sin \phi_x \cos \phi_z (\dot{\theta}_y + \Omega_y) + \cos \phi_x \cos \phi_z (\ddot{\theta}_y + \dot{\Omega}_y) \\ & + (-\dot{\phi}_x \sin \phi_x \sin \phi_y \sin \phi_z + \dot{\phi}_x \cos \phi_x \cos \phi_y) (\dot{\theta}_z - \theta_x \Omega_y) \\ & + (\cos \phi_x \sin \phi_y \sin \phi_z + \sin \phi_x \cos \phi_y) (\ddot{\theta}_z - \theta_x \dot{\Omega}_y - \dot{\theta}_x \Omega_y) \\ & + (\dot{\phi}_x \sin \phi_x \cos \phi_y \sin \phi_z + \dot{\phi}_x \cos \phi_x \sin \phi_y) (\dot{\theta}_x + \theta_z \Omega_y) \\ & + (-\cos \phi_x \cos \phi_y \sin \phi_z + \sin \phi_x \sin \phi_y) (\ddot{\theta}_x + \theta_z \dot{\Omega}_y + \dot{\theta}_z \Omega_y) \end{aligned} \quad (4.22)$$

$$\begin{aligned} \dot{\omega}_{g_k} = & -\dot{\phi}_x \cos \phi_x \cos \phi_z (\dot{\theta}_y + \Omega_y) - \sin \phi_x \cos \phi_z (\ddot{\theta}_y + \dot{\Omega}_y) \\ & + (-\dot{\phi}_x \sin \phi_x \cos \phi_y - \dot{\phi}_x \cos \phi_x \sin \phi_y \sin \phi_z) (\dot{\theta}_z - \theta_x \Omega_y) \\ & + (\cos \phi_x \cos \phi_y - \sin \phi_x \sin \phi_y \sin \phi_z) (\ddot{\theta}_z - \theta_x \dot{\Omega}_y - \dot{\theta}_x \Omega_y) \\ & + (-\dot{\phi}_x \sin \phi_x \sin \phi_y + \dot{\phi}_x \cos \phi_x \cos \phi_y \sin \phi_z) (\dot{\theta}_x + \theta_z \Omega_y) \\ & + (\cos \phi_x \sin \phi_y + \sin \phi_x \cos \phi_y \sin \phi_z) (\ddot{\theta}_x + \theta_z \dot{\Omega}_y + \dot{\theta}_z \Omega_y) \end{aligned} \quad (4.23)$$

Substituting equations (4.18), (4.19), (4.20), (4.21), (4.22) and (4.23) into equations (4.1), (4.2), and (4.3) yields for the components of torque on the gyroscope gimbal along the gyroscope axes

$$\begin{aligned} T_{g_i g} = & I_g \left[ \sin \phi_z (\ddot{\theta}_y + \dot{\Omega}_y) - \sin \phi_y \cos \phi_z (\ddot{\theta}_z - \theta_x \dot{\Omega}_y - \dot{\theta}_x \Omega_y) \right. \\ & \left. + \cos \phi_y \cos \phi_z (\ddot{\theta}_x + \theta_z \dot{\Omega}_y + \dot{\theta}_z \Omega_y) + \ddot{\phi}_x \right] \quad (4.24) \\ & + H_r \left[ \sin \phi_x \cos \phi_z (\dot{\theta}_y + \Omega_y) - (\cos \phi_x \cos \phi_y - \sin \phi_x \sin \phi_y \sin \phi_z) \right. \\ & \left. (\dot{\theta}_z - \theta_x \Omega_y) - (\cos \phi_x \sin \phi_y + \sin \phi_x \cos \phi_y \sin \phi_z) (\dot{\theta}_x + \dot{\theta}_z \Omega_y) \right] \end{aligned}$$

$$\begin{aligned} T_{g_j g} = & I_g \left[ -\dot{\phi}_x \sin \phi_x \cos \phi_z (\dot{\theta}_y + \Omega_y) + \cos \phi_x \cos \phi_z (\ddot{\theta}_y + \dot{\Omega}_y) \right. \quad (4.25) \\ & \left. + (-\dot{\phi}_x \sin \phi_x \sin \phi_y \sin \phi_z + \dot{\phi}_x \cos \phi_x \cos \phi_y) (\ddot{\theta}_z - \theta_x \dot{\Omega}_y) \right. \\ & \left. + (\cos \phi_x \sin \phi_y \sin \phi_z + \sin \phi_x \cos \phi_y) (\ddot{\theta}_z - \theta_x \dot{\Omega}_y - \dot{\theta}_x \Omega_y) \right. \\ & \left. + (\dot{\phi}_x \sin \phi_x \cos \phi_y \sin \phi_z + \dot{\phi}_x \cos \phi_x \sin \phi_y) (\ddot{\theta}_x + \theta_z \dot{\Omega}_y) \right. \\ & \left. + (-\cos \phi_x \cos \phi_y \sin \phi_z + \sin \phi_x \sin \phi_y) (\ddot{\theta}_x + \theta_z \dot{\Omega}_y + \dot{\theta}_z \Omega_y) \right] \end{aligned}$$

$$\begin{aligned} T_{g_k g} = & I_g \left[ -\dot{\phi}_x \cos \phi_x \cos \phi_z (\dot{\theta}_y + \Omega_y) - \sin \phi_x \cos \phi_z (\ddot{\theta}_y + \dot{\Omega}_y) \right. \quad (4.26) \\ & \left. - (\dot{\phi}_x \sin \phi_x \cos \phi_y + \dot{\phi}_x \cos \phi_x \sin \phi_y \sin \phi_z) (\dot{\theta}_z - \theta_x \dot{\Omega}_y) \right. \\ & \left. + (\cos \phi_x \cos \phi_y - \sin \phi_x \sin \phi_y \sin \phi_z) (\ddot{\theta}_z - \theta_x \dot{\Omega}_y - \dot{\theta}_x \Omega_y) \right. \\ & \left. + (-\dot{\phi}_x \sin \phi_x \sin \phi_y + \dot{\phi}_x \cos \phi_x \cos \phi_y \sin \phi_z) (\ddot{\theta}_x + \theta_z \dot{\Omega}_y) \right. \\ & \left. + (\cos \phi_x \sin \phi_y + \sin \phi_x \cos \phi_y \sin \phi_z) (\ddot{\theta}_x + \theta_z \dot{\Omega}_y + \dot{\theta}_z \Omega_y) \right] \\ & + H_r \left[ \sin \phi_z (\dot{\theta}_y + \Omega_y) - \sin \phi_y \cos \phi_z (\ddot{\theta}_z - \theta_x \dot{\Omega}_y) \right. \\ & \left. + \cos \phi_y \cos \phi_z (\dot{\theta}_x + \theta_z \dot{\Omega}_y) + \dot{\phi}_x \right] \end{aligned}$$

It is now necessary to express the component of torque on the gyroscope gimbal in terms of the body coordinate axes. This is accomplished by utilizing the inverse transformation of equation (4.6)

$$A^{-1} = \begin{pmatrix} \cos \phi_x \cos \phi_z & -\sin \phi_x \cos \phi_z & \sin \phi_z \\ \cos \phi_x \sin \phi_y \sin \phi_z & -\sin \phi_x \sin \phi_y \sin \phi_z & -\sin \phi_y \cos \phi_z \\ + \sin \phi_x \cos \phi_y & + \cos \phi_x \cos \phi_y & \\ -\cos \phi_x \cos \phi_y \sin \phi_z & \sin \phi_x \cos \phi_y \sin \phi_z & \cos \phi_y \cos \phi_z \\ + \sin \phi_x \sin \phi_y & + \cos \phi_x \sin \phi_y & \end{pmatrix} \quad (4.27)$$

Utilizing the inverse matrix,

$$\begin{pmatrix} T_{g_{j_b}} \\ T_{g_{k_b}} \\ T_{g_{i_b}} \end{pmatrix} = \begin{pmatrix} \\ \\ \\ \end{pmatrix} A^{-1} \begin{pmatrix} T_{g_{j_g}} \\ T_{g_{k_g}} \\ T_{g_{i_g}} \end{pmatrix} \quad (4.28)$$

expanding and performing algebraic simplifications, one obtains for the components of torque on the gyroscope gimbal along the body coordinate axes

$$\begin{aligned} T_{g_{i_b}} = I_g & \left[ -\dot{\phi}_x \sin \phi_y \cos \phi_z (\dot{\theta}_y + \Omega_y) + (\ddot{\theta}_x + \theta_z \dot{\Omega}_y + \dot{\theta}_z \Omega_y) \right. \\ & \left. + (\cos \phi_y \cos \phi_z \dot{\phi}_x) - \dot{\phi}_x \sin \phi_z (\dot{\theta}_z - \theta_x \Omega_y) \right] \\ & + H_r \left[ (\sin \phi_x \cos \phi_y + \cos \phi_x \sin \phi_y \sin \phi_z) (\dot{\theta}_y + \Omega_y) \right. \\ & \left. - \cos \phi_x \cos \phi_z (\dot{\theta}_z - \theta_x \Omega_y) + (\cos \phi_x \sin \phi_y + \right. \\ & \left. \sin \phi_x \cos \phi_y \sin \phi_z) \dot{\phi}_x \right] \end{aligned} \quad (4.29)$$

$$\begin{aligned} T_{g_{j_b}} = I_g & \left[ (\ddot{\theta}_y + \dot{\Omega}_y) + \sin \phi_z \ddot{\phi}_x + \dot{\phi}_x \cos \phi_y \cos \phi_z (\dot{\theta}_z - \theta_x \Omega_y) \right. \\ & \left. + \dot{\phi}_x \sin \phi_y \cos \phi_z (\dot{\theta}_x + \theta_z \Omega_y) \right] + H_r \left[ (\sin \phi_x \sin \phi_y \right. \\ & \left. - \cos \phi_x \cos \phi_y \sin \phi_z) (\dot{\theta}_z - \theta_x \Omega_y) - (\sin \phi_x \cos \phi_y \right. \\ & \left. + \cos \phi_x \sin \phi_y \sin \phi_z) (\dot{\theta}_x + \theta_z \Omega_y) - \dot{\phi}_x \sin \phi_x \cos \phi_z \right] \end{aligned} \quad (4.30)$$

$$\begin{aligned}
T_{g_{k_b}} = I_g & \left[ -\dot{\phi}_x \cos \phi_y \cos \phi_z (\dot{\phi}_y + \Omega_y) + (\ddot{\phi}_z - \dot{\phi}_x \dot{\Omega}_y - \dot{\phi}_x \Omega_y) \right. \\
& \left. - \sin \phi_y \cos \phi_z \ddot{\phi}_x + \dot{\phi}_x \sin \phi_y (\dot{\phi}_x + \dot{\phi}_z \Omega_y) \right] \\
+ H_r & \left[ \cos \phi_x \cos \phi_z (\dot{\phi}_x + \dot{\phi}_z \Omega_y) + (\cos \phi_x \cos \phi_y \right. \\
& \left. - \sin \phi_x \sin \phi_y \sin \phi_z) \dot{\phi}_x + (-\sin \phi_x \sin \phi_y \right. \\
& \left. + \cos \phi_x \cos \phi_y \sin \phi_z) (\dot{\phi}_y + \Omega_y) \right]
\end{aligned} \tag{4.31}$$

The equation of constraint relating the gyroscope precession angle ( $\phi_x$ ) to the body angular deviations ( $\theta_x$ ,  $\phi_y$  and  $\theta_z$ ) can be obtained from the fact that the component of torque on the gyroscope gimbal along the X axis of the gyroscope is given by

$$T_{g_{i_g}} = -D \dot{\phi}_x + T_c \tag{4.32}$$

where  $D$  represents the damping coefficient  
 $T_c$  represents a control torque applied to the gyroscope.

Equating the right side of equation (4.32) to the component of torque on the gyroscope along the  $i_g$  direction (equation 4.24) yields for the equation of constraint

$$\begin{aligned}
-D \dot{\phi}_x + T_c = I_g & \left[ \sin \phi_z (\ddot{\phi}_y + \dot{\Omega}_y) - \sin \phi_y \cos \phi_z \right. \\
& \left. (\ddot{\phi}_z - \dot{\phi}_x \dot{\Omega}_y - \dot{\phi}_x \Omega_y) + \cos \phi_y \cos \phi_z (\ddot{\phi}_x + \dot{\phi}_z \dot{\Omega}_y + \dot{\phi}_z \Omega_y) + \ddot{\phi}_x \right] \\
+ H_r & \left[ \sin \phi_x \cos \phi_z (\dot{\phi}_y + \Omega_y) - (\cos \phi_x \cos \phi_y - \sin \phi_x \right. \\
& \left. \sin \phi_y \sin \phi_z) (\dot{\phi}_z - \dot{\phi}_x \Omega_y) - (\cos \phi_x \sin \phi_y + \sin \phi_x \cos \phi_y \right. \\
& \left. \sin \phi_z) (\dot{\phi}_x + \dot{\phi}_z \Omega_y) \right]
\end{aligned} \tag{4.33}$$

Equations (4.29), (4.30), (4.31) and (4.33) are completely general. For appropriate values of  $\phi_y$  and  $\phi_z$  the equations for any desired orientation of the precession axis can be obtained. In Section D, the equations for several different gyroscope configurations will be tabulated though by no means will this list be exhaustive.

#### D) The Gyroscope Equations for Particular Configurations

Although the gyroscope equations (4.29), (4.30), (4.31) and (4.33) are completely general, it will be convenient to reduce the gyroscope equations for somewhat more restrictive configurations. Several of the more important configurations are listed below.

1) The gyroscope precession axis is located in the  $X_b Y_b$  plane. (see Fig. 4-2)

For this configuration,  $\phi_y = 0^\circ$  and the location of the precession axis is determined by  $\phi_z$  .  $\phi_x$  , of course, determines the location of the spin axis. Setting  $\phi_y = 0^\circ$  in equations (4.29), (4.30) and (4.31) yields the equations for the components of torque on the gyroscope when the precession axis is located arbitrarily in the  $X_b Y_b$  plane

$$T_{g_{i_b}} = I_g \left[ \ddot{\theta}_x + \theta_z \dot{\Omega}_y + \dot{\theta}_z \Omega_y + \cos \phi_z \ddot{\phi}_x - \dot{\phi}_x \sin \phi_z (\dot{\theta}_z - \theta_x \Omega_y) \right] \quad (4.34)$$

$$+ H_r \left[ \sin \phi_x (\dot{\theta}_y + \Omega_y) - \cos \phi_x \cos \phi_z (\dot{\theta}_z - \theta_x \Omega_y) + \sin \phi_x \sin \phi_z \dot{\phi}_x \right]$$

$$T_{g_{j_b}} = I_g \left[ \ddot{\theta}_y + \dot{\Omega}_y + \sin \phi_z \ddot{\phi}_x + \dot{\phi}_x \cos \phi_z (\dot{\theta}_z - \theta_x \Omega_y) \right] \quad (4.35)$$

$$+ H_r \left[ -\cos \phi_x \sin \phi_z (\dot{\theta}_z - \theta_x \Omega_y) - \sin \phi_x (\dot{\theta}_x + \theta_z \Omega_y) - \dot{\phi}_x \sin \phi_x \cos \phi_z \right]$$

$$T_{g_{k_b}} = I_g \left[ -\dot{\phi}_x \cos \phi_z (\dot{\theta}_y + \Omega_y) + \ddot{\theta}_z - \theta_x \dot{\Omega}_y - \dot{\theta}_x \Omega_y \right] \quad (4.36)$$

$$+ \dot{\phi}_x \sin \phi_z (\dot{\theta}_x + \theta_z \Omega_y) + H_r \left[ \cos \phi_x \cos \phi_z (\dot{\theta}_x + \theta_z \Omega_y) + \cos \phi_x \dot{\phi}_x + \cos \phi_x \sin \phi_z (\dot{\theta}_y + \Omega_y) \right]$$

Setting  $\phi_y = 0^\circ$  in equation (4.33) yields the equation of constraint.

$$-D \phi_x + T_c = I_g \left[ \sin \phi_z (\ddot{\theta}_y + \dot{\Omega}_y) \right] \quad (4.37)$$

$$+ \cos \phi_z (\ddot{\theta}_x + \theta_z \dot{\Omega}_y + \dot{\theta}_z \Omega_y) + \ddot{\phi}_x$$

$$+ H_r \left[ \sin \phi_x \cos \phi_z (\dot{\theta}_y + \Omega_y) - \cos \phi_x (\theta_z - \theta_x \Omega_y) - \sin \phi_x \sin \phi_z (\dot{\theta}_x + \theta_z \Omega_y) \right]$$

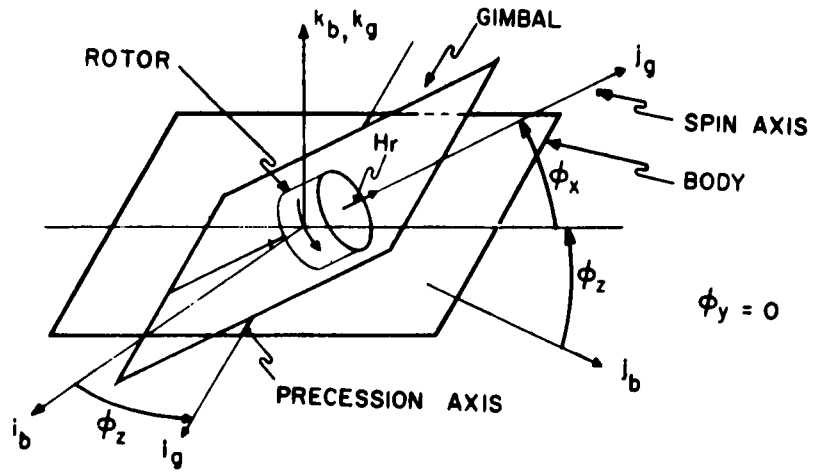


Fig. 4-2 Gyroscope precession axis in the  $X_b Y_b$  plane

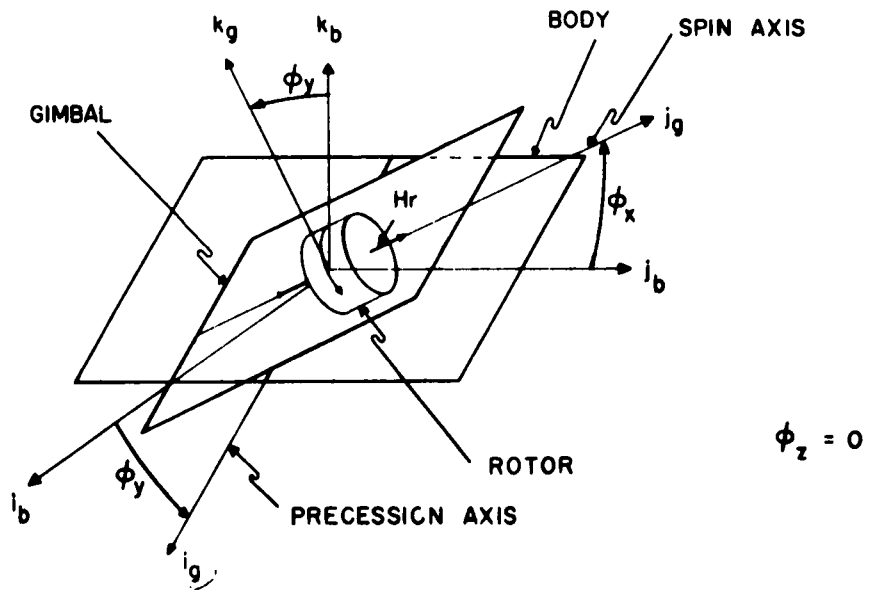


Fig. 4-3 Gyroscope precession axis in the  $X_b Z_b$  plane



2) The gyroscope precession axis is located in the  $X_b Z_b$  plane. (see Fig. 4-3)

For this configuration  $\phi_z = 0^\circ$  and the location of the precession axis is determined by  $\phi_y$ . Setting  $\phi_z = 0^\circ$  in equations (4.29), (4.30) and (4.31) yields the equations for the components of torque on the gyroscope when the precession axis is located arbitrarily in the  $X_b Z_b$  plane.

$$T_{g_{i_b}} = I_g \left[ -\dot{\phi}_x \sin \phi_y (\dot{\theta}_y + \Omega_y) + \ddot{\theta}_x + \dot{\epsilon}_z \dot{\Omega}_y + \dot{\epsilon}_z \Omega_y + \cos \phi_y \ddot{\phi}_x \right] \quad (4.38)$$

$$+ H_r \left[ \sin \phi_x \cos \phi_y (\dot{\theta}_y + \Omega_y) - \cos \phi_x (\dot{\epsilon}_z - \theta_x \Omega_y) + \cos \phi_x \sin \phi_y \dot{\phi}_x \right]$$

$$T_{g_{j_b}} = I_g \left[ \ddot{\theta}_y + \dot{\Omega}_y + \dot{\phi}_x \cos \phi_y (\dot{\theta}_z - \theta_x \Omega_y) + \dot{\phi}_x \sin \phi_y (\dot{\epsilon}_x + \theta_z \Omega_y) \right] \quad (4.39)$$

$$+ H_r \left[ \sin \phi_x \sin \phi_y (\dot{\epsilon}_z - \theta_x \Omega_y) - \sin \phi_x \cos \phi_y (\dot{\theta}_x + \theta_z \Omega_y) - \dot{\phi}_x \sin \phi_x \right]$$

$$T_{g_{k_b}} = I_g \left[ -\dot{\phi}_x \cos \phi_y (\dot{\theta}_y + \Omega_y) + \ddot{\theta}_z - \theta_x \dot{\Omega}_y - \dot{\theta}_x \Omega_y - \sin \phi_y \ddot{\phi}_x \right] \quad (4.40)$$

$$+ H_r \left[ \cos \phi_x (\dot{\theta}_x + \theta_z \Omega_y) + \cos \phi_x \cos \phi_y \dot{\phi}_x - \sin \phi_x \sin \phi_y (\dot{\theta}_y + \Omega_y) \right]$$

Setting  $\phi_z = 0^\circ$  in equation (4.33) yields the equation of constraint

$$-D \dot{\phi}_x + T_c = I_g \left[ -\sin \phi_y (\ddot{\theta}_z - \theta_x \dot{\Omega}_y - \dot{\theta}_x \Omega_y) \right] \quad (4.41)$$

$$+ \cos \phi_y (\ddot{\theta}_x + \dot{\epsilon}_z \dot{\Omega}_y + \dot{\epsilon}_z \Omega_y) + \ddot{\phi}_x \right] + H_r \left[ \sin \phi_x (\dot{\theta}_y + \Omega_y) - \cos \phi_x \cos \phi_y (\dot{\theta}_z - \theta_x \Omega_y) - \cos \phi_x \sin \phi_y (\dot{\theta}_x + \theta_z \Omega_y) \right]$$

3) The gyroscope precession axis is located in the  $Y_b Z_b$  plane. (See Fig. 4-4)

For this configuration  $\phi_y = 90^\circ$  and the location of the precession axis is determined by  $\phi_z$ . Setting  $\phi_y = 90^\circ$  in equations (4.29), (4.30) and (4.31) yields the equations for the components of torque on the gyroscope when the precession axis is located arbitrarily in the  $Y_b Z_b$  plane.

$$T_{g_{i_b}} = I_g \left[ -\dot{\phi}_x \cos \phi_z (\dot{\theta}_y + \Omega_y) + \ddot{\theta}_x + \dot{\epsilon}_z \dot{\Omega}_y + \dot{\epsilon}_z \Omega_y - \dot{\phi}_x \sin \phi_z (\dot{\epsilon}_z - \theta_x \Omega_y) \right] \quad (4.42)$$

$$+ H_r \left[ \cos \phi_x \sin \phi_z (\dot{\theta}_y + \Omega_y) - \cos \phi_x \cos \phi_z (\dot{\theta}_z - \theta_x \Omega_y) + \cos \phi_x \dot{\phi}_x \right]$$

$$T_{g_{j_b}} = I_g \left[ \ddot{\theta}_y + \dot{\Omega}_y \sin \phi_z \ddot{\phi}_x + \dot{\phi}_x \cos \phi_z (\dot{\theta}_x + \theta_z \Omega_y) \right] + H_r \left[ \sin \phi_x (\dot{\theta}_z - \theta_x \Omega_y) - \cos \phi_x \sin \phi_z (\dot{\theta}_x + \theta_z \Omega_y) - \dot{\phi}_x \sin \phi_x \cos \phi_z \right] \quad (4.43)$$

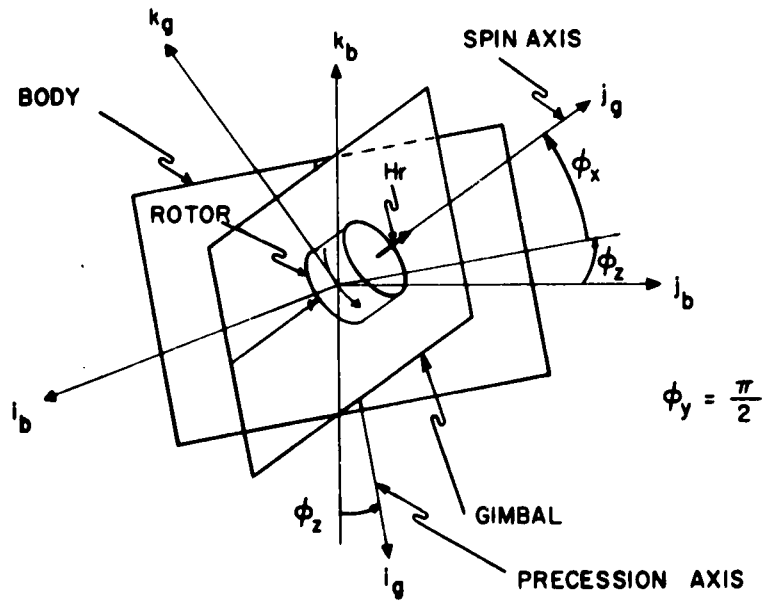


Fig. 4-4 Gyroscope precession axis in the  $Y_b Z_b$  plane

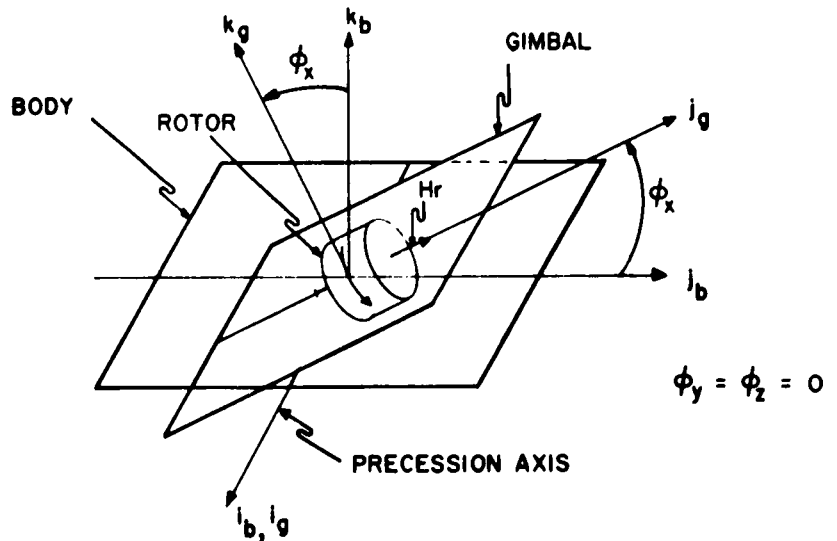


Fig. 4-5 Gyroscope precession axis along the  $X_b$  axis

$$T_{g_{k_b}} = I_g \left[ \ddot{\theta}_z - \theta_x \dot{\Omega}_y - \dot{\theta}_x \Omega_y - \cos \phi_z \ddot{\phi}_x + \dot{\phi}_x \sin \phi_z (\dot{\theta}_x + \theta_z \Omega_y) \right] + H_r \left[ \cos \phi_x \cos \phi_z (\dot{\theta}_x + \theta_z \Omega_y) - \sin \phi_x \sin \phi_z \dot{\phi}_x - \sin \phi_x (\dot{\theta}_y + \Omega_y) \right] \quad (4.44)$$

Setting  $\phi_y = 90^\circ$  in equation (4.33) yields the equation of constraint.

$$-D \dot{\phi}_x + T_c = I_g \left[ \sin \phi_z (\ddot{\theta}_y + \dot{\Omega}_y) - \cos \phi_z (\ddot{\theta}_z - \theta_x \dot{\Omega}_y - \dot{\theta}_x \Omega_y) + \ddot{\phi}_x \right] + H_r \left[ \sin \phi_x \cos \phi_z (\dot{\theta}_y + \Omega_y) + \sin \phi_x \sin \phi_z (\dot{\theta}_z - \theta_x \Omega_y) - \cos \phi_x (\dot{\theta}_x + \theta_z \Omega_y) \right] \quad (4.45)$$

4) The gyroscope precession axis is located along  $X_b$ . (See Fig. 4-5)

Although the set of equations for this configuration can be obtained from the general equations (4.29), (4.30) and (4.31) by setting  $\phi_y = \phi_z = 0^\circ$ , they can also be obtained as a special case of (1) by setting  $\phi_z = 0^\circ$  since, in that case,  $\phi_y$  was already taken to be zero. At any rate, the resulting equations are

$$T_{g_{i_b}} = I_g \left[ \ddot{\theta}_x + \theta_z \dot{\Omega}_y + \dot{\theta}_z \Omega_y + \ddot{\phi}_x \right] + H_r \left[ -\cos \phi_x (\dot{\theta}_z - \theta_x \Omega_y) + \sin \phi_x (\dot{\theta}_y + \Omega_y) \right] \quad (4.46)$$

$$T_{g_{j_b}} = I_g \left[ \ddot{\theta}_y + \dot{\Omega}_y + \dot{\phi}_x (\dot{\theta}_z - \theta_x \Omega_y) \right] - H_r \left[ \sin \phi_x (\dot{\theta}_x + \theta_z \Omega_y + \dot{\phi}_x) \right] \quad (4.47)$$

$$T_{g_{k_b}} = I_g \left[ -\dot{\phi}_x (\dot{\theta}_y + \Omega_y) + \ddot{\theta}_z - \theta_x \dot{\Omega}_y - \dot{\theta}_x \Omega_y \right] + H_r \left[ \cos \phi_x (\dot{\theta}_x + \theta_z \Omega_y + \dot{\phi}_x) \right] \quad (4.48)$$

Setting  $\phi_y = \phi_z = 0^\circ$  in equation (4.33) or setting  $\phi_z = 0^\circ$  in equation (4.37), yields the equation of constraint.

$$-D \dot{\phi}_x + T_c = I_g \left[ \ddot{\theta}_x + \theta_z \dot{\Omega}_y + \dot{\theta}_z \Omega_y + \ddot{\phi}_x \right] + H_r \left[ \sin \phi_x (\dot{\theta}_y + \Omega_y) - \cos \phi_x (\dot{\theta}_z - \theta_x \Omega_y) \right] \quad (4.49)$$

5) The precession axis of the gyroscope is along the  $Y_b$  axis. (See Fig. 4-6)

As in (4), the set of equations for this configuration can be obtained by setting  $\phi_y = 0^\circ$  and  $\phi_z = 90^\circ$  in the general equations (4.29), (4.30), and (4.31) or as a special case of (1) by setting  $\phi_z = 90^\circ$ . Either way, the resulting equations are

$$T_{g_{i_b}} = I_g \left[ \ddot{\theta}_x + \theta_z \dot{\Omega}_y + \dot{\theta}_z \Omega_y - \dot{\phi}_x (\dot{\theta}_z - \theta_x \Omega_y) \right] + H_r \left[ \sin \phi_x (\dot{\theta}_y + \Omega_y + \dot{\phi}_x) \right] \quad (4.50)$$

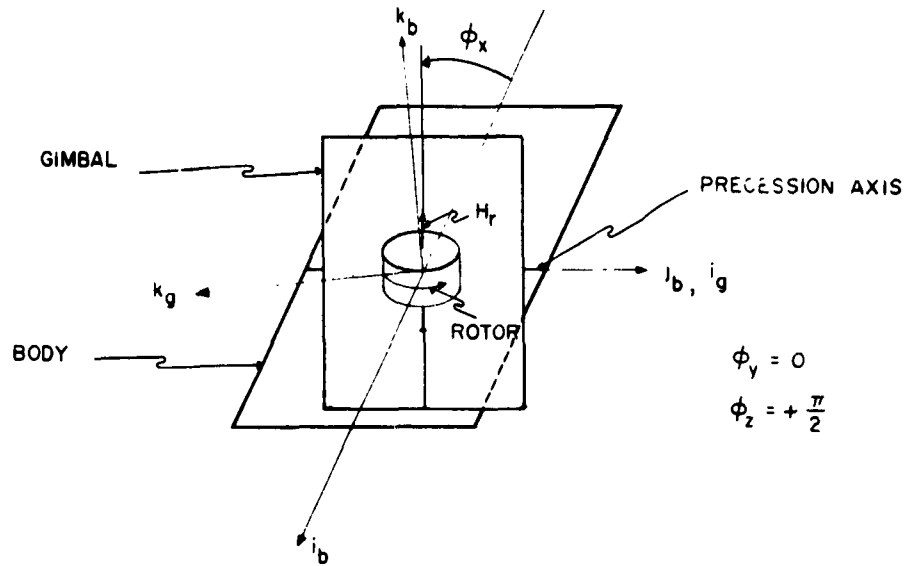


Fig. 4-6 Gyroscope precession axis along the  $Y_b$  axis

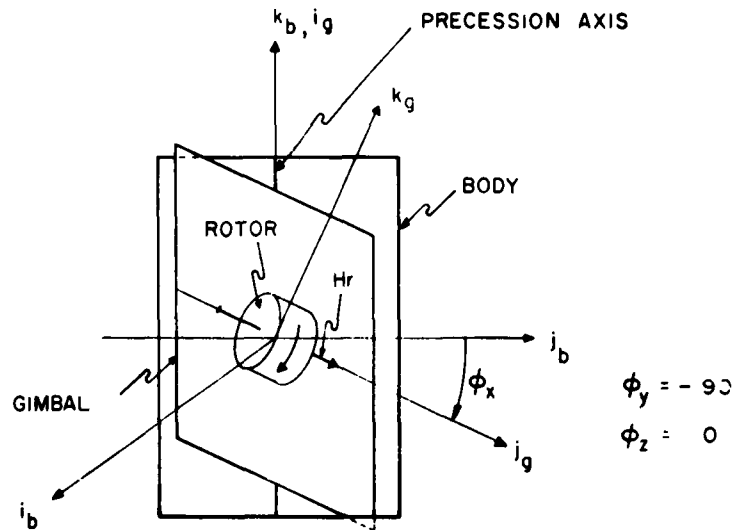


Fig. 4-7 Gyroscope precession axis along the  $Z_b$  axis

$$T_{g_{j_b}} = I_g \left[ \ddot{\theta}_y + \dot{\Omega}_y + \dot{\phi}_x \right] - H_r \left[ \cos \phi_x (\dot{\theta}_z - \theta_x \Omega_y) + \sin \phi_x (\dot{\theta}_x + \theta_z \Omega_y) \right] \quad (4.51)$$

$$T_{g_{k_b}} = I_g \left[ \ddot{\theta}_z - \theta_x \dot{\Omega}_y - \dot{\theta}_x \Omega_y + \dot{\phi}_x (\dot{\theta}_x + \theta_z \Omega_y) \right] + H_r \left[ \cos \phi_x (\dot{\phi}_x + \dot{\theta}_y + \Omega_y) \right] \quad (4.52)$$

Setting  $\phi_y = 0^\circ$  and  $\phi_z = 90^\circ$  in equation (4.33) or setting  $\phi_z = 90^\circ$  in equation (4.37) yields the equation of constraint.

$$-D \dot{\phi}_x + T_c = I_g \left[ \ddot{\theta}_y + \dot{\Omega}_y + \dot{\phi}_x \right] - H_r \left[ \cos \phi_x (\dot{\theta}_z - \theta_x \Omega_y) + \sin \phi_x (\dot{\theta}_x + \theta_z \Omega_y) \right] \quad (4.53)$$

6) The gyroscope precession axis is along the  $Z_b$  axis. (See Fig. 4-7)

The set of equations for this configuration can be obtained from the general equations (4.29), (4.30) and (4.31) by setting  $\phi_y = -90^\circ$  and  $\phi_z = 0^\circ$ , or as a special case of (2) by setting  $\phi_y = -90^\circ$  since  $\phi_z$  is already zero. At any rate, the resulting equations are

$$T_{g_{i_b}} = I_g \left[ \dot{\phi}_x (\dot{\theta}_y + \Omega_y) + \ddot{\theta}_x + \theta_z \dot{\Omega}_y + \dot{\theta}_z \Omega_y \right] - H_r \left[ \cos \phi_x (\dot{\theta}_z - \theta_x \Omega_y + \dot{\phi}_x) \right] \quad (4.54)$$

$$T_{g_{j_b}} = I_g \left[ \ddot{\theta}_y + \dot{\Omega}_y - \dot{\phi}_x (\dot{\theta}_x + \theta_z \Omega_y) \right] - H_r \left[ \sin \phi_x (\dot{\theta}_z - \theta_x \Omega_y + \dot{\phi}_x) \right] \quad (4.55)$$

$$T_{g_{k_b}} = I_g \left[ \ddot{\theta}_z - \theta_x \dot{\Omega}_y - \dot{\theta}_x \Omega_y + \dot{\phi}_x \right] + H_r \left[ \cos \phi_x (\dot{\theta}_x + \theta_z \Omega_y) + \sin \phi_x (\dot{\theta}_y + \Omega_y) \right] \quad (4.56)$$

Setting  $\phi_y = -90^\circ$  and  $\phi_z = 0^\circ$  in equation (4.33) or setting  $\phi_y = -90^\circ$  in equation (4.41) yields the equation of constraint.

$$-D \dot{\phi}_x + T_c = I_g \left[ \ddot{\theta}_z - \theta_x \dot{\Omega}_y - \dot{\theta}_x \Omega_y + \dot{\phi}_x \right] + H_r \left[ \sin \phi_x (\dot{\theta}_y + \Omega_y) + \cos \phi_x (\dot{\theta}_x + \theta_z \Omega_y) \right] \quad (4.57)$$

With the equations for a gyroscope and the equations developed in Chapter II for a rigid body, it is now possible to obtain the equations of motion for a vehicle containing any configuration of gyroscopes. In order to intelligently choose a configuration, it is necessary to first consider the nature of the steady state response. This is the subject matter of Chapter V.

## CHAPTER V - STEADY STATE REQUIREMENTS FOR AN ORBITING VEHICLE

Consider a vehicle in orbit of the earth that contains internally mounted gyroscopes for damping purposes. If no disturbance torques are applied, steady state will eventually be attained. If the vehicle's orbit is circular, and the gyroscope configuration is chosen such that the resultant torque exerted by the gyroscopes on the body at steady state is zero, the body coordinate system will become aligned with the reference coordinate system; the body will then have an angular velocity of  $\Omega_y j_b$ . If the orbit is elliptical, and the gyroscope configuration is chosen such that no resultant torque is exerted on the body at steady state,  $\theta_x$ ,  $\theta_z$  and their derivatives will vanish but  $\theta_y$  and its derivatives will not vanish. This is because an elliptical orbit requires the vehicle to have a variable angular acceleration. Since the restoring torques are produced through the mechanism of differential gravity and gyroscopic cross-coupling of the vehicle's orbital rate, it is necessary that an angular deviation appear about the  $Y_b$  axis. It should be noted that a vehicle in an elliptical orbit can never attain complete alignment with the reference coordinate system. If a less restrictive gyroscope configuration is employed, the gyroscopes will, at steady state, exert a torque on the vehicle. In order to counter this torque, steady state will be reached with the body axes offset from the reference coordinate system, so that counterbalancing differential gravity and gyroscopic cross coupling torques are produced. Therefore, in steady state, the best that can be expected is that

$$\dot{\theta}_x = \ddot{\theta}_x = \dot{\theta}_z = \ddot{\theta}_z = 0 \quad (5.1)$$

$$\theta_x \neq 0 \quad \theta_y \neq 0 \quad \theta_z \neq 0 \quad \dot{\theta}_y \neq 0 \quad \ddot{\theta}_y \neq 0 \quad (5.2)$$

Even though, for an arbitrary gyroscope configuration, an offset will occur from the reference coordinate system, the offset can be determined in advance, permitting the orientation of data gathering equipment to be adjusted to compensate for the angular error. It is therefore anticipated that permitting the vehicle to have a small offset from the reference coordinate system will not produce any serious problems. At steady state, it is also necessary for all of the gyroscopes in the configuration to be at rest with respect to the body; that is, the angular velocity and acceleration of each gyroscope gimbal with respect to the body be zero. Therefore,

$$\dot{\phi}_x = \ddot{\phi}_x = 0 \quad (5.3)$$

for each gyroscope in the configuration at steady state. The desired orientation of each gyroscope at steady state will, of course, depend on the vehicle design. The question immediately arises as to the nature of the torque that must be supplied to each gyroscope to maintain it at rest in its desired orientation at steady state, and

how this torque will be supplied.

#### A) The General Steady State Torque Equations

When a gyroscope is mounted within an orbiting vehicle, it is subjected to an angular velocity and acceleration due to the vehicle's orbital rate. If the gyroscope is at rest with respect to the body, the angular velocity and acceleration of the gyroscope gimbal with respect to inertial space, is the same as the angular velocity and acceleration of the body with respect to inertial space. For a vehicle with an arbitrary gyroscope configuration at steady state in an elliptical orbit, the angular velocity and acceleration of the body with respect to inertial space can be obtained from equations (2.14) through (2.19) by setting

$$\dot{\theta}_x = \ddot{\theta}_x = \dot{\theta}_z = \ddot{\theta}_z = \Omega_x = \Omega_z = 0 \quad (5.4)$$

$$\omega_{b/I.S.} = \omega_{g/I.S.} = \theta_z \Omega_y i_b + (\dot{\theta}_y + \Omega_y) j_b - \theta_x \Omega_y k_b \quad (5.5)$$

$$\dot{\omega}_{b/I.S.} = \dot{\omega}_{g/I.S.} = \theta_z \dot{\Omega}_y i_b + (\ddot{\theta}_y + \dot{\Omega}_y) j_b - \theta_x \dot{\Omega}_y k_b \quad (5.6)$$

The components of the torque on the gyroscope, necessary to produce this angular velocity and acceleration at steady state, can be obtained along the gyroscope axes from equations (4.24), (4.25) (4.26) and along the body axes from equations (4.29), (4.30), (4.31) by setting

$$\dot{\theta}_x = \ddot{\theta}_x = \dot{\theta}_z = \ddot{\theta}_z = 0 \quad (5.7)$$

The required components of torque on the gyroscope along the gyroscope axes are

$$\begin{aligned} T_{g_i g} = I_g & \left[ \sin \phi_z (\ddot{\theta}_y + \dot{\Omega}_y) + \sin \phi_y \cos \phi_z \theta_x \dot{\Omega}_y \right. \\ & + (\cos \phi_y \cos \phi_z \theta_z \dot{\Omega}_y) + H_r \left[ \sin \phi_x \cos \phi_z (\dot{\theta}_y + \Omega_y) \right. \\ & + (\cos \phi_x \cos \phi_y - \sin \phi_x \sin \phi_y \sin \phi_z) \theta_x \Omega_y - (\cos \phi_x \sin \phi_y \\ & \left. + \sin \phi_x \cos \phi_y \sin \phi_z) \theta_z \Omega_y \right] \end{aligned} \quad (5.8)$$

$$\begin{aligned} T_{g_j g} = I_g & \left[ \cos \phi_x \cos \phi_z (\ddot{\theta}_y + \dot{\Omega}_y) - (\cos \phi_x \sin \phi_y \sin \phi_z \right. \\ & + \sin \phi_x \cos \phi_y) \theta_x \dot{\Omega}_y - (\cos \phi_x \cos \phi_y \sin \phi_z \\ & \left. - \sin \phi_x \sin \phi_y) \theta_z \dot{\Omega}_y \right] \end{aligned} \quad (5.9)$$

$$\begin{aligned} T_{g_k g} = I_g & \left[ -\sin \phi_x \cos \phi_z (\ddot{\theta}_y + \dot{\Omega}_y) - (\cos \phi_x \cos \phi_y \right. \\ & - \sin \phi_x \sin \phi_y \sin \phi_z) \theta_x \dot{\Omega}_y + (\cos \phi_x \sin \phi_y \\ & + \sin \phi_x \cos \phi_y \sin \phi_z) \theta_z \dot{\Omega}_y \left. \right] + H_r \left[ \sin \phi_z (\dot{\theta}_y + \Omega_y) \right. \\ & \left. + \sin \phi_y \cos \phi_z \theta_x \Omega_y + \cos \phi_y \cos \phi_z \theta_z \Omega_y \right] \end{aligned} \quad (5.10)$$

and along the body axes are

$$T_{g_{i_b}} = I_g \dot{\theta}_z \dot{\Omega}_y + H_r \left[ (\sin \phi_x \cos \phi_y + \cos \phi_x \sin \phi_y \sin \phi_z) (\dot{\theta}_y + \dot{\Omega}_y) + \cos \phi_x \cos \phi_z \dot{\theta}_x \dot{\Omega}_y \right] \quad (5.11)$$

$$T_{g_{j_b}} = I_g (\ddot{\theta}_y + \dot{\Omega}_y) + H_r \left[ (\cos \phi_x \cos \phi_y \sin \phi_z - \sin \phi_x \sin \phi_y) \dot{\theta}_x \dot{\Omega}_y - (\sin \phi_x \cos \phi_y + \cos \phi_x \sin \phi_y \sin \phi_z) \dot{\theta}_z \dot{\Omega}_y \right] \quad (5.12)$$

$$T_{g_{k_b}} = -I_g \dot{\theta}_x \dot{\Omega}_y + H_r \left[ \cos \phi_x \cos \phi_z \dot{\theta}_z \dot{\Omega}_y + (\cos \phi_x \cos \phi_y \sin \phi_z - \sin \phi_x \sin \phi_y) (\dot{\theta}_y + \dot{\Omega}_y) \right] \quad (5.13)$$

B) Specialization for several restrictive cases.

It is advantageous to specialize these equations for somewhat more restrictive conditions.

1) Consider a satellite in an elliptical orbit with a gyroscope configuration chosen such that the components of the resultant torque exerted by the gyroscopes on the body along the  $X_b$  and  $Z_b$  axes are zero. In steady state, the components of torque on each gyroscope in the configuration can be obtained along the gyroscope axes from equations (5.8), (5.9), (5.10) and along the body axes from equations (5.11), (5.12), (5.13) by setting

$$\theta_x = \theta_z = 0 \quad (5.14)$$

The required components of torque on the gyroscope along the gyroscope axes are

$$T_{g_{i_g}} = I_g \sin \phi_z (\dot{\theta}_y + \dot{\Omega}_y) + H_r \sin \phi_x \cos \phi_z (\dot{\theta}_y + \dot{\Omega}_y) \quad (5.15)$$

$$T_{g_{j_g}} = I_g \cos \phi_x \cos \phi_z (\ddot{\theta}_y + \dot{\Omega}_y) \quad (5.16)$$

$$T_{g_{k_g}} = -I_g \sin \phi_x \cos \phi_z (\ddot{\theta}_y + \dot{\Omega}_y) + H_r \sin \phi_z (\dot{\theta}_y + \dot{\Omega}_y) \quad (5.17)$$

and along the body axes are

$$T_{g_{i_b}} = H_r (\sin \phi_x \cos \phi_y + \cos \phi_x \sin \phi_y \sin \phi_z) (\dot{\theta}_y + \dot{\Omega}_y) \quad (5.18)$$

$$T_{g_{j_b}} = I_g (\ddot{\theta}_y + \dot{\Omega}_y) \quad (5.19)$$

$$T_{g_{k_b}} = H_r (\cos \phi_x \cos \phi_y \sin \phi_z - \sin \phi_x \sin \phi_y) (\dot{\theta}_y + \dot{\Omega}_y) \quad (5.20)$$



2) Consider a satellite in a circular orbit with a completely arbitrary gyroscope configuration employed. In steady state a resultant torque will, in general, be exerted on the body by the gyroscopes. Therefore,  $\theta_x$ ,  $\theta_y$  and  $\theta_z$  will, in general not be zero. In steady state, the components of torque on each gyroscope in the configuration can be obtained along the gyroscope axes from equations (5.8), (5.9) (5.10) and along the body axes from equations (5.11), (5.12), (5.13) by setting

$$\ddot{\theta}_y = \dot{\theta}_y = \dot{\Omega}_y = 0 \quad (5.21)$$

The components of the torque on the gyroscope required along the gyroscope axes are

$$T_{g_{ig}} = H_r \left[ \sin \phi_x \cos \phi_z \Omega_y + (\cos \phi_x \cos \phi_y - \sin \phi_x \sin \phi_y \sin \phi_z) \theta_x \Omega_y - (\cos \phi_x \sin \phi_y + \sin \phi_x \cos \phi_y \sin \phi_z) \theta_z \Omega_y \right] \quad (5.22)$$

$$T_{g_{jg}} = 0 \quad (5.23)$$

$$T_{g_{kg}} = H_r \left[ \sin \phi_y \cos \phi_z \theta_x \Omega_y + \cos \phi_y \cos \phi_z \theta_z \Omega_y + \sin \phi_z \Omega_y \right] \quad (5.24)$$

and along the body axes are

$$T_{g_{ib}} = H_r \left[ (\sin \phi_x \cos \phi_y + \cos \phi_x \sin \phi_y \sin \phi_z) \Omega_y + \cos \phi_x \cos \phi_z \theta_x \Omega_y \right] \quad (5.25)$$

$$T_{g_{jb}} = H_r \left[ (\cos \phi_x \cos \phi_y \sin \phi_z - \sin \phi_x \sin \phi_y) \theta_x \Omega_y - (\sin \phi_x \cos \phi_y + \cos \phi_x \sin \phi_y \sin \phi_z) \theta_z \Omega_y \right] \quad (5.26)$$

$$T_{g_{kb}} = H_r \left[ \cos \phi_x \cos \phi_z \theta_z \Omega_y + (\cos \phi_x \cos \phi_y \sin \phi_z - \sin \phi_x \sin \phi_y) \Omega_y \right] \quad (5.27)$$

3) Consider a satellite in a circular orbit with a gyroscope configuration chosen such that no resultant torque is exerted by the gyroscopes on the body at steady state. The equations for this case can be obtained from the general equations (5.8) through (5.13) by setting

$$\theta_x = \theta_y = \theta_z = \dot{\theta}_y = \ddot{\theta}_y = \dot{\Omega}_y = 0 \quad (5.28)$$

The required components of the torque on the gyroscope along the gyroscope axes are

$$T_{g_i g} = H_r \sin \phi_x \cos \phi_z \Omega_y \quad (5.29)$$

$$T_{g_j g} = 0 \quad (5.30)$$

$$T_{g_k g} = H_r \sin \phi_z \Omega_y \quad (5.31)$$

and along the body axes are

$$T_{g_i b} = H_r (\sin \phi_x \cos \phi_y + \cos \phi_x \sin \phi_y \sin \phi_z) \Omega_y \quad (5.32)$$

$$T_{g_j b} = 0 \quad (5.33)$$

$$T_{g_k b} = H_r (\cos \phi_x \cos \phi_y \sin \phi_z - \sin \phi_x \sin \phi_y) \Omega_y \quad (5.34)$$

For a circular orbit, and steady state, an equivalent form for the torque on each gyroscope in a configuration, is, of course, given by

$$T_g = \Omega_y \times H_r \quad (5.35)$$

The resultant torque on all the gyroscopes for a circular orbit at steady state, is therefore given by

$$\sum (\Omega_y \times H_r) = \Omega_y \times \sum H_r \quad (5.36)$$

The resultant torque on the body is the negative of the resultant torque on the gyroscopes. Therefore, at steady state, the resultant torque on the body will be zero, when either  $\sum H_r = 0$  (the  $H_r$  vectors form a closed polygon) or the  $\sum H_r$  is along  $\Omega_y$ .

At steady state, it is necessary for the required torque, predicted by the equations, to be present on each of the gyroscopes of the configuration. Since none of the gyroscopes are constrained about their precession axes, it will be necessary to utilize a gyroscope torquer to furnish the  $i_g$  component of the torque for each gyroscope for which this component is not zero. For a circular orbit, the required torque will be a constant. For an elliptical orbit, it will be necessary to supply a time

varying torque which will undoubtedly require the use of programmed digital equipment. It would be interesting to consider what would happen if gyroscope torquers are not utilized. For a circular orbit, the precession angle of each gyroscope in the configuration, and the body angular deviations, will adjust themselves so that the resultant torque on the body will be zero. If desired, the values of the precession angles and body deviation angles can be obtained by first setting equation (5.22) equal to zero to obtain a relation between the precession angle and the body deviation angles, and then equating the negative of the resultant torque applied to the gyroscopes (the resultant torque is obtained by summing equations (5.25), (5.26), (5.27) for each gyroscope in the configuration) to the torque on the body, equations (2.52), (2.54), (2.56) after setting all the derivatives equal to zero.

$$-\sum T_{g_{i_b}} = -(I_{z_b} - I_{y_b}) 4 \theta_x \Omega_y^2 \quad (5.37)$$

$$-\sum T_{g_{j_b}} = 3 (I_{x_b} - I_{z_b}) \theta_y \Omega_y^2 \quad (5.38)$$

$$-\sum T_{g_{k_b}} = (I_{y_b} - I_{x_b}) \theta_z \Omega_y^2 \quad (5.39)$$

If the orbit is elliptical, the gyroscope will never reach a state of rest with respect to the body. Therefore, energy will be constantly dissipated due to gyroscope damping. The only sources of this energy are the kinetic and potential energy of the satellite. Invariably, as time progresses, the orbital parameters will therefore be altered.

### C) Choice of a Gyroscope Configuration

Consider briefly the problem of choosing a gyroscope configuration for a vehicle in a circular orbit. The configuration must, of course, be chosen to provide damping about all vehicle axes. (This aspect of the problem will be considered in detail in Chapter VI.) If possible, the gyroscope configuration should be chosen so that no resultant torque is exerted on the body due to the gyroscopes at steady state. If this cannot be achieved, it will be necessary to determine the steady state offset angles from equations (5.37), (5.38), and (5.39). (The precession angle of each gyroscope is specified by the configuration.) The torque which the torquer must supply to each gyroscope, is given by the  $i_g$  component of the torque on the gyroscope.

$$T_{\text{torquer}} = T_{g_{i_g}} \quad (5.40)$$

It is also necessary for each gyroscope in a configuration to be in a state of stable equilibrium. The nature of the equilibrium can be easily established for each gyroscope by substituting the value of  $\phi_x$  specified by the design into the derivative of equation (5.22) with respect to  $\phi_x$ .

$$\frac{d}{d\phi_x} T_{g_i} = H_r \left[ \cos \phi_x \cos \phi_z \Omega_y - (\sin \phi_x \cos \phi_y + \cos \phi_x \sin \phi_y \sin \phi_z) \theta_x \Omega_y - (\cos \phi_x \cos \phi_y \sin \phi_z - \sin \phi_x \sin \phi_y) \theta_z \Omega_y \right] \quad (5.41)$$

If equation (5.41) is positive, a state of stable equilibrium exists. If equation (5.41) is negative, a state of unstable equilibrium exists. The explanation for this test is as follows: Equation (5.41) is the derivative of the torque required to maintain the gyroscope at any specified position at steady state. If the derivative is positive, at the specified position, a positive angular displacement of the gyroscope will require a larger torque than is being supplied to maintain the new position. A negative angular displacement will require a smaller torque than is being supplied to maintain the displacement. Hence, in either case, a resultant torque will be established such that the gyroscope will return to its original position. If the derivative is negative, a positive angular displacement will require a smaller torque than is being supplied, and a negative angular displacement will require a larger torque than is being supplied. In either case, the resultant torque will be established such that the gyroscope will continue to move in the direction displaced.

In order to obtain a better understanding of the principles involved, an example will be considered. Consider the configuration shown in Fig 4-5 where a single gyroscope is mounted with its precession axis along the  $X_b$  axis of the vehicle. The satellite design requires the spin axis of the gyroscope to be at an angle  $\phi_x$  with the  $Y_b$  axis. It will be assumed for convenience that the satellite is in a circular orbit. It is immediately apparent that if  $\phi_x$  is not zero, steady state will be established with the body offset from the reference coordinate system. If the vehicle was aligned with the reference coordinate system at steady state, the angular momentum vector  $H_r$ , will not be along  $\Omega_y$ . The angular offset, at steady state, can be obtained by setting  $\phi_y = \phi_z = 0$  in equations (5.25), (5.26) and (5.27) and substituting in equations (5.37), (5.38) and (5.39)

$$- H_r (\sin \phi_x \Omega_y + \cos \phi_x \theta_x \Omega_y) = - (I_{z_b} - I_{y_b}) \theta_x \Omega_y^2 \quad (5.42)$$

$$H_r \sin \phi_x \theta_x \Omega_y = 3(I_{x_b} - I_{z_b}) \theta_y \Omega_y^2 \quad (5.43)$$

$$- H_r \cos \phi_x \theta_z \Omega_y = (I_{y_b} - I_{x_b}) \theta_z \Omega_y^2 \quad (5.44)$$

Solution of these equations, yields the offset angles of the vehicle at steady state.

$$\theta_x = \frac{H_r \sin \phi_x}{(I_{z_b} - I_{x_b}) 4\Omega_y - \cos \phi_x H_r} \quad (5.45)$$

If

$$H_r \cos \phi_x - (I_{x_b} - I_{y_b}) \Omega_y \neq 0 \quad (5.46)$$

then

$$\theta_y = \theta_z = 0 \quad (5.47)$$

If the left side of equation (5.46) is equal to zero,  $\theta_y$  and  $\theta_z$  are indeterminate.

The torque which must be supplied by the gyroscope torquer is given by

$$T_{\text{torquer}} = H_r \Omega_y (\cos \phi_x \theta_x + \sin \phi_x) \quad (5.48)$$

If a gyroscope torquer is not utilized, steady state will be established with  $\phi_x = 0$  and the vehicle aligned with the reference coordinate axes.

If another gyroscope is added to the configuration of Fig. 4-5 so that the configuration of Fig. 6-2, with  $\phi_z = 0$  results, steady state will be established with the vehicle axes aligned with the reference coordinate axes, since for this configuration, the resultant angular momentum vector, at steady state, is along  $\Omega_y$ . This configuration is known as a "V" configuration and will be discussed further in Chapter VI.

In Chapter VI, the results of Chapters II, IV and V will be combined to obtain the equations describing the dynamics of an orbiting vehicle with internally mounted gyroscopes. Several configurations will be considered that provide damping about all of the vehicle axes. For simplicity, the treatment will be restricted to vehicles in a circular orbit.

CHAPTER VI - THE DYNAMICS OF AN ORBITING VEHICLE WITH INTERNALLY  
MOUNTED GYROSCOPES FOR A CIRCULAR ORBIT

The dynamics of an orbiting vehicle in a circular orbit with internally mounted gyroscopes will be developed for several gyroscope configurations. There is no contention that the configurations chosen for presentation are, in any sense, optimal; they are presented to illustrate the principles involved. The gyroscope configurations chosen for analysis, will provide indirect damping about all three of the vehicle axes. It was noted in Chapter III that a smaller settling time could be obtained through the utilization of indirect damping than with direct damping. It is for this reason that all the configurations presented are chosen to provide indirect damping. In fact, if direct damping was desirable, it would be merely necessary to construct the vehicle in two parts, coupled viscously, since the mechanism of gyroscope precession is not involved. It has been shown in the literature, and should be expected from the results of Chapter III of this report, that direct vehicle damping will result in excessive settling time.

The dynamics of an orbiting vehicle with internally mounted gyroscopes can be developed by combining the results obtained in Chapter II for an orbiting rigid body and the results obtained in Chapter IV for a gyroscope under various constraints. The torque exerted on the body is equal to the vector sum of the external disturbance torques (exclusive of the differential gravity torque) exerted on the body and the torques exerted by the gyroscopes on the body. For a symmetrically designed gyroscope, there is no differential gravity torque on the gyroscope, hence the torque exerted by the gyroscope on the body is the negative of the torque exerted on the gyroscope.

$$T_e = T_d + \sum_{n=1}^N T_{g_n} \quad (6.1)$$

where  $T_e$  is the external torque applied to the body less the differential gravity torque.  
 $T_d$  is the total torque on the body less the differential gravity torque.  
 $T_{g_n}$  is the torque on the  $n^{\text{th}}$  gyroscope of the configuration.

A) Analysis of a Configuration Employing Gyroscopes with Precession axes  
along  $X_b$  and  $Z_b$  .

Fig. 6-1 shows a configuration employing two gyroscopes which will provide damping about all vehicle axes. One of the gyroscopes is oriented with its precession axis along the  $Z_b$  axis (precession angle denoted by  $\phi_{x_1}$ ) and the other

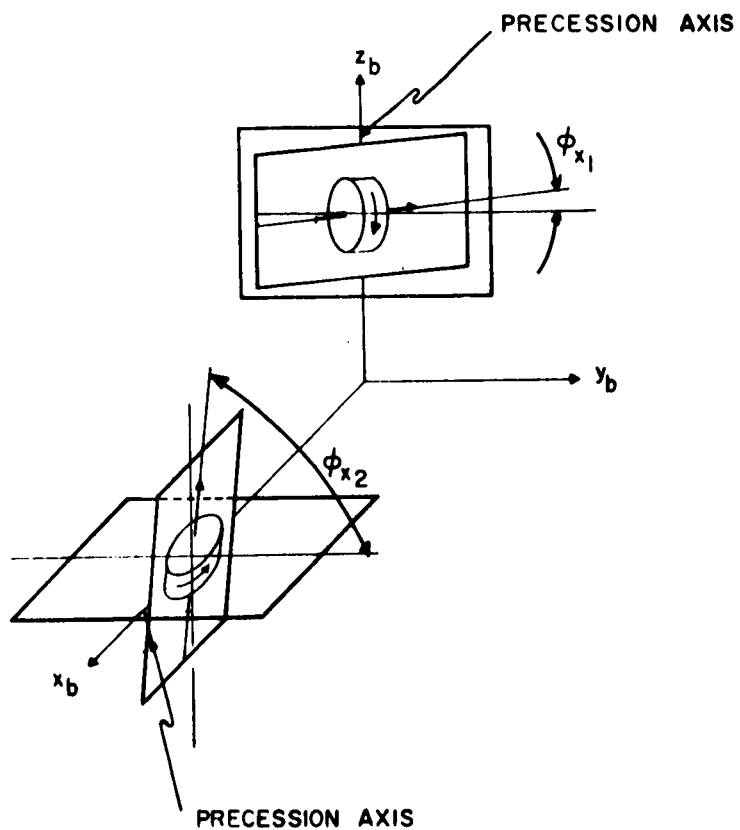


Fig. 6-1 Configuration Employing Gyroscopes with Precession Axes Along  $X_b$  and  $Z_b$

with its precession axis along the  $X_b$  axis, (precession angle denoted by  $\phi_{x_2}$ ). If gyroscope torquers are not utilized for both gyroscopes, at steady state, the body will be aligned with the reference coordinate axes and the steady state values of  $\phi_{x_1}$  and  $\phi_{x_2}$ ,  $\phi_{x_{1_0}}$  and  $\phi_{x_{2_0}}$ , will be zero. For such a condition, indirect damping will not be attainable about the  $Y_b$  axis. To obtain indirect damping about the  $Y_b$  axis, it is necessary that at least one of the steady state gyroscope precession angles,  $\phi_{x_{1_0}}$  or  $\phi_{x_{2_0}}$ , be non-zero. In general, for arbitrary values of  $\phi_{x_{1_0}}$  and  $\phi_{x_{2_0}}$  indirect damping about the  $X_b$  axis is provided by the  $Z_b$  oriented gyroscope, indirect damping about the  $Y_b$  axis is provided by both the  $X_b$  and  $Z_b$  oriented gyroscopes, and indirect damping is provided about the  $Z_b$  axis by the  $X_b$  oriented gyroscope. For arbitrary values of  $\phi_{x_{1_0}}$  and  $\phi_{x_{2_0}}$ , a gyroscope torquer will be required for each gyroscope.

The angular deviations of the vehicle as a function of  $\phi_{x_{1_0}}$  and  $\phi_{x_{2_0}}$  at steady state can be calculated from equations (5.25), (5.26), (5.27), (5.37), (5.38) and (5.39). Solution of these equations yields:

$$\theta_{x_0} = \frac{H_r \sin \phi_{x_{2_0}}}{4(I_{z_b} - I_{y_b}) \Omega_y - H_r (\cos \phi_{x_{1_0}} + \cos \phi_{x_{2_0}})} \quad (6.2)$$

$$\theta_{z_0} = \frac{-H_r \sin \phi_{x_{1_0}}}{(I_{y_b} - I_{x_b}) \Omega_y + H_r (\cos \phi_{x_{1_0}} + \cos \phi_{x_{2_0}})} \quad (6.3)$$

$$\theta_{y_0} = \frac{H_r (\sin \phi_{x_{2_0}} \theta_{z_0} - \sin \phi_{x_{1_0}} \theta_{x_0})}{3(I_{x_b} - I_{z_b}) \Omega_y} \quad (6.4)$$

The torque which each gyroscope torquer must supply can be determined from equation (5.40). For the  $X_b$  oriented gyroscope, the torque required is obtained from equation (5.22) with  $\phi_y = \phi_z = 0$ .

$$T_{\text{torquer}_x} = H_r \Omega_y (\sin \phi_{x_{2_0}} + \cos \phi_{x_{2_0}} \theta_{x_0}) \quad (6.5)$$



For the  $Z_b$  oriented gyroscope, the torque required is obtained from equation (5.22) with  $\phi_y = -90^\circ$  and  $\phi_z = 0$ .

$$T_{\text{torquer}_z} = H_r \Omega_y (\sin \phi_{x_{1_0}} + \cos \phi_{x_{1_0}} \theta_{z_0}) \quad (6.6)$$

where  $\theta_{x_0}$  and  $\theta_{z_0}$  are obtained from equations (6.2) and (6.3)

The values of  $\phi_{x_{1_0}}$  and  $\phi_{x_{2_0}}$  must, of course, be chosen so that the gyroscopes, at steady state, are in a state of stable equilibrium. To check the nature of the equilibrium it is merely necessary to substitute the steady state deviation angles (equations (6.2), (6.3), (6.4)) into equation (5.41) for each gyroscope and examine the sign.

For stability

$$\cos \phi_{x_{1_0}} + \frac{H_r \sin^2 \phi_{x_{1_0}}}{(I_{y_b} - I_{x_b}) \Omega_y + H_r (\cos \phi_{x_{1_0}} + \cos \phi_{x_{2_0}})} > 0 \quad (6.7)$$

$$\cos \phi_{x_{2_0}} - \frac{H_r \sin^2 \phi_{x_{2_0}}}{4(I_{z_b} - I_{y_b}) \Omega_y - H_r (\cos \phi_{x_{1_0}} + \cos \phi_{x_{2_0}})} > 0 \quad (6.8)$$

The dynamic performance of the vehicle with internally mounted gyroscopes can be obtained from the body equations for a circular orbit (2.52), (2.54), (2.56), from the equations of an  $X_b$  oriented gyroscope (4.46), (4.47), (4.48), from the equations of a  $Z_b$  oriented gyroscope (4.54), (4.55), (4.56) and from equation (6.1). The resulting equations are:

$$\begin{aligned} T_{e_{i_b}} = & (I_{x_b} + 2 I_g) (\ddot{\theta}_x + \dot{\theta}_z \Omega_y) + (I_{z_b} - I_{y_b}) (\dot{\theta}_z \Omega_y - 4 \theta_x \Omega_y^2) \\ & + I_g [\ddot{\phi}_{x_2} + \dot{\phi}_{x_1} (\dot{\theta}_y + \Omega_y)] + H_r [\sin \phi_{x_2} (\dot{\theta}_y + \Omega_y) \\ & + (\cos \phi_{x_1} + \cos \phi_{x_2}) (\dot{\theta}_z - \theta_x \Omega_y) - \dot{\phi}_{x_1} \cos \phi_{x_1}] \end{aligned} \quad (6.9)$$

$$\begin{aligned} T_{e_{j_b}} = & (I_{y_b} + 2I_g) \ddot{\theta}_y + 3(I_{x_b} - I_{z_b}) \theta_y \Omega_y^2 + I_g \left[ \dot{\phi}_{x_2} (\dot{\theta}_z - \theta_x \Omega_y) \right. \\ & \left. - \dot{\phi}_{x_1} (\dot{\theta}_x + \theta_z \Omega_y) \right] - H_r \left[ \sin \phi_{x_1} (\dot{\theta}_z - \theta_x \Omega_y) + \sin \phi_{x_2} (\dot{\theta}_x + \theta_z \Omega_y) \right. \\ & \left. + \dot{\phi}_{x_1} \sin \phi_{x_1} + \dot{\phi}_{x_2} \sin \phi_{x_2} \right] \end{aligned} \quad (6.10)$$

$$\begin{aligned} T_{e_{k_b}} = & (I_{z_b} + 2I_g) (\ddot{\theta}_z - \dot{\theta}_x \Omega_y) + (I_{y_b} - I_{x_b}) (\dot{\theta}_x \Omega_y + \theta_z \Omega_y^2) \\ & + I_g \left[ \ddot{\phi}_{x_1} - \dot{\phi}_{x_2} (\dot{\theta}_y + \Omega_y) \right] + H_r \left[ \dot{\phi}_{x_2} \cos \phi_{x_2} \right. \\ & \left. + \sin \phi_{x_1} (\dot{\theta}_y + \Omega_y) + (\cos \phi_{x_1} + \cos \phi_{x_2}) (\dot{\theta}_x + \theta_z \Omega_y) \right] \end{aligned} \quad (6.11)$$

The equation of constraint for the  $X_b$  oriented gyroscope, relating  $\phi_{x_2}$  to the body deviation angles, can be obtained from equation (4.49), where  $T_c$  is equal to  $T_{\text{torquer}_x}$  given by equation (6.5)

$$\begin{aligned} T_{\text{torquer}_x} = & D\dot{\phi}_{x_2} + I_g (\ddot{\theta}_x + \dot{\theta}_z \Omega_y + \ddot{\phi}_{x_2}) + H_r \left[ \sin \phi_{x_2} (\dot{\theta}_y + \Omega_y) \right. \\ & \left. - \cos \phi_{x_2} (\dot{\theta}_z - \theta_x \Omega_y) \right] \end{aligned} \quad (6.12)$$

The equation of constraint for the  $Z_b$  oriented gyroscope can be obtained from equation (4.57) where  $T_c$  is equal to  $T_{\text{torquer}_z}$  given by equation (6.6)

$$\begin{aligned} T_{\text{torquer}_z} = & D\dot{\phi}_{x_1} + I_g (\ddot{\theta}_z - \dot{\theta}_x \Omega_y + \ddot{\phi}_{x_1}) + H_r \left[ \sin \phi_{x_1} (\dot{\theta}_y + \Omega_y) \right. \\ & \left. + \cos \phi_{x_1} (\dot{\theta}_x + \theta_z \Omega_y) \right] \end{aligned} \quad (6.13)$$

The equations developed in this section characterize the steady state and dynamic performance of an orbiting vehicle for the configuration of Fig. 6-1 for arbitrary  $\phi_{x_1_0}$  and  $\phi_{x_2_0}$ . Since the equations are nonlinear, the dynamic performance of a vehicle containing this configuration can best be analyzed using an analog or digital simulation. It will be necessary to choose values of  $\phi_{x_1_0}$ ,  $\phi_{x_2_0}$  and find a suitable vehicle geometry so that both adequate settling time is attained and the vehicle angular deviations at steady state are small. Indeed, for large angular deviations, the approximations made in Chapter II will probably invalidate the results.

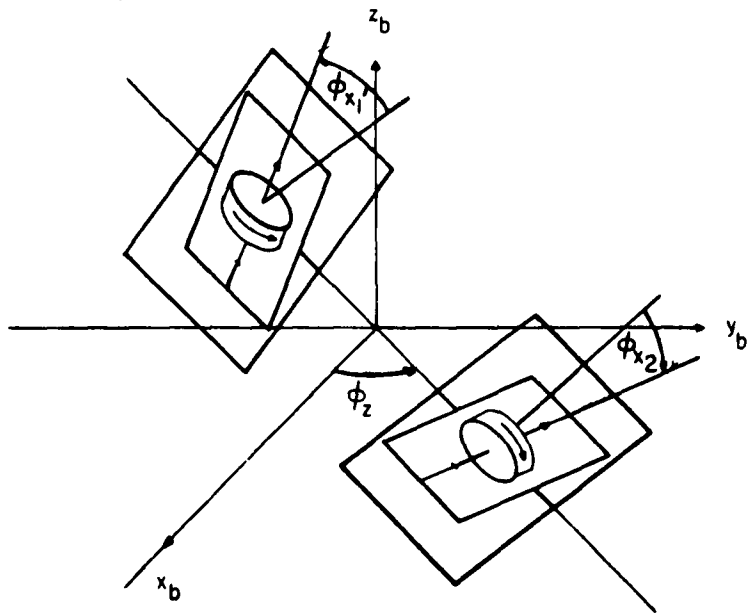


Fig. 6-2 "V" Configuration in the  $X_b Y_b$  Plane

B) Analysis of a "V" configuration in the  $X_b Y_b$  plane.

Fig. 6-2 shows two gyroscopes with their precession axes in the  $X_b Y_b$  plane forming a "V" configuration. This configuration will provide indirect damping about all three of the vehicle axes. At steady state, one of the gyroscopes will have its spin axis above the  $X_b Y_b$  plane by an angle  $\phi_{x_1}$ . This gyroscope will, for convenience, be referred to as "gyro I". The other gyroscope will, at steady state, have its spin axis below the  $X_b Y_b$  plane by an angle  $\phi_{x_2}$ . This gyroscope will, for convenience, be referred to as "gyro II". The precession angle of gyro I will be denoted by  $\phi_{x_1}$  and the precession angle of gyro II will be denoted by  $\phi_{x_2}$ . At steady state

$$\phi_{x_1} = \phi_{x_{10}} \quad (6.14)$$

$$\phi_{x_2} = 360^\circ - \phi_{x_{10}} \quad (6.15)$$

The angular deviations of the vehicle as a function of  $\phi_{x_1}$  at steady state can be calculated from equations (5.25), (5.26), (5.27), (5.37), (5.38) and (5.39).

$$H_r \cos \phi_{x_{10}} \cos \phi_z \theta_{x_0} = 2(I_{z_b} - I_{y_b}) \theta_{x_0} \Omega_y \quad (6.16)$$

$$2 H_r \cos \phi_{x_{10}} \sin \phi_z \theta_{x_0} = 3(I_{z_b} - I_{x_b}) \theta_{y_0} \Omega_y \quad (6.17)$$

$$\begin{aligned} 2 H_r (\cos \phi_{x_{10}} \cos \phi_z \theta_{z_0} + \cos \phi_{x_{10}} \sin \phi_z) \\ = (I_{x_b} - I_{y_b}) \theta_{z_0} \Omega_y \end{aligned} \quad (6.18)$$

Solution of these equations yields the offset angles of the vehicle at steady state.

$$\theta_{z_0} = - \frac{2 H_r \cos \phi_{x_{10}} \sin \phi_z}{(I_{y_b} - I_{x_b}) \Omega_y + 2 H_r \cos \phi_{x_{10}} \cos \phi_z} \quad (6.19)$$

If

$$H_r \cos \phi_{x_{10}} \cos \phi_z - 2(I_{z_b} - I_{y_b}) \Omega_y \neq 0 \quad (6.20)$$

then

$$\theta_{x_0} = \theta_{y_0} = 0 \quad (6.21)$$

If the left side of equation (6.20) is equal to zero,  $\theta_{x_0}$  and  $\theta_{y_0}$  are indeterminate. Note, that if  $\phi_z = 0$ ,  $\theta_{z_0}$  will also be zero and hence, at steady state, the vehicle will be perfectly aligned with the reference coordinate axes.

The torque which each gyroscope torquer must supply can be determined from equation (5.40). For gyro I, the torque required is obtained from equation (5.22) with  $\phi_y = 0$ .

$$T_{\text{torquer I}} = \frac{H_r \Omega}{r} y (\sin \phi_{x_{1_0}} \cos \phi_z + \cos \phi_{x_{1_0}} \theta_{x_0} - \sin \phi_{x_{1_0}} \sin \phi_z \theta_{z_0}) \quad (6.22)$$

For gyro II, the torque required is obtained from equation (5.22) with  $\phi_y = 0$  and  $\phi_{x_{2_0}} = 360^\circ - \phi_{x_{1_0}}$

$$T_{\text{torquer II}} = H_r \Omega y (\cos \phi_{x_{1_0}} \theta_{x_0} - \sin \phi_{x_{1_0}} \cos \phi_z + \sin \phi_{x_{1_0}} \sin \phi_z \theta_{z_0}) \quad (6.23)$$

Since  $\theta_{x_0} = 0$

$$T_{\text{torquer I}} = H_r \Omega y \sin \phi_{x_{1_0}} (\cos \phi_z - \sin \phi_z \theta_{z_0}) \quad (6.24)$$

$$T_{\text{torquer II}} = H_r \Omega y \sin \phi_{x_{1_0}} (\sin \phi_z \theta_{z_0} - \cos \phi_z) \quad (6.25)$$

where  $\theta_{z_0}$  is obtained from equation (6.19).

The value of  $\phi_{x_{1_0}}$  must, of course, be chosen so that both gyroscopes, at steady state, are in a state of stable equilibrium. To check the nature of the equilibrium, it is merely necessary to substitute the steady state deviation angles (6.19) and (6.21) into equation (5.41) for each gyroscope and examine the sign. For stability of both gyroscopes

$$\cos \phi_{x_{1_0}} \cos \phi_z + \frac{2H_r \cos^2 \phi_{x_{1_0}} \sin^2 \phi_z}{(I_{y_b} - I_{x_b}) \Omega y + 2H_r \cos \phi_{x_{1_0}} \cos \phi_z} > 0 \quad (6.26)$$

If the precession axes of the gyroscopes are along  $X_b$  ( $\phi_z = 0$ ), the condition for stability reduces to

$$\cos \phi_{x_{1_0}} > 0 \quad (6.27)$$

Clearly, the gyroscopes will be in a state of stable equilibrium when

$$-90^\circ < \phi_{x_1} < +90^\circ \quad (6.28)$$

The dynamic performance of the vehicle with internally mounted gyroscopes can be obtained from the body equations for a circular orbit (2.52), (2.54), (2.56), from the equations for a gyroscope whose precession axis is in the  $X_b Y_b$  plane (4.34), (4.35), (4.36) and from equation (6.1). The resulting equations are:

$$\begin{aligned} T_{e_{ib}} = & (I_{x_b} + 2I_g) (\ddot{\theta}_x + \dot{\theta}_z \Omega_y) + (I_{z_b} - I_{y_b}) (\dot{\theta}_z \Omega_y - 4\theta_x \Omega_y^2) \\ & + I_g \left[ \cos \phi_z (\ddot{\phi}_{x_1} + \ddot{\phi}_{x_2}) - \sin \phi_z (\dot{\theta}_z - \theta_x \Omega_y) (\dot{\phi}_{x_1} + \dot{\phi}_{x_2}) \right] \\ & + H_r \left[ (\dot{\theta}_y + \Omega_y) (\sin \phi_{x_1} + \sin \phi_{x_2}) - \cos \phi_z (\dot{\theta}_z - \theta_x \Omega_y) (\cos \phi_{x_1} + \cos \phi_{x_2}) \right. \\ & \left. + \sin \phi_z (\dot{\phi}_{x_1} \sin \phi_{x_1} + \dot{\phi}_{x_2} \sin \phi_{x_2}) \right] \end{aligned} \quad (6.29)$$

$$\begin{aligned} T_{e_{jb}} = & (I_{y_b} + 2I_g) \ddot{\theta}_y + 3(I_{x_b} - I_{z_b}) \theta_y \Omega_y^2 + I_g \left[ \sin \phi_z (\ddot{\phi}_{x_1} + \ddot{\phi}_{x_2}) \right. \\ & \left. + \cos \phi_z (\dot{\theta}_z - \theta_x \Omega_y) (\dot{\phi}_{x_1} + \dot{\phi}_{x_2}) \right] - H_r \left[ \cos \phi_z (\dot{\phi}_{x_1} \sin \phi_{x_1} + \dot{\phi}_{x_2} \sin \phi_{x_2}) \right. \\ & \left. + \sin \phi_z (\dot{\theta}_z - \theta_x \Omega_y) (\cos \phi_{x_1} + \cos \phi_{x_2}) + (\dot{\theta}_x + \theta_z \Omega_y) (\sin \phi_{x_1} + \sin \phi_{x_2}) \right] \end{aligned} \quad (6.30)$$

$$\begin{aligned} T_{e_{kb}} = & (I_{z_b} + 2I_g) (\ddot{\theta}_z - \dot{\theta}_x \Omega_y) + (I_{y_b} - I_{x_b}) (\dot{\theta}_x \Omega_y + \theta_z \Omega_y^2) \\ & + I_g \left[ \sin \phi_z (\dot{\theta}_x + \theta_z \Omega_y) (\dot{\phi}_{x_1} + \dot{\phi}_{x_2}) - \cos \phi_z (\dot{\theta}_y + \Omega_y) (\phi_{x_1} + \phi_{x_2}) \right] \\ & + H_r \left[ \dot{\phi}_{x_1} \cos \phi_{x_1} + \dot{\phi}_{x_2} \cos \phi_{x_2} + \cos \phi_z (\dot{\theta}_x + \theta_z \Omega_y) (\cos \phi_{x_1} + \cos \phi_{x_2}) \right. \\ & \left. + \sin \phi_z (\dot{\theta}_y + \Omega_y) (\cos \phi_{x_1} + \cos \phi_{x_2}) \right] \end{aligned} \quad (6.31)$$

The equation of constraint for gyro I, relating its precession angle to the body deviation angles, can be obtained from equation (4.37), where  $T_c$  is equal to

$T_{\text{torquer}_I}$  given in equation (6.24)

$$\begin{aligned} T_{\text{torquer}_I} = & D\dot{\phi}_{x_1} + I_g \left[ \ddot{\theta}_y \sin \phi_z + \cos \phi_z (\ddot{\theta}_x + \dot{\theta}_z \Omega_y) + \ddot{\phi}_{x_1} \right] \\ & + H_r \left[ \sin \phi_{x_1} \cos \phi_z (\dot{\theta}_y + \Omega_y) - \cos \phi_{x_1} (\dot{\theta}_z - \theta_x \Omega_y) \right. \\ & \left. - \sin \phi_{x_1} \sin \phi_z (\dot{\theta}_x + \theta_z \Omega_y) \right] \end{aligned} \quad (6.32)$$

The equation of constraint for gyro II is identical with that for gyro I (equation (6.32)) with  $\phi_{x_1}$  replaced by  $\phi_{x_2}$  and  $T_{\text{torquer}_I}$  replaced by  $T_{\text{torquer}_{II}}$ .

Although the development for the "V" configuration in this section was for equal and opposite displacement angles from the  $X_b Y_b$  plane, the development could have been easily extended to the case where the displacement angles are arbitrary. In fact, an extension to a "V" configuration, where the precession axes lie on any line relative to the body coordinate system, can be easily accomplished from the equations developed in Chapters II, IV and V in a manner similar to that used in this section.

### C) A Configuration Employing a Single Gyroscope to Provide Three Axis Vehicle Damping .

Fig. 6-3 shows a configuration employing a single, one degree of freedom, gyroscope whose precession axis is located in the  $X_b Z_b$  plane. This configuration will provide damping about all three of the vehicle axes. Since only one gyroscope is used, no subscripting is necessary therefore, the gyroscope precession angle will be denoted merely by  $\phi_x$ , and the value of the gyroscope precession angle at steady state will be denoted by  $\phi_{x_0}$ .

The angular deviations of the vehicle as a function of  $\phi_x$  at steady state can be calculated from equations (5.25), (5.26) and (5.27) with  $\phi_z = 0$  and from equations (5.37), (5.38) and (5.39). Solution of these equations yields:

$$\theta_{x_0} = \frac{H_r \sin \phi_{x_0} \cos \phi_y}{4(I_{z_b} - I_{y_b})\Omega_y - H_r \cos \phi_{x_0}} \quad (6.33)$$

$$\theta_{z_0} = \frac{H_r \sin \phi_{x_0} \sin \phi_y}{(I_{y_b} - I_{x_b})\Omega_y + H_r \cos \phi_{x_0}} \quad (6.34)$$

$$\theta_{y_0} = \frac{H_r \sin \phi_{x_0} (\sin \phi_y \theta_{x_0} + \cos \phi_y \theta_{z_0})}{3(I_{x_b} - I_{z_b})\Omega_y} \quad (6.35)$$

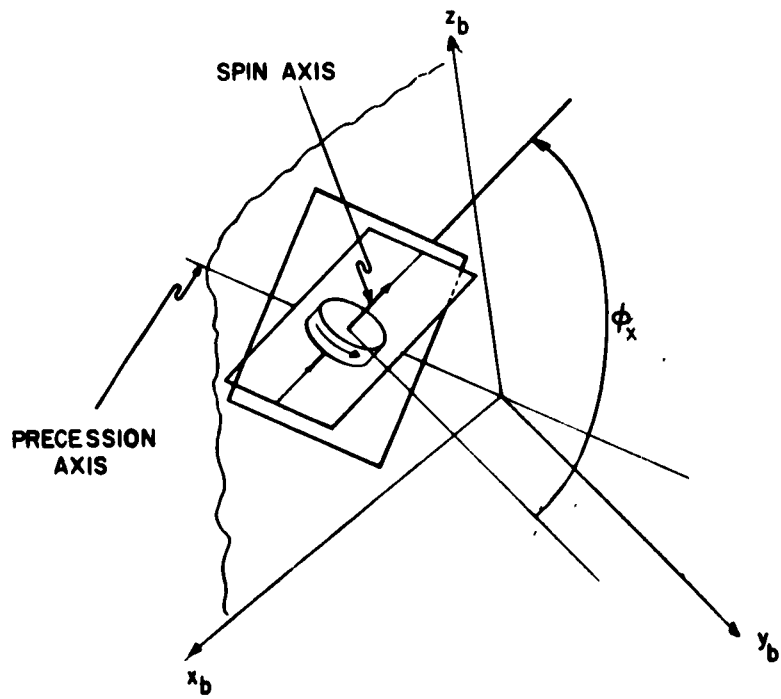


**Fig. 6-3 Configuration Employing a Simple Gyroscope**



The torque which the gyroscope torquer must supply can be obtained from equation (5.22) with  $\phi_z = 0$  and from equation (5.40)

$$T_{\text{torquer}} = H_r \Omega_y (\sin \phi_{x_0} + \cos \phi_{x_0} \cos \phi_y \theta_{x_0} - \cos \phi_{x_0} \sin \phi_y \theta_{z_0}) \quad (6.36)$$

where  $\theta_{x_0}$  and  $\theta_{z_0}$  are obtained from equations (6.33) and (6.34)

The value of  $\phi_{x_0}$  must, of course, be chosen so that the gyroscope, at steady state, is in a state of stable equilibrium. To check the nature of the equilibrium it is merely necessary to substitute the steady state deviation angles (equations (6.33), (6.34), (6.35) into equation (5.41) and examine the sign. For stability

$$\cos \phi_{x_0} \cos \phi_z - \sin \phi_{x_0} \cos \phi_y \theta_{x_0} + \sin \phi_{x_0} \sin \phi_y \theta_{z_0} > 0 \quad (6.37)$$

The dynamic performance of the vehicle can be obtained from the body equations for a circular orbit (2.52), (2.54), (2.56), from the equations for a gyroscope constrained to rotate in the  $X_b Z_b$  plane (4.38), (4.39), (4.40) and equation (6.1).

The resulting equations are:

$$\begin{aligned} T_{e_{ib}} = & (I_{x_b} + I_g) (\ddot{\theta}_x + \dot{\theta}_z \Omega_y) + (I_{z_b} - I_{y_b}) (\dot{\theta}_z \Omega_y - 4\theta_x \Omega_y^2) \\ & + I_g \left[ \ddot{\phi}_x \cos \phi_y - \dot{\phi}_x (\dot{\theta}_y + \Omega_y) \sin \phi_y \right] + H_r \left[ (\dot{\theta}_y + \Omega_y) \sin \phi_x \cos \phi_y \right. \\ & \left. - \cos \phi_x (\dot{\theta}_z - \theta_x \Omega_y - \ddot{\phi}_x \sin \phi_y) \right] \end{aligned} \quad (6.38)$$

$$\begin{aligned} T_{e_{jb}} = & (I_{y_b} + I_g) \ddot{\theta}_y + 3(I_{x_b} - I_{z_b}) \theta_y \Omega_y^2 + I_g \ddot{\phi}_x \left[ (\dot{\theta}_z - \theta_x \Omega_y) \cos \phi_y \right. \\ & \left. + (\dot{\theta}_x + \theta_z \Omega_y) \right] + H_r \sin \phi_x \left[ (\dot{\theta}_z - \theta_x \Omega_y) \sin \phi_y - \dot{\phi}_x - (\dot{\theta}_x + \theta_z \Omega_y) \cos \phi_y \right] \end{aligned} \quad (6.39)$$

$$\begin{aligned} T_{e_{kb}} = & (I_{z_b} + I_g) (\ddot{\theta}_z - \dot{\theta}_x \Omega_y) + (I_{y_b} - I_{x_b}) (\dot{\theta}_x \Omega_y + \theta_z \Omega_y^2) \\ & - I_g \left[ \dot{\phi}_x (\dot{\theta}_y + \Omega_y) \cos \phi_y + \ddot{\phi}_x \sin \phi_y \right] - H_r \left[ (\dot{\theta}_y + \Omega_y) \sin \phi_x \sin \phi_y \right. \\ & \left. - \cos \phi_x (\dot{\theta}_x + \theta_z \Omega_y + \ddot{\phi}_x \cos \phi_y) \right] \end{aligned} \quad (6.40)$$

The equation of constraint relating the gyroscope precession angle to body deviation angles can be obtained from equation (4.41) where  $T_c$  is equal to  $T_{\text{torquer}}$  given by equation (6.36)

$$T_{\text{torquer}} = D\dot{\phi}_x + I_g \left[ \cos \phi_y (\ddot{\theta}_x + \dot{\theta}_z \Omega_y) - \sin \phi_y (\ddot{\theta}_z - \dot{\theta}_x \Omega_y) + \dot{\phi}_x \right] \quad (6.41)$$

$$+ H_r \left[ \sin \phi_x (\ddot{\theta}_y + \Omega_y) - \cos \phi_x \cos \phi_y (\dot{\theta}_z - \theta_x \Omega_y) - \cos \phi_x \sin \phi_y (\dot{\theta}_x + \theta_z \Omega_y) \right]$$

The procedure involved for developing the equations describing the statics and dynamics of an orbiting vehicle for an arbitrary configuration should be clear from the examples that have been presented. The equations developed in Chapters II, IV and V can be used to analyze any configuration in a circular orbit. Furthermore, many of the equations can be applied to a vehicle in an elliptical orbit. Chapter VII will summarize the results thus far obtained and will indicate the areas in which further study is warranted.

## Chapter VII - CONCLUSION

The analyses given in this report are valid if the following assumptions are satisfied:

1. Attitude deviations are small so that the equations of motion for the body can be linearized.
2. With the exception of the internally mounted gyroscopes, the satellite comprises a rigid body with no moving internal parts.
3. Control is desired about the principal axes of the vehicle.
4. The earth is assumed to be a homogeneous sphere, and therefore the gravitational field is inverse square.
5. All gyroscopes are assumed symmetric.

It is further assumed in the latter part of Chapter V and Chapter VI that the orbit is circular.

With the above assumptions the following has been accomplished:

1. The equations of motion of a rigid body in an elliptical orbit were obtained with the inclusion of the gravity gradient torque.
2. An analysis of a simple configuration employing gyroscope damping was considered to furnish an insight into the mechanism of gyroscope damping and its properties.
3. The equations of a symmetrical one degree of freedom gyroscope mounted in an arbitrary position within the vehicle in an elliptical orbit were obtained and several specialized cases were cited.
4. The steady state requirements for an orbiting vehicle containing internally mounted gyroscopes were considered. In the latter part of this analysis the vehicle's orbit was assumed circular.
5. The equations of motion for a vehicle containing internally mounted gyroscopes were obtained for several gyroscope configurations for a circular orbit.

There are several areas of investigation that have been neglected in this work and should be the topic of future study in this field.

1. The effects of large angular deviations should be considered since at the time of insertion of the vehicle into its orbit large angular deviations will invariably occur.

2. The effects of an non-spherical, non-homogeneous earth should be considered.
3. The effects of moving internal components should be investigated. The acceleration and deceleration of internally moving parts (such as tape recorders) will produce reaction torques on the vehicle. Motion of components may also cause the moments of inertia and location of the vehicle's principal axes to become time varying.
4. The analysis should be extended to include non-symmetrically designed gyroscopes.
5. A computer study of several gyroscope configurations is essential to obtain both an optimum vehicle geometry and optimum gyroscope configuration.

APPENDIX ADerivation of Euler's Equations

For any system of particles, the angular momentum of that system about any point in space (see Figure A-1)

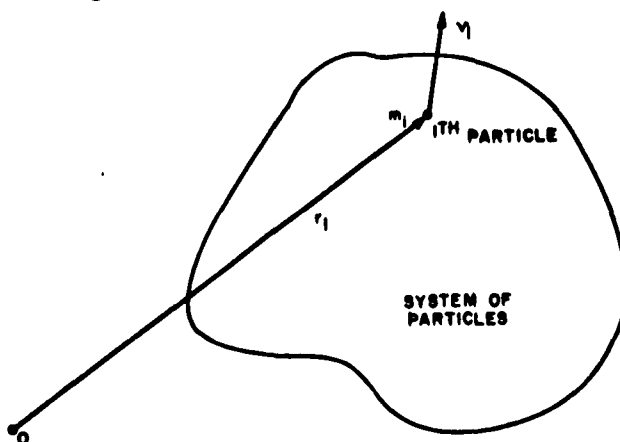


Fig. A-1 System of Particles

is given by

$$h = \sum_{i=1}^n r_i \times m_i v_i \quad (\text{A.1})$$

where  $m_i$  is the mass of the  $i^{\text{th}}$  particle

$r_i$  is the radius vector from the point about which the angular momentum is to be obtained to the  $i^{\text{th}}$  particle.

$v_i$  is the velocity of the  $i^{\text{th}}$  particle relative to the point about which the angular momentum of the system is to be obtained.

This definition is meaningful regardless of whether the reference point be fixed or translating with respect to inertial space.

The case where the system of particles comprises a rigid body, and the point about which the angular momentum is to be obtained is the mass center of the body, is of particular interest. For this case, the velocity of an arbitrary ( $i^{\text{th}}$ ) particle is given by

$$v_i = \omega \times r_i \quad (\text{A.2})$$

where  $\omega$  is the angular velocity of the rigid body with respect to inertial space  
 $r_i$  is the radius vector from the mass center to the  $i^{\text{th}}$  particle.

Substituting into the general equation for the angular momentum, (A.1) one obtains for the angular momentum about the mass center

$$h_{c.g.} = \sum_{i=1}^n r_i \times m_i (\omega \times r_i) \quad (\text{A. 3})$$

Using the vector identity for a triple cross product

$$A \times (B \times C) = B(A \cdot C) - C(A \cdot B) \quad (\text{A. 4})$$

one obtains

$$r_i \times m_i (\omega \times r_i) = m_i \left[ \omega r_i^2 - r_i (\omega \cdot r_i) \right] \quad (\text{A. 5})$$

Resolving  $r_i$  and  $\omega$  into a system of rectangular coordinates

$$r_i = x_i i + y_j j + z_k k \quad (\text{A. 6})$$

$$\omega = \omega_i i + \omega_j j + \omega_k k \quad (\text{A. 7})$$

and performing the indicated operations, one obtains

$$h_{c.g.} = h_i i + h_j j + h_k k \quad (\text{A. 8})$$

where

$$h_i = A \omega_i - H \omega_j - G \omega_k \quad (\text{A. 9})$$

$$h_j = -H \omega_i + B \omega_j - F \omega_k \quad (\text{A. 10})$$

$$h_k = -G \omega_i - F \omega_j + C \omega_k \quad (\text{A. 11})$$

Equations (A. 9), (A. 10) and (A. 11) can be expressed in matrix notation by representing the angular momentum vector and the angular velocity vector as column matrices

$$\begin{pmatrix} h_i \\ h_j \\ h_k \end{pmatrix} = \begin{pmatrix} A & -H & -G \\ -H & B & -F \\ -G & -F & C \end{pmatrix} \begin{pmatrix} \omega_i \\ \omega_j \\ \omega_k \end{pmatrix} \quad (\text{A. 12})$$

The first term on the right side of the equation is referred to as the inertia tensor.

Where  $A = \sum m_i (y^2 + z^2)$  (A.13)

$$B = \sum m_i (x^2 + z^2) \quad (\text{A.14})$$

$$C = \sum m_i (x^2 + y^2) \quad (\text{A.15})$$

are the polar moments of inertia about the  $i$ ,  $j$  and  $k$  axes respectively

and

$$H = \sum m_i xy \quad (\text{A.16})$$

$$G = \sum m_i xz \quad (\text{A.17})$$

$$F = \sum m_i yz \quad (\text{A.18})$$

are the products of inertia in the  $i$ - $j$ ,  $i$ - $k$ , and  $j$ - $k$  planes respectively.

If  $i$ ,  $j$  and  $k$  are body fixed vectors, the components of the inertia tensor are constant.

It is shown in any text of classical mechanics that the torque exerted on a body about its center of gravity is equal to the rate of change of its angular momentum about its center of gravity as seen from inertial space.

$$T_{c.g.} = \dot{h}_{c.g.} \quad (\text{A.19})$$

where

$$\dot{h}_{c.g.} = \frac{\delta h_{c.g.}}{\delta t} + \omega \times h_{c.g.} \quad (\text{A.20})$$

where

$\delta/\delta t$  denotes a partial differentiation in which the  $i$ - $j$ - $k$  vectors are held fixed,

$\omega$  is the angular velocity of the  $i$ - $j$ - $k$  coordinate system with respect to inertial space (which need not be that of the body).

It can also be shown in advanced books of classical mechanics that there exists at least one set of axes for which the product of inertia terms ( $H$ ,  $G$ ,  $F$ ) vanish. Such axes are known as principal axes. For the principal axes, the inertia tensor is diagonal.

$$\begin{pmatrix} A & 0 & 0 \\ 0 & B & 0 \\ 0 & 0 & C \end{pmatrix} \quad (\text{A.21})$$

It will be assumed that the  $i$ - $j$ - $k$  vectors are fixed in the body and coincide with the principal axes.

Therefore

$$h_{c.g.} = A \dot{\omega}_i i + B \dot{\omega}_j j + C \dot{\omega}_k k \quad (A.22)$$

and

$$\begin{aligned} \dot{h}_{c.g.} &= A \ddot{\omega}_i i + B \ddot{\omega}_j j + C \ddot{\omega}_k k \\ &+ \omega \times [A \omega_i i + B \omega_j j + C \omega_k k] \end{aligned} \quad (A.23)$$

Expanding and equating (A.23) component wise to the torque yields the following equations:

$$T_i = A \ddot{\omega}_i + (C - B) \omega_j \omega_k \quad (A.24)$$

$$T_j = B \ddot{\omega}_j + (A - C) \omega_i \omega_k \quad (A.25)$$

$$T_k = C \ddot{\omega}_k + (B - A) \omega_i \omega_j \quad (A.26)$$

These are Euler's equations.



APPENDIX BDerivation of Gyroscope Equations.

A gyroscope consists of two basic components. An inertia wheel or rotor which rotates at a high speed and a gimbal to which the rotor is mounted and which permits angular motion of the rotor with respect to inertial space. (Refer to Fig. B-1).

The torque on the rotor and gimbal which comprise the gyroscope, about the center of gravity of the gyroscope is given by the time derivative of its angular momentum about its center of gravity with respect to inertial space.

$$T_{g.c.g.} = \frac{d}{dt} h_{g.c.g.} \quad (B.1)$$

The angular momentum of the gyroscope can be considered to be composed of two parts. One due to the angular velocity of the rotor and the other due to the angular velocity of the gimbal. The component of angular momentum due to the angular velocity of the gimbal, is computed by considering the rotor to be stationary.

$$h_{g.c.g.} = \sum r_i \times m_i v_i \Big|_{\text{rotor}} + \sum r_i \times m_i v_i \Big|_{\substack{\text{gimbal plus} \\ \text{stationary rotor}}} \quad (B.2)$$

Now

$$\sum r_i \times m_i v_i \Big|_{\text{rotor}} = H_r j_g \quad (B.3)$$

$$H_r = J_r \omega_r \quad (B.4)$$

where  $J_r$  represents the polar moment of inertia of the rotor about its axis of rotation.

$\omega_r$  is the angular velocity of the rotor about its axis of rotation.

$$\sum r_i \times m_i v_i \Big|_{\substack{\text{gimbal plus} \\ \text{stationary rotor}}} = A_g \omega_i i_g + B_g \omega_j j_g + C_g \omega_k k_g \quad (B.5)$$

As was done in deriving Euler's equations in Appendix A

$$\frac{d}{dt} h_{g.c.g.} = \frac{\delta h}{\delta t} + \omega_g \times h_g \quad (B.6)$$

where

$$\omega_g = \omega_i i_g + \omega_j j_g + \omega_k k_g \quad (B.7)$$

is the angular velocity of the gimbal axes with respect to inertial space.

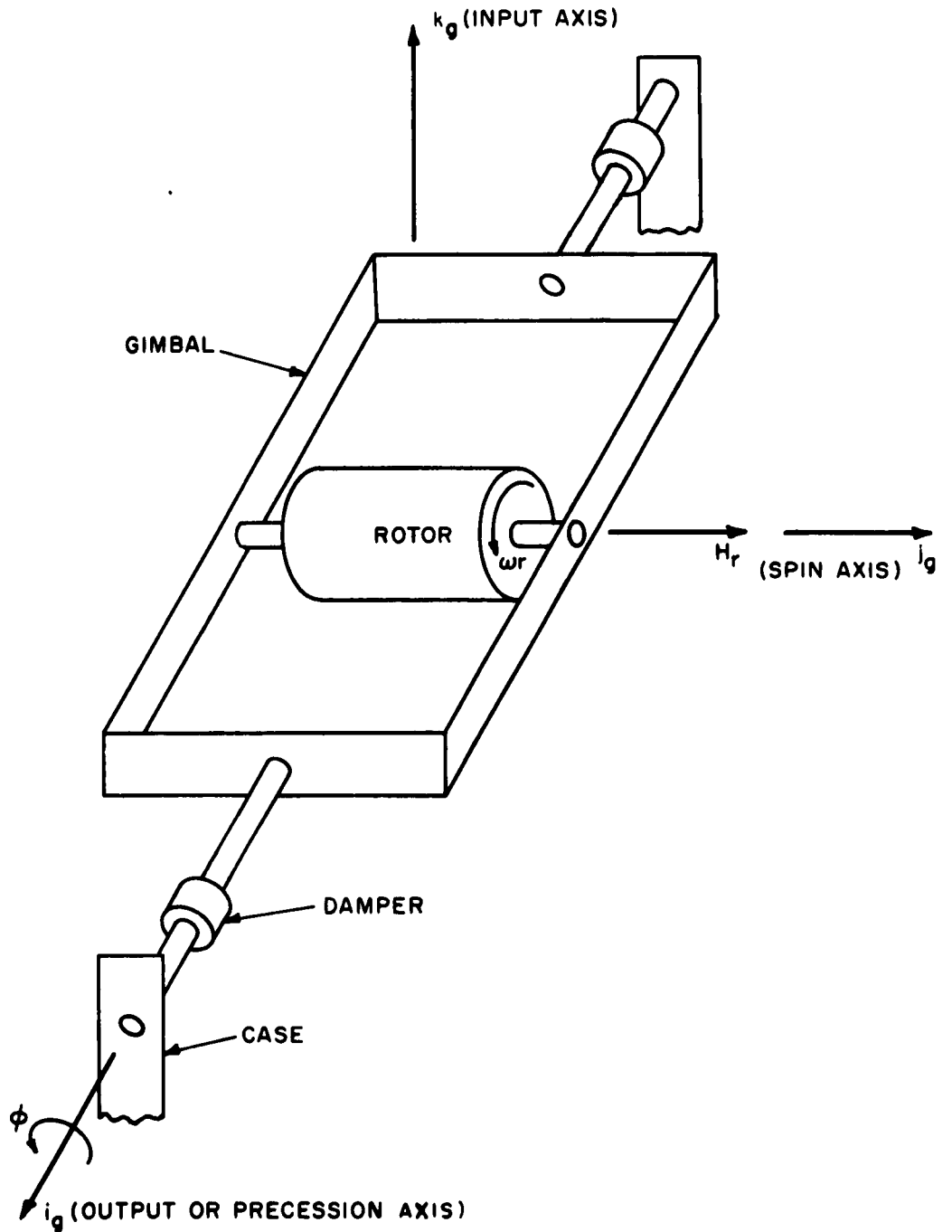


Fig. B-1 Single Degree of Freedom Gyroscope

Therefore

$$\begin{aligned} \frac{d}{dt} h_{g.c.g.} = & A_g \dot{\omega}_{i_g} i_g + (\dot{H}_r + B_g \dot{\omega}_{j_g}) j_g + C_g \dot{\omega}_{k_g} k_g \\ & + i_g \left[ (C_g - B_g) \omega_{j_g} \omega_{k_g} - H_r \omega_{k_g} \right] + j_g \left[ (A_g - C_g) \omega_{i_g} \omega_{k_g} \right] \\ & + k_g \left[ (B_g - A_g) \omega_{i_g} \omega_{j_g} + H_r \omega_{i_g} \right] \end{aligned} \quad (B.8)$$

Grouping terms and equating component wise to the torque one obtains

$$T_{g_{i_g}} = A_g \dot{\omega}_{i_g} + (C_g - B_g) \omega_{j_g} \omega_{k_g} - H_r \omega_{k_g} \quad (B.9)$$

$$T_{g_{j_g}} = \dot{H}_r + B_g \dot{\omega}_{j_g} + (A_g - C_g) \omega_{i_g} \omega_{k_g} \quad (B.10)$$

$$T_{g_{k_g}} = C_g \dot{\omega}_{k_g} + (B_g - A_g) \omega_{i_g} \omega_{j_g} + H_r \omega_{i_g} \quad (B.11)$$

Examination of these equations reveals that the torque on the gyroscope is composed of two parts. The first part is given by

$$T_{g_{i_g}} = A_g \dot{\omega}_{i_g} + (C_g - B_g) \omega_{j_g} \omega_{k_g} \quad (B.12)$$

$$T_{g_{j_g}} = B_g \dot{\omega}_{j_g} + (A_g - C_g) \omega_{i_g} \omega_{k_g} \quad (B.13)$$

$$T_{g_{k_g}} = C_g \dot{\omega}_{k_g} + (B_g - A_g) \omega_{i_g} \omega_{j_g} \quad (B.14)$$

and the second part is given by

$$T_{g_{i_g}} = - H_r \dot{\omega}_{k_g} \quad (B.15)$$

$$T_{g_{j_g}} = \dot{H}_r \quad (B.16)$$

$$T_{g_{k_g}} = H_r \omega_{i_g} \quad (B.17)$$

The first part is seen to be a restatement of Euler's Equations, (A.24), (A.25), (A.26). It describes the rigid body dynamics that do not depend upon the angular momentum

of the rotor. The second part of the equation, which is known as the gyroscopic torque, is provided by the angular momentum of the rotor. If the angular velocity of the rotor is assumed to be constant ( $\dot{H}_r = 0$ ), the equation of gyroscopic torque takes a particularly simple form. Namely

$$T_g = \omega \times H_r \quad (\text{B.18})$$

where  $\omega$  is the angular velocity of the gimbal with respect to inertial space.

$H_r$  is the angular momentum of the rotor.

This form of the equation is extensively used in the literature.

APPENDIX CDerivation of the Gravity Gradient Torque.

Consider a rigid system of particles in orbit around the earth. (See Fig. C-1). The force on the  $i^{\text{th}}$  particle is given by

$$\underline{W}_i = -m_i g_i \frac{\underline{\rho}_i}{\rho_i} \quad (\text{C.1})$$

Where

$m_i$  is the mass of the  $i^{\text{th}}$  particle

$g_i$  is the acceleration due to gravity at the position of the  $i^{\text{th}}$  particle.

$\underline{\rho}_i$  is the vector displacement from the center of the earth to the  $i^{\text{th}}$  particle.

$$\text{Now } g_i = \frac{g_s R_e^2}{\rho_i^2} \quad (\text{C.2})$$

where  $g_s$  is the acceleration due to gravity at the surface of the earth.

$R_e$  is the mean radius of the earth.

Substituting eq. (C.2) into eq. (C.1) yields:

$$\underline{W}_i = -m_i g_s \frac{R_e^2}{\rho_i^3} \underline{\rho}_i \quad (\text{C.3})$$

The torque exerted on the system of particles about its center of gravity due to the earth's gravitational field, is given by

$$\underline{T}_{dg} = \sum_{i=1}^n \underline{r}_i \times \underline{W}_i \quad (\text{C.4})$$

where  $\underline{T}_{dg}$  is the gravity gradient torque on the body (differential gravity torque)

$\underline{r}_i$  is the vector displacement from the center of gravity to the  $i^{\text{th}}$  particle.

Substituting eq. (C.3) into eq. (C.4) yields:

$$\underline{T}_{dg} = -g_s R_e^2 \sum_{i=1}^n \frac{m_i}{\rho_i^3} (\underline{r}_i \times \underline{\rho}_i) \quad (\text{C.5})$$

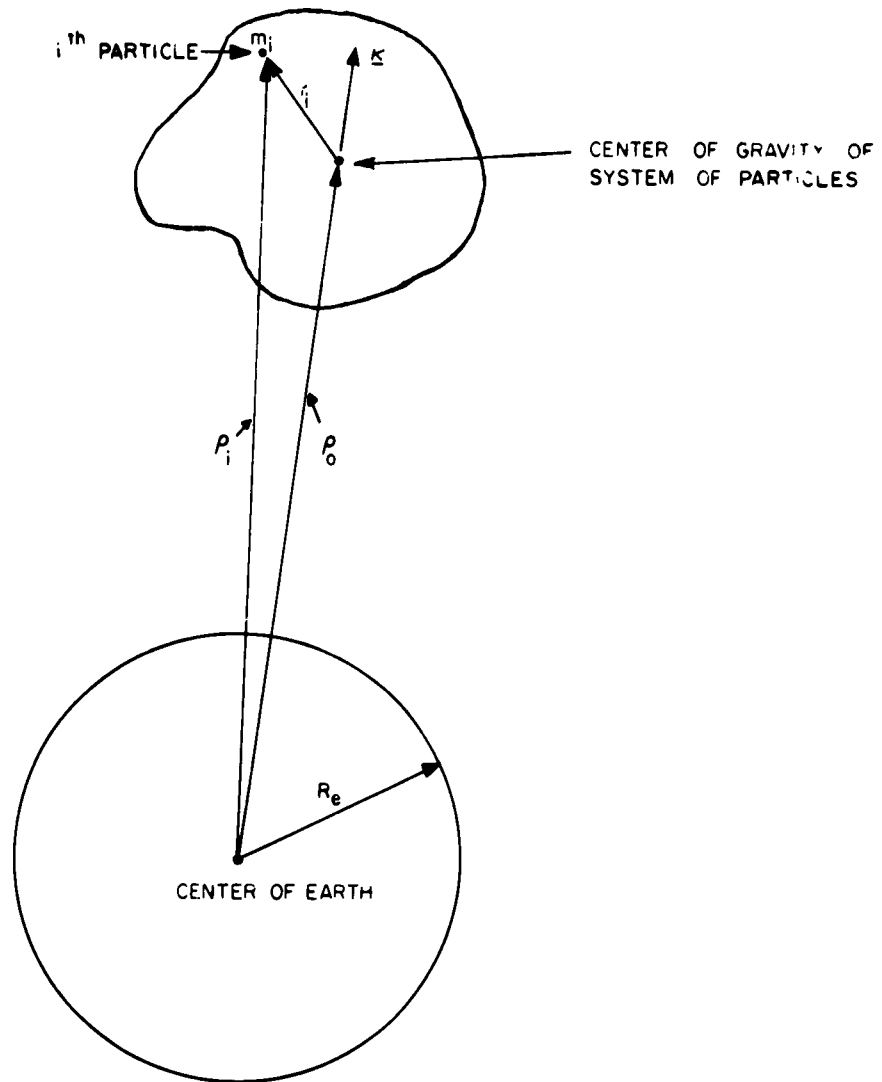


Fig. C-1 An Arbitrary Shaped Orbiting Vehicle

From Fig. (C-1) it is seen that

$$\underline{\rho}_i = \rho_o \underline{k} + \underline{r}_i \quad (\text{C. 6})$$

where

$\rho_o$  is the distance from the center of the earth to the mass center of the system of particles.

$\underline{k}$  is a unit vector outward along the geocentric vertical.

Now

$$\rho_i^{-3} = (\underline{\rho}_i \cdot \underline{\rho}_i)^{-\frac{3}{2}} \quad (\text{C. 7})$$

Substituting eq. (C. 6) and simplifying yields:

$$\rho_i^{-3} = \rho_o^{-3} \left[ 1 + \frac{2\underline{k} \cdot \underline{r}_i}{\rho_o} + \left( \frac{r_i}{\rho_o} \right)^2 \right]^{-\frac{3}{2}} \quad (\text{C. 8})$$

Since

$$\frac{r_i}{\rho_o} \ll 1 \quad (\text{C. 9})$$

$$\rho_i^{-3} \approx \rho_o^{-3} \left[ 1 + \frac{2\underline{k} \cdot \underline{r}_i}{\rho_o} \right]^{-\frac{3}{2}} \quad (\text{C. 10})$$

Expanding in a power series and taking only the first terms yields:

$$\rho_i^{-3} \approx \rho_o^{-3} \left[ 1 - \frac{3\underline{k} \cdot \underline{r}_i}{\rho_o} \right] \quad (\text{C. 11})$$

Substituting eq. (C. 6) and (C. 11) into eq. (C. 5) and expanding the vector product yields:

$$\underline{T}_{dg} = \frac{g_s R_e^2}{\rho_o^2} \underline{k} \times \sum_{i=1}^n m_i \underline{r}_i + \frac{3 g_s R_e^2}{\rho_o^3} \sum_{i=1}^n m_i (\underline{r}_i \times \underline{k})(\underline{r}_i \cdot \underline{k}) \quad (\text{C. 12})$$

But

$$\sum_{i=1}^n m_i \underline{r}_i = 0 \quad (\text{C. 13})$$

defines the center of mass of the system. Therefore

$$\underline{T}_{dg} = \frac{3 g_s R_e^2}{\rho_o^3} \sum_{i=1}^n m_i (\underline{r}_i \times \underline{k})(\underline{r}_i \cdot \underline{k}) \quad (\text{C. 14})$$

For a circular orbit

$$\rho_o \Omega_y^2 = g_o = \frac{g_s R_e^2}{\rho_o} \quad (C.15)$$

where

$g_o$  is the acceleration due to gravity at the mass center.

Therefore

$$\frac{g_s R_e^2}{\rho_o^3} = \Omega_y^2 \quad (C.16)$$

Substituting eq. (C.16) into equation (C.14) yields for a circular orbit.

$$\underline{T}_{dg} = 3 \Omega_y^2 \sum_{i=1}^n m_i (\underline{r}_i \cdot \underline{x} \underline{k}) (\underline{r}_i \cdot \underline{k}) \quad (C.17)$$

Let  $X_b$ ,  $Y_b$  and  $Z_b$  be the coordinate system formed by the body principal axes, with corresponding unit vectors  $i_b$ ,  $j_b$  and  $k_b$ . Let  $X$ ,  $Y$  and  $Z$  be the reference coordinate system with corresponding unit vectors  $i$ ,  $j$  and  $k$ . (Refer to Chapter II sections A and B.) The set of Eulerian angles relating the body coordinate system to the reference coordinate system is denoted by  $\theta_x$ ,  $\theta_y$  and  $\theta_z$ . The transformation matrix relating the two coordinate systems is given in equation (2.5). (Refer to Chapter II, section C.)

Expressing the vector  $\underline{r}_i$  in terms of body coordinates yields:

$$\underline{r}_i = x_b i_b + y_b j_b + z_b k_b \quad (C.18)$$

Using the transformation matrix (2.5) yields:

$$\underline{k} = -\theta_y i_b + \theta_x j_b + k_b \quad (C.19)$$

Substituting equations (C.19) and (C.18) into eq. (C.14) yields:

$$\underline{T}_{dg} = \frac{3 g_s R_e^2}{\rho_o^3} \sum_{i=1}^n m_i \left[ i_b (y_b - \theta_x z_b) + j_b (-x_b - \theta_y z_b) + k_b (\theta_x x_b + \theta_y y_b) \right] \left[ -\theta_y x_b + \theta_x y_b + z_b \right] \quad (C.20)$$



Expanding eq. (C. 20) and noting that the product of inertia terms vanish (see eqs. (A. 16), (A. 17), (A. 18) yields:

$$\underline{T}_{dg} = \frac{3 g_s R_e^2}{\rho_o^3} \sum_{i=1}^{n'} m_i \left[ i_b \theta_x (y_b^2 - z_b^2) + j_b \theta_y (x_b^2 - z_b^2) + k_b \theta_x \theta_y (y_b^2 - x_b^2) \right] \quad (C. 21)$$

The  $k_b$  component will be neglected since it involves the product of two small angles. Substituting eqs. (A. 13), (A. 14) and (A. 15) into eq. (C. 21) yields the final result for the gravity gradient torque.

$$\underline{T}_{dg} = \frac{3 g_s R_e^2}{\rho_o^3} \left[ i_b \theta_x (I_{z_b} - I_{y_b}) + j_b \theta_y (I_{z_b} - I_{x_b}) \right] \quad (C. 22)$$

Substituting eq. (C. 16) into eq. (C. 22), one obtains the corresponding equation for a circular orbit.

$$\underline{T}_{dg} = 3 \Omega_y^2 \left[ i_b \theta_x (I_{z_b} - I_{y_b}) + j_b \theta_y (I_{z_b} - I_{x_b}) \right] \quad (C. 23)$$

REFERENCES

1. J.S. Ausman, "Theory of Inertial Sensing Devices", Autonetics, Downey, California, Technical Memorandum 3242-3-3, Feb. 1961
2. E.G.C. Burt, "On the attitude Control of Earth Satellites", Guided Weapons Department, Royal Aircraft Establishment, Farnborough, 1961
3. J. DeLisle, G. Ogletree, B.M. Hildebrant, "Attitude Control of Satellites using Integrating Gyroscopes", Instrumentation Laboratory, Massachusetts Institute of Technology, Cambridge, 1961
4. W.A. Lynch and J.G. Truxal, "Signals and Systems in Electrical Engineering", pp 365-379, 397-409, McGraw-Hill Book Co., Inc., New York 1962
5. J. Marino, "Feasibility of a Space Vehicle Gyro-Stabilizer", M.S. Thesis, Department of Electrical Engineering, Polytechnic Institute of Brooklyn, June 1961
6. C. McClure, "Theory of Inertial Guidance" pp 57-115, Prentice-Hall, Inc. New Jersey 1960
7. R. A. Nidey, "Gravitational Torque on a Satellite of Arbitrary Shape", Ball Brothers Research Corp., Boulder, Colo., February 1960.
8. G. Ogletree, S. J. Sklar and J.G. Mangan, "Satellite Attitude Control Study", Instrumentation Laboratory, Massachusetts Institute of Technology, Parts I and II, Cambridge, 1961, 1962
9. R. Schindwolf, "Geocentric Attitude Control of an Earth Satellite", Ph. D. Dissertation, Department of Electrical Engineering, Polytechnic Institute of Brooklyn, June 1962.
10. E.D. Scott, "The V-CMG System", Lockheed Aircraft Corporation, Sunnyvale, California, LMSC/A083727 SA/62-43/324, April 1962
11. E.D. Scott, "General CMG Attitude Control System", Lockheed Aircraft Corporation, Sunnyvale, California, LMSC/A056549, SA/62-43/422, 1962
12. M. L. Shooman and H. Perkel, "A Preliminary Evaluation of Passive and Semi-Passive Attitude Control Techniques", Radio Corporation of America, Princeton, New Jersey, 1963
13. J. Synge and B. Griffith, "Principles of Mechanics", McGraw-Hill Book Co., Inc., New York 1959
14. L. B. Taplin and B. R. Teitelbaum, "The State-of-the-Art of Space Vehicle Attitude Control", The Bendix Corporation Research Laboratories Division, Energy Conversion and Dynamic Controls Laboratory, Southfield, Michigan, 1962
15. J.G. Truxal and E. Mishkin, "On the Evaluation of an Attitude Control System", Proceedings of the Symposium on Active Networks and Feedback Systems. Polytechnic Institute of Brooklyn, April, 1962

**TECHNICAL AND FINAL REPORT DISTRIBUTION LIST**  
**PHYSICAL SCIENCES DIRECTORATE**

Commander AF Office of Scientific Research ATTN: SRY Washington 25, D. C.	3	Chief of Research and Development 1 ATTN: Scientific Information Branch Department of the Army Washington 25, D. C.
Commander AF Office of Scientific Research ATTN: SRGL Washington 25, D. C.	2	Chief, Physics Branch 1 Division of Research U. S. Atomic Energy Commission Washington 25, D. C.
Commander Wright Air Development Division ATTN: WWAD Wright-Patterson Air Force Base Ohio	4	U. S. Atomic Energy Commission 1 Technical Information Extension P. O. Box 62 Oak Ridge, Tennessee
Commander AF Cambridge Research Laboratories ATTN: CRRELA L. G. Hanscom Field Bedford, Massachusetts	1	National Bureau of Standards Library 1 Room 203, Northwest Building Washington 25, D. C.
Commander European Office Office of Aerospace Research The Shell Building Brussels, Belgium	2	Physics Program 1 National Science Foundation Washington 25, D. C.
P. O. Box AA Wright-Patterson Air Force Base Ohio	1	Director, Office of Ordnance Research Box CM, Duke Station 1 Durham, North Carolina
Aeronautical Research Laboratories 1 ATTN: Technical Library Building 450 Wright-Patterson Air Force Base Ohio	1	Director, Department of Commerce 1 Office of Technical Services Washington 25, D. C.
Armed Services Technical Info. Agency ATTN: TIPCR Arlington Hall Station Arlington 12, Virginia	10	AEDC (AEOIM) 1 Arnold Air Force Station Tullahoma, Tennessee
Director of Research and Development Headquarters, USAF ATTN: AFDRD Washington 25, D. C.	1	Commander 1 AF Flight Test Center ATTN: FTOTL Edwards Air Force Base, California
Office of Naval Research Department of the Navy ATTN: Code 420 Washington 25, D. C.	1	Commander 1 AF Special Weapons Center ATTN: SWOI Kirtland Air Force Base, New Mexico
Director, Naval Research Laboratory ATTN: Technical Info. Officer Washington 25, D. C.	1	Commander 1 AF Missile Development Center ATTN: HDOI Holloman Air Force Base New Mexico
		Commander 1 Army Rocket and Guided Missile Agency ATTN: ORD XR-OTL Redstone Arsenal, Alabama

Commandant Air Force Institute of Technology AU Library M0 LI-LIB, Bldg. 125, Area B Wright-Patterson Air Force Base Ohio	1
Commander Air Force Systems Command ATTN: RDRS Andrews Air Force Base Washington 25, D. C.	6
Commanding General U. S. Army Signal Corps Research and Development Laboratory ATTN: SIGFM/EL-RPO Ft. Monmouth, New Jersey	1
National Aeronautics and Space Administration ATTN: Library 1520 H Street, N. W. Washington 25, D. C.	6
Advanced Research Projects Agency Washington 25, D. C.	1
Rand Corporation 1700 Main Street Santa Monica, California	1
Chairman (Unclass. Reports) Canadian Joint Staff For DRB/DSIS 2450 Massachusetts Ave., N. W. Washington 25, D. C.	1